Building and characterization of a DSSC cell with TiO2 nanotubes

UNIVERSITY OF TRENTO

· **Autor:** Adrián García Ramos

· **Universidad de realización del proyecto durante intercambio Erasmus:**

Università degli studi di Trento.

· **Tutor del proyecto en la Universidad de destino:** Claudio della Volpe.

· **Coordinador Académico y Cotutor en UCIIIM:** J. M. Torralba.

· **Calificación obtenida:** 30 / 30

Resumen

El siguiente proyecto fin de carrera denominado: Construcción y caracterización de una célula DSSC usando nanotubos de TiO2 ha sido realizado en la Universidad de Trento (Italia) en el departamento de materiales de la facultad de ingeniería. Durante mi estancia como becario erasmus en Italia, tuve la oportunidad de conocer al profesor Claudio della Volpe que fue quien me presentó la idea de trabajar con células solares fotovoltaicas y especialmente como aplicación de nanotubos de titanio.

En su dilatada carrera como investigador, el profesor della Volpe había realizado el seguimiento como tutor de un gran número proyectos relacionados con las aplicaciones solares de nanoestructuras de titanio sensitivizado. Estas aplicaciones fueron publicadas por primera vez en 1991 por el profesor M. Gräetzel en su articulo: "*Low-cost, high-efficiency solar cell based on dye-sensitized colloidal TiO2 films".*

Durante todos estos años, muchos grupos han intentado encontrar nuevas técnicas que reduzcan el principal problema de las células fotovoltaicas tradicionales. Este "handicap" no es otro que el alto coste de fabricación que implica el uso y procesamiento del silicio como material base. De este modo, hoy en día encontramos en el mercado fotovoltaico un alto porcentaje de células solares con un buen rendimiento global pero con un ciclo de vida energético deficiente en muchos casos.

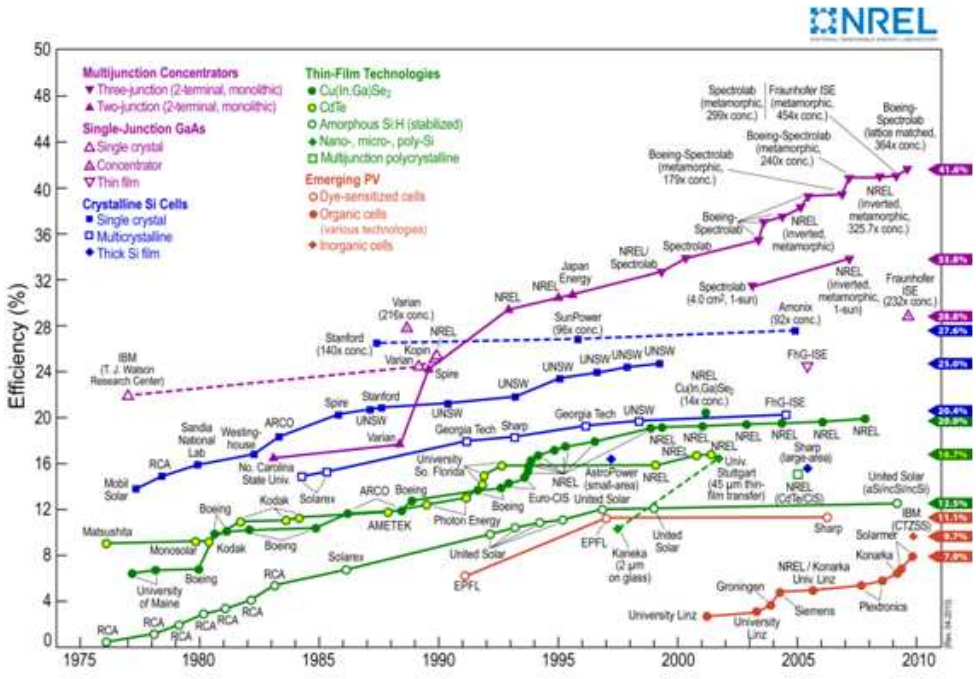

El principal objetivo de las “Dye sensitized solar cells” o simplemente “DSSC” es disminuir este coste; para ello, se utilizan áreas con superficies especificas muy altas donde la conversión de la luz (fotones) en corriente eléctrica (electrones) es posible. Estas superficies conductoras necesitan un colorante (dye en inglés) donde se produce la conversión antes mencionada. De esta manera, la luz incide sobre el colorante que baña las estructuras con alta superficie específica y se produce el proceso de generación de corriente eléctrica a través de la banda de conducción del material metálico.

En la siguiente figura se representa el comportamiento esquemático del principio de operación de una célula fotovoltaica a partir de colorante sensitivizado. Como se puede observar, los fotones (hv) inciden sobre las estructuras conductoras sensitivizadas que

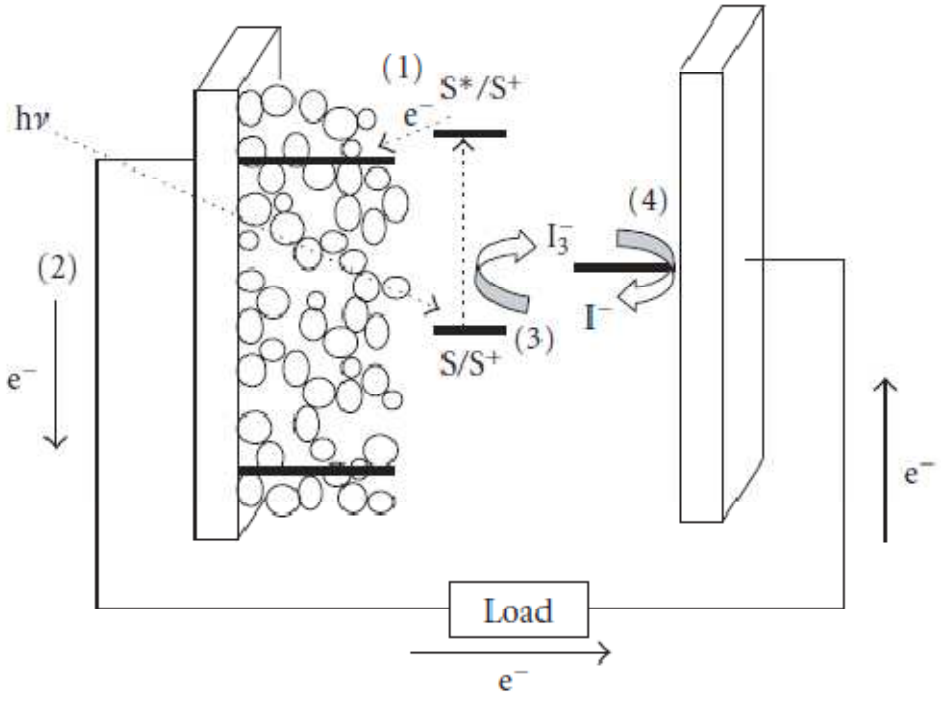

convierten e introducen electrones en la banda de conducción de los coloides de titanio, en este punto, el contraelectrodo se encarga de neutralizar la reacción y cerrar el circuito eléctrico para poder producir una carga constante.

Alrededor de este tema fueron realizadas investigaciones por el propio profesor della Volpe durante años además de otros grupos, con el objetivo de conseguir un rendimiento de las células competitivo que pudiera establecer un nuevo mercado fotovoltaico.

No obstante, gracias a las investigaciones llevadas a cabo por el profesor A. Grimes, la aplicación de nanotubos sensitivizados de titanio como electrodo dentro de la célula fotovoltaica es por primera vez utilizada en 2009. La alta superficie específica que ofrecen estas estructuras pone de relieve un marco óptimo para el desarrollo de aplicaciones solares "DSSC".

Es a raíz de este momento cuando surge el interés en este nuevo campo, manteniendo los trabajos realizados por la universidad anteriormente con las estructuras coloidales de titanio.

De esta forma, la misión del proyecto era entender cómo se podían reproducir los nanotubos y en qué condiciones, e intentar trasladarlos a una superficie de vidrio conductora similar a la usada durante estos años en la universidad con las células que usaban estructuras de titanio coloidal.

El primer paso fue controlar el proceso de formación de nanotubos; éste se llevaba a cabo, de entre varias maneras, como pudimos recoger en la literatura, a través de un dispositivo electroquímico similar al mostrado en la figura.

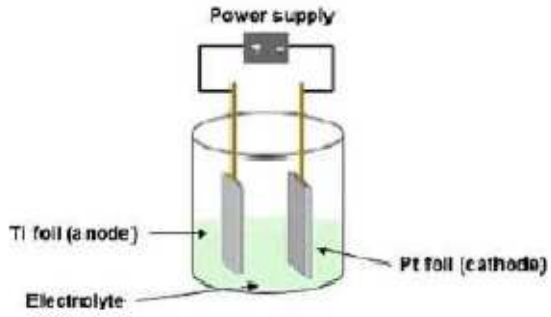

En él se pueden diferenciar la fuente de alimentación de corriente continua, el ánodo de titanio que pretendemos oxidar, el cátodo de platino y la solución electrolítica donde están contenidos ambos.

Al principio nuestra idea fue oxidar directamente muestras de cristal conductor con un film de titanio depositado y continuar con el montaje de la célula que había sido realizado en trabajos anteriores en el departamento. Sin embargo, debido a problemas

durante los experimentos con la separación del film decidimos continuar la parte experimental utilizando en primer lugar placas de titanio para conseguir las condiciones óptimas de proceso.

Llegados a este punto tuvimos que diseñar nuevos elementos que nos permitieran realizar las anodizaciones en condiciones reproducibles. Los principales problemas que encontramos estuvieron relacionados con la geometría de las placas de titanio de las que disponíamos (botones cilíndricos de 6 mm. de diámetro) que no nos permitían trabajar de manera estanca (contacto eléctrico con el electrolito) y de paralelismo entre el cátodo y el ánodo. No obstante, fueron conseguidos resultados apreciables aunque en zonas muy concretas de la muestra analizada con un área muy pequeña.

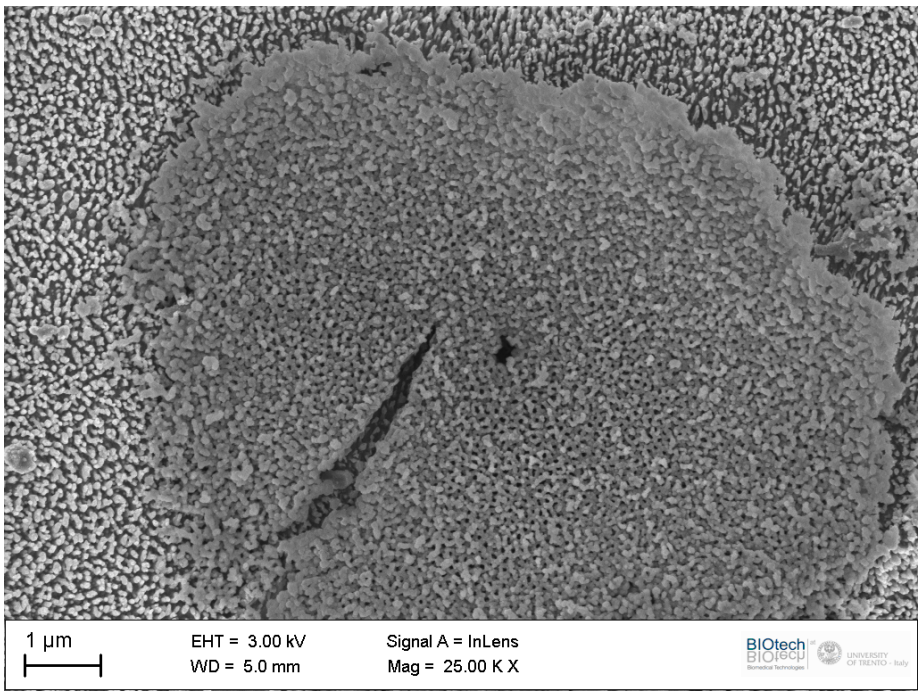

Precisamente por este motivo, probamos nuevas geometrías que dieran como resultado superficies de nanotubos homogéneas de acuerdo a nuestras necesidades. Esto es, una superficie continua de nanotubos sobre toda la superficie de la muestra. De cualquier forma, pronto llegaron nuevas muestras de placas de titanio que nos permitieron resolver los problemas antes mencionados con las placas originales, pudiendo realizar

los experimentos de forma cómoda y sin problemas. Fue en este momento cuando conseguimos que toda la parte oxidada de la muestra tuviera presente la existencia de estructuras de nanotubos homogénea. En la figura se pueden apreciar los nanotubos que se extendían por toda la superficie.

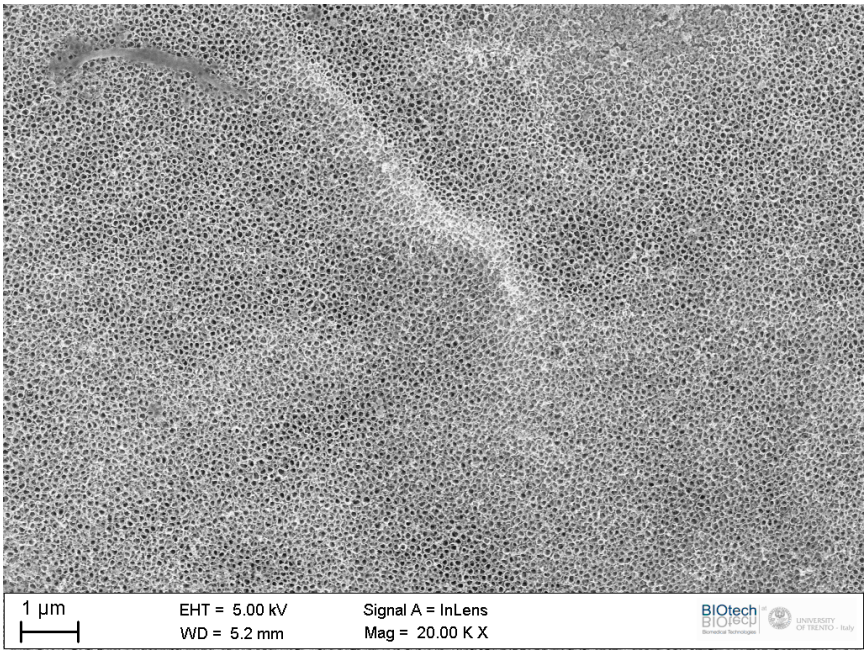

Una vez el principal objetivo de la síntesis de nanotubos fue conseguido, realizamos distintos experimentos para comprobar el efecto de la temperatura durante la oxidación de las muestras y su influencia sobre las propiedades geométricas de las estructuras formadas.

Estas características fueron analizadas posteriormente utilizando un software de tratamiento de imágenes "ImageJ" a través de las fotografías obtenidas en el microscopio electrónico.

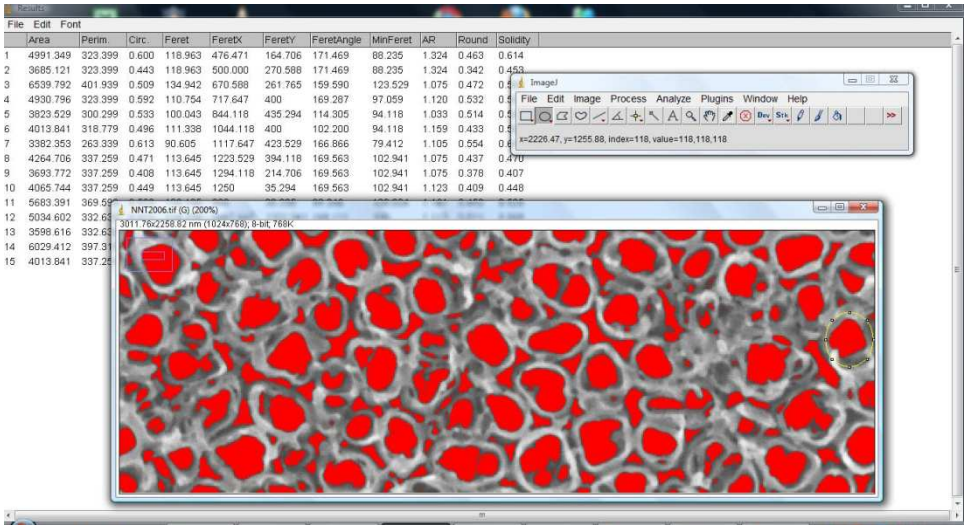

El siguiente punto del trabajo experimental consistía en la oxidación de las muestras de cristal conductor con el film depositado de titanio como habíamos hecho al principio. Sin embargo, debido a dificultades con la disponibilidad de los equipos de "Sputtering" (encargados de la deposición de espesores de microns sobre la superficie de vidrio) en Trento, tuvimos que contactar con el profesor Maggioni en Padova, que utilizaba en sus investigaciones estos aparatos.

De este modo y tras una visita de un día para conocer los equipos que podrían proporcionarnos las nuevas muestras, realizamos un viaje de cuatro días a la ciudad de Padova desde Trento para trabajar en las instalaciones con el profesor Maggioni.

Cabe destacar, que durante esta estancia trabajamos tanto con técnicas de sputtering de radio frecuencia como magnetron.

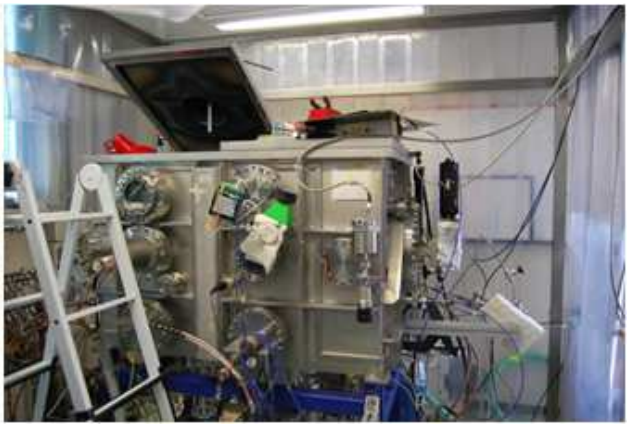

En este tiempo diversas muestras fueron realizadas con la consecución de espesores diversos; en total regresamos a Trento con 22 muestras de espesores de 1, ½ y ¼ de micron.

Una vez ya en los laboratorios de la universidad, comenzamos con la oxidación de las muestras realizadas en Padova. Durante los primeros experimentos pudimos observar, como la capa de titanio se separaba espontáneamente del vidrio; esto nos hizo darnos cuenta de que los parámetros de proceso que habíamos definido para los experimentos con placas eran completamente diferentes a los realizados con muestras de vidrio con titanio depositado.

Así, tuvimos que ser más cuidadosos con las nuevas muestras, controlando en todo momento la permanencia del film durante las pruebas.

Finalmente, conseguimos algunas estructuras nanoporosas que nos fueron útiles para fabricación de las células fotovoltaicas.

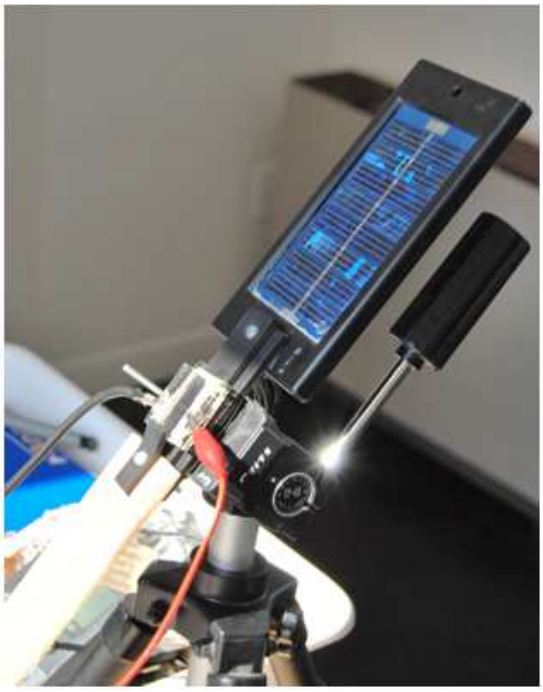

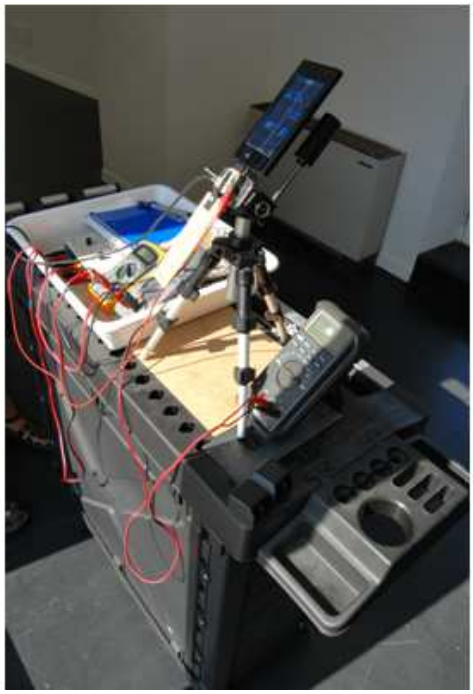

De este modo, utilizamos los conocimientos adquiridos en la realización de células con titanio coloidal (llegamos a fabricar algunas pruebas) para el montaje de los nuevos dispositivos con las estructuras de titanio depositado.

En la fotografía de la página anterior se puede observar cómo tras el montaje de las células, estas eran expuestas a la luz para medir su rendimiento. En este procedimiento fue utilizado un dispositivo fotovoltaico tradicional que servía de referencia para las mediciones realizadas.

Como quiera que sea, el resultado de estas células experimentales no fue especialmente bueno debido a nuestro desconocimiento en detalle de las técnicas de sputtering necesarias para un buen resultado posterior durante las anodizaciones de los films y sobretodo de las condiciones específicas encontradas en la segunda parte del proyecto durante las oxidaciones que hacían que no se pudieran aplicar plenamente los primeros resultados.

No obstante, todos los medios materiales y humanos fueron puestos en juego en nuestro equipo y la síntesis de nanotubos en placas de titanio fue satisfactoria. Concretamente, los parámetros geométricos fueron analizados en función de su dependencia con la temperatura dando lugar a interesantes resultados.

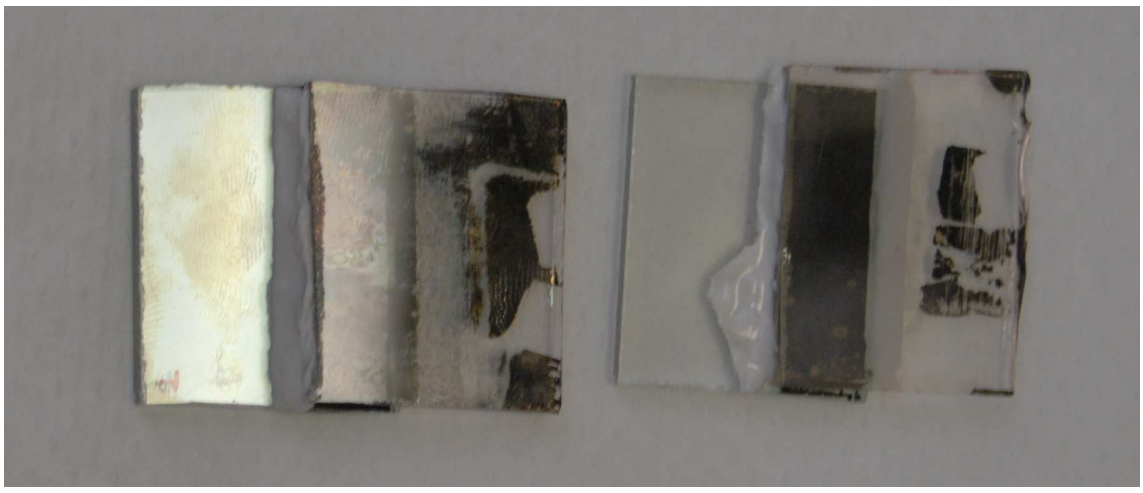

En la fotografía se pueden observar las células que construimos basadas en las estructuras nanoporosas anodizadas previamente en un baño electrolítico. Es interesante destacar que éstas fueron realizadas de manera experimental y las áreas de las muestras útiles con las que trabajábamos no superaban los 3 cm^2 en ningún caso.

Building and characterization of a DSSC cell with TiO2 nanotubes

UNIVERSITY OF TRENTO

Author: Adrián García Ramos

Supervisor: Prof. Claudio della Volpe.

Madrid, August 2010.

Contents

Foreword

First, I would like to thank professor Claudio della Volpe for giving me a research topic which was both interesting and fun to work at, as well as the motivation and support along the period I was in Trento. Also, the inestimable help I got from Mattia was substantial and it got me past the difficulties that came along the way.

Of course, everything in this work is not done by me, especially I would like to thank Lorenzo Moschini for his time on ESEM microscope.

I would also like to thank the Laboratory of Fisica Nucleare in Padova for allowing us to freely use their equipment, concretely professor Maggioni.

In the same way, I would like to thank my parents for giving me the moral and financial support to conclude this stage of my life. And finally, I would like to thank Elma for being there with me.

1. Introduction

1.1 Global energy situation.

The lifestyle and culture are based on current usable energy. The road to current living standards began precisely at the time were available enough energy. A secure energy supply, cost, not harmful to the environment and sustainable development is absolutely indispensable to the world in which we live.

Fossil fuels are currently the backbone of energy supply in Europe and worldwide. These fuels do not lose such importance in the coming decades and, therefore, continue remain essential. Their extraction and use, however, imply various environmental damage, mainly gas emissions greenhouse gases, especially CO2 and methane. On the other hand, their use has led to Europe depends on a very high level of imports of the subject essential raw, being expected that the dependence will increase in the future, particularly on oil peak and gradually and in relation to natural gas as well.

It is clear that the EU energy policy must take all necessary steps to reduce long-term dependence, including measures of saving and more efficient use of all sources of energy, such as increased use of alternative energy systems, such as renewables. In this context is particularly important the improvement of alternative energy systems. A prerequisite for progress in the field of energy efficiency is to intensify the research and development.

Moreover, that production and energy use are linked to pollution environment. None of the options and techniques that can contribute to future energy supply is technically perfect, neither is wholly free of disturbance to the environment, nor is it sufficient to cover all needs, and it can provide evolution of its price and availability for a period sufficiently long. Apart of this, is added the issue of shortage of reserves and resources, with all that entails. It is expected that the problem will increase considerably with overall population growth, growing demand energy in developing countries and in particular, the needs increasing energy by large latest industrializing countries like China, India and Brazil.

Thus, an important objective should be to ensure a providing long-term energy that respects the environment that is competitive. For the reasons already mentioned, that policy can not be limited to the use of a few sources of energy. On the contrary, the problems of power shortages and other risks must be to deal with through a highly diversified energy mix using

and developing all the techniques and available energy sources to undergo finally, in the context of accepted environmental requirements, to changing conditions.

1.1.1 Future prospects for renewable energy.

In general, all predictions about future developments depend (and therefore, there are differences in point of view adopted and, sometimes, we have a small stake in the business) of hypotheses about the future demographic and economic evolution, on the development of other scanning and exploration techniques, and the particular conditions in different countries. This is concretely applicable to nuclear energy, as well as the importance building measures for renewable energy sources.

The rapid increase in world energy prices from 2003 to 2008, combined with concerns about the environmental consequences of greenhouse gas emissions, has led to renewed interest in alternatives to fossil fuels—particularly, nuclear power and renewable resources—. As a result, long-term prospects continue to improve for generation from both nuclear and renewable energy sources—supported by government incentives and by higher fossil fuel prices [1].

According to *IEO2010*[2], renewable energy is the fastest-growing source of electricity generation in the reference case. From 2007 to 2035, world renewable energy use for electricity generation grows by an average of 3.0 percent per year , and the renewable share of world electricity generation increases from 18 percent in 2007 to 23 percent in 2035.

Much of the world increase in renewable electricity supplies fueled by hydropower and wind power. Except for those two sources, most renewable generation technologies are not economically competitive with fossil fuels over the projection period, outside a limited number of niche markets. Typically, government incentives or policies provide the primary support for construction of renewable generation facilities. Although they remain a small part of total renewable generation, renewables other than hydroelectricity and wind—including solar, geothermal, biomass, waste, and tidal/wave/oceanic energy—do increase at a rapid rate over the projection period.

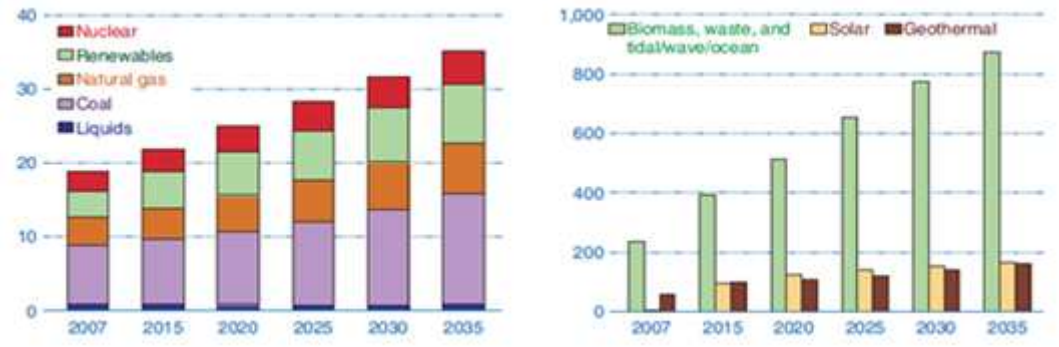

Figure 1. World net electricity region by fuel (trillion kilowatthours) andworld renewable electricity generation by energy source, excluding wind and hydropower (billion kilowatts.

Although renewable energy sources have positive environmental and energy security attributes, most renewable technologies other than hydroelectricity are not able to compete economically with fossil fuels during the projection period outside of a few regions. Solar power, for instance, is currently a "niche" source of renewable energy but can be economical where electricity prices are especially high, where peak load pricing occurs, or where government incentives are available. Government policies or incentives often provide the primary economic motivation for construction of renewable generation facilities.

Wind and solar are intermittent technologies that can be used only when resources are available. Once built, the cost of operating wind or solar technologies when the resource is available is generally much less than the cost of operating conventional renewable generation. However, high construction costs can make the total cost to build and operate renewable generators higher than those for conventional power plants. The intermittence of wind and solar can further hinder the economic competitiveness of those resources, as they are not operator controlled and are not necessarily available when they would be of greatest value to the system. The use of energy storage (such as hydroelectric pumped storage, compressed air storage, and batteries) and a wide geographic dispersal of wind and solar generating facilities could mitigate many of the problems associated with intermittence in the future.

Region	2007	2015	2020	2025	2030	2035	Average annual percent change, 2007-2035
OECD							
Hydropower	1,246	1,384	1,460	1,530	1,585	1,624	0.9
Wind	144	525	671	803	846	898	6.8
Geothermal	37	57	61	66	73	80	2.8
Solar	6	85	104	107	114	122	11.6
Other	195	253	318	398	456	485	3.3
Total OECD	**1,628**	**2,303**	**2,614**	**2,904**	**3,074**	**3,208**	**2.5**
Non-OECD							
Hydropower	1,753	2,305	2,706	3,061	3,449	3,795	2.8
Wind	21	157	231	312	388	457	11.7
Geothermal	21	41	47	52	68	80	5.0
Solar	0	10	23	33	39	44	21.7
Other	40	141	196	255	317	389	8.4
Total Non-OECD	**1,834**	**2,654**	**3,203**	**3,714**	**4,263**	**4,764**	**3.5**
World							
Hydropower	2,999	3,689	4,166	4,591	5,034	5,418	2.1
Wind	165	682	902	1,115	1,234	1,355	7.8
Geothermal	57	98	108	119	142	160	3.7
Solar	6	95	126	140	153	165	12.7
Other	235	394	515	653	773	874	4.8
Total World	**3,462**	**4,958**	**5,817**	**6,618**	**7,336**	**7,972**	**3.0**

Note: Totals may not equal sum of components due to independent rounding.

Figure 2. OECD and Non-OECD net renewable electricity generation by source (billion kilowatthours). OECD menas Organization for Economic Cooperation and Development.

1.2 Evolution of solar photovoltaic technologies.

Solar cells, also called photovoltaic (PV) cells by scientists, convert sunlight directly into electricity. PV gets its name from the process of converting light (photons) to electricity (voltage), which is called the *PV effect*. The PV effect was first recognized in 1834 by Becquerel. However, it was not until 1883 that the first solar cell was built, by Charles Fritts, who coated the semiconductor selenium with an extremely thin layer of gold to form the junctions. Soon solar cells were being used to power space satellites and smaller items like calculators and watches. Today, thousands of people power their homes and businesses with individual solar PV systems. Utility companies are also using PV technology for large power stations.

Traditional solar cells are made from silicon, are usually flat-plate, and generally are the most efficient. Second-generation solar cells are called thin-film solar cells because they are made from amorphous silicon or non-silicon materials such as cadmium telluride. Thin film solar cells use layers of semiconductor materials only a few micrometers thick. Because of

their flexibility, thin film solar cells can double as rooftop shingles and tiles, building facades, or the glazing for skylights.

Third-generation solar cells are being made from variety of new materials besides silicon, including solar inks using conventional printing press technologies, solar dyes, and conductive plastics. They still do not guarantee performance to make the devices marketed but are generating enormous interest in research given their potential and future low cost production. Some new solar cells use plastic lenses or mirrors to concentrate sunlight onto a very small piece of high efficiency PV material. The PV material is more expensive, but because so little is needed, these systems are becoming cost effective for use by utilities and industry. However, because the lenses must be pointed at the sun, the use of concentrating collectors is limited to the sunniest parts of the country. In figure 3 we can see the progress made in different generations[4].

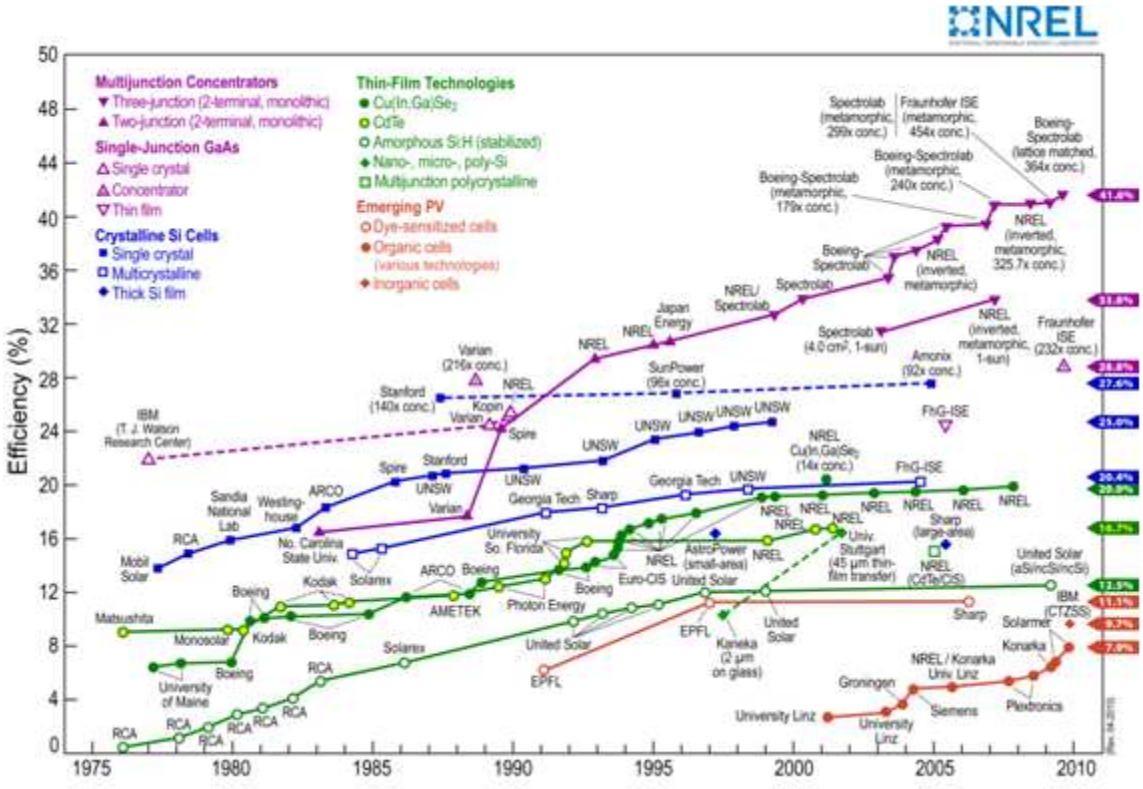

Figure 3. Best research-cells efficiencies.

1.3 Work motivation.

Nowadays, the technology with more commercial use is with no doubts the mono and polycrystalline silicon ensuring outputs around 14% working in standard conditions with a long lifetime as well. Even so, costs of ingot shaping and wafer slicing industries which manufacture silicon solar cells are very high. This has led to the search for new technologies that reduce the cost of manufacturing solar cells to improve the price/performance ratio. One of these emerging technologies is based on Dye-sensitized solar cell developed by Michael Grätzel in 1991[3].

As shown in the figure 2 the average annual percentage percent change for next years in electricity due to solar sources is the higher one among the renewable sources. Apart of this, within the framework of the photovoltaic cell technologies, dye-sensitized has been recognized as a viable competitor to the well developed but expensive solid-state solar cells. All these reasons, besides of shorter energy pay-back, influence to temperature changes and easy fabrication on rigid and flexible substrates make of dye-sensitized solar cells one of the better options to research and invest in these moments[2].

1.4 Theoretical introduction of operation.

"How a solar cell works?" This is one of the main points to understand the substance of this project. The goal of this part is to give a simple explanation of the different principles behind the working of a solar cell described before.

According to the bibliography [5] investigations focused on two types of cells whose principle of operation is shown in figure 4 . The first type is the regenerative cell, which converts light to electric power leaving no net chemical change behind. Photons of energy exceeding that of the band gap generate electron–hole pairs, which are separated by the electric field present in the space-charge layer. The negative charge carriers move through the bulk of the semiconductor to the current collector and the external circuit. The positive holes are driven to the surface where they are scavenged by the reduced form of the redox relay molecule (R), oxidizing it: $h^+ + R \rightarrow O$. The oxidized form O is reduced back to R by the electrons that re-enter the cell from the external circuit. Much of the work on

regenerative cells has focused on electron-doped (*n*-type), semiconductors using electrolytes based on sulphide/polysulphide, vanadium(II)/vanadium(III) or I_2/I^- redox couples. Conversion efficiencies of up to 19.6% have been reported for multijunction regenerative cells.

The second type, photosynthetic cells, operate on a similar principle except that there are two redox systems: one reacting with the holes at the surface of the semiconductor electrode and the second reacting with the electrons entering the counter-electrode. In the example shown, water is oxidized to oxygen at the semiconductor photoanode and reduced to hydrogen at the cathode. The overall reaction is the cleavage of water by sunlight. Titanium dioxide has been the favoured semiconductor for these studies, following its use by Fujishima and Honda for water photolysis. Unfortunately, because of its large band gap, TiO2 absorbs only the ultraviolet part of the solar emission and so has low conversion efficiencies. Numerous attempts to shift the spectral response of TiO2 into the visible, or to develop alternative oxides affording water cleavage by visible light, have so far failed.

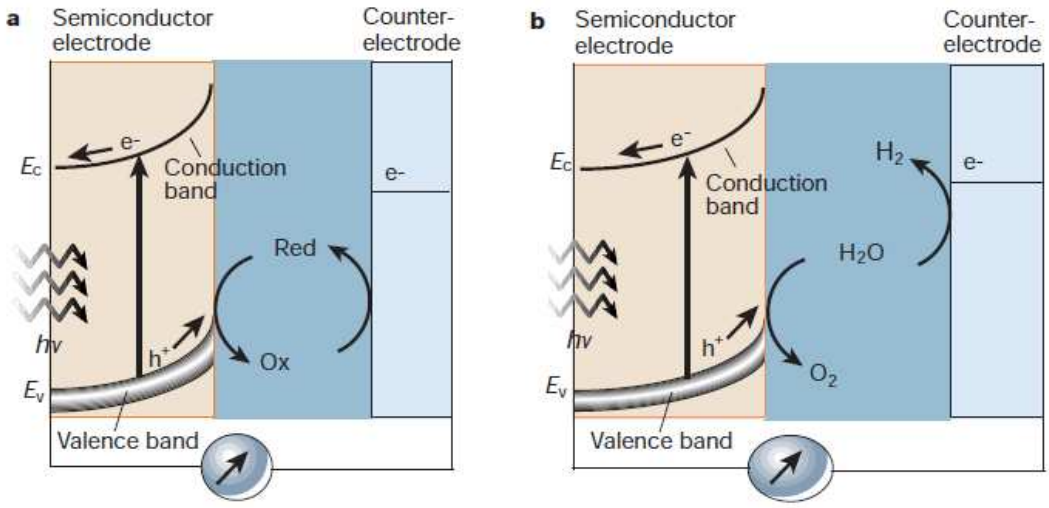

Figure 4. Principle of operation of photoelectrochemical cells based on n-type semiconductors. a, Regenerative-type cell producing electric current from sunlight; b, a cell that generates a chemical fuel, hydrogen, through the photo-cleavage of water [13].

In view of these prolonged efforts, disillusionment has grown about the prospects of photoelectrochemical cells being able to give rise to competitive photovoltaic devices, as those semiconductors with band gaps narrow enough for efficient absorption of visible light are unstable against photocorrosion. The width of the band gap is a measure of the chemical bond strength. Semiconductors stable under illumination, typically oxides of metals such as

titanium or niobium, therefore have a wide band gap, an absorption edge towards the ultraviolet and consequently an insensitivity to the visible spectrum. The resolution of this dilemma came in the separation of the optical absorption and charge-generating functions, using an electron transfer sensitizer absorbing in the visible to inject charge carriers across the semiconductor–electrolyte junction into a substrate with a wide band gap, and therefore stable. Figure 5 shows the operational principle of such a device.

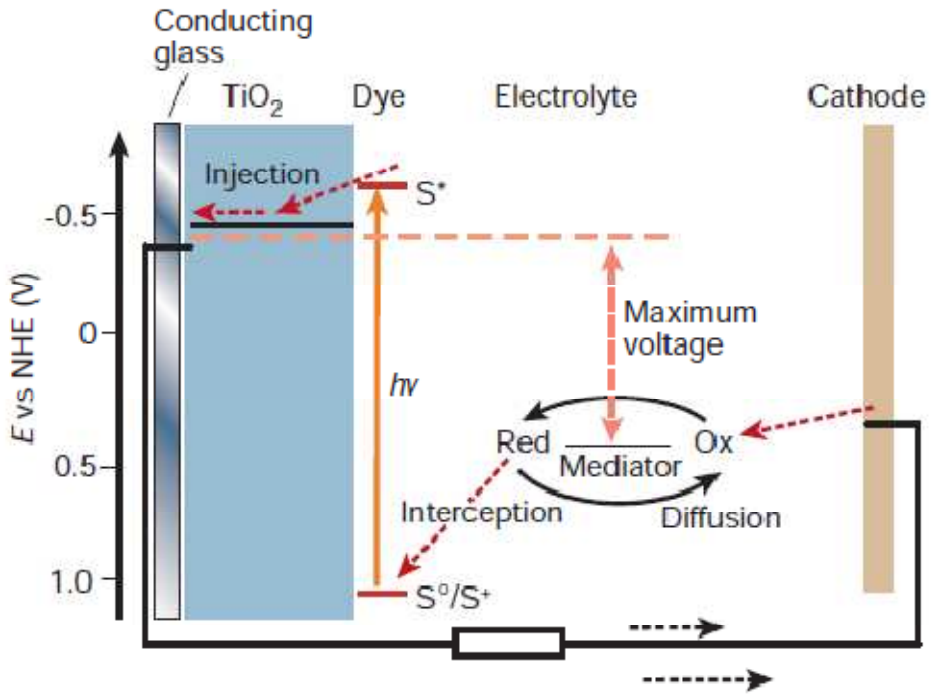

Figure 5. Schematic of operation of the dye-sensitized electrochemical photovoltaic cell.

The need for dye-sensitized solar cells to absorb far more of the incident light was the driving force for the development of mesoscopic semiconductor materials — minutely structured materials with an enormous internal surface area — which have attracted great attention during recent years. Mesoporous oxide films are made up of arrays of tiny crystals measuring a few nanometres across. Oxides such as TiO2, ZnO, SnO2 and Nb2O5, or chalcogenides such as CdSe, are the preferred compounds. These are interconnected to allow electronic conduction to take place. Between the particles are mesoscopic pores filled with a semiconducting or a conducting medium, such as a *p*-type semiconductor, a polymer, a hole transmitter or an electrolyte. The net result is a junction of extremely large contact area between two interpenetrating, individually continuous networks. Particularly intriguing

is the ease with which charge carriers percolate across the mesoscopic particle network, making the huge internal surface area electronically addressable. Charge transport in such mesoporous systems is under intense investigation today and is best described by a random walk model [13].

However, recent advances suggest that the most promising nanoarchitecture for solar energy conversion appears to be an array of highly orderer vertically aligned titania nanotubes grown by anodic oxidation of titanium, offering electron transport properties superior to randomly oriented titania nanoparticles.

1.4.1 Dye-Sensitized Solar cells with TiO2 Nanoube Arrays as a Base Material.

As explained above, a dye-sensitized solar cell (DSSC) is a relatively low cost photovoltaic device using a photosensitized anode and hole transporting electrolyte, where charge separation occurs at the dye layer between the semiconductor and electrolyte. DSSC efficiencies have reached over 11% using nanocrystalline TiO2 films. In this part is presented the progress with respect to the use of anodically grown and crystallized TiO2 nanotube arrays as the base electron transporting material for DSSC use, offering large surface areas with vectorial charge transport along the length of the nanotubes.

To overcome the charge transport limitation of isotropic bulk heterojunction solar cells, it has been proposed that the ideal heterojunction geometry of an inorganic-organic device should consist of a vertical array of highly crystallized nanostructures, such as nanotubes or nanorods, encased in a polymer film with size and spacing of the nanostructures controlled to be on the order of the exciton diffusion length. Such geometry provides, respectively, direct and spatially separated charge transport channels for electron and holes. In response, many efforts have been devoted to create films with ordered one-dimensional architectures, such as TiO2 nanopores and nanotubes.

The working electrodes in typical DSSCs consist of a 10 mm thick film comprised of a three-dimensional network of interconnected nanocrystalline semiconductor nanoparticles, typically 15 to 20 nm in diameter. The large surface area associated with such films enables efficient light harvesting that in turn maximizes the amount of photogenerated charge. However the structural disorder at the contact between two crystalline nanoparticles leads to enhanced scattering of free electrons, thus, reducing electron mobility. From the light

intensity dependence of the electron diffusion coefficient in randomly packed TiO2 nanoparticle films, it has been inferred that transport is limited by the residence time of electrons in traps and the morphology associated with both the particle network and the interparticle contact area.

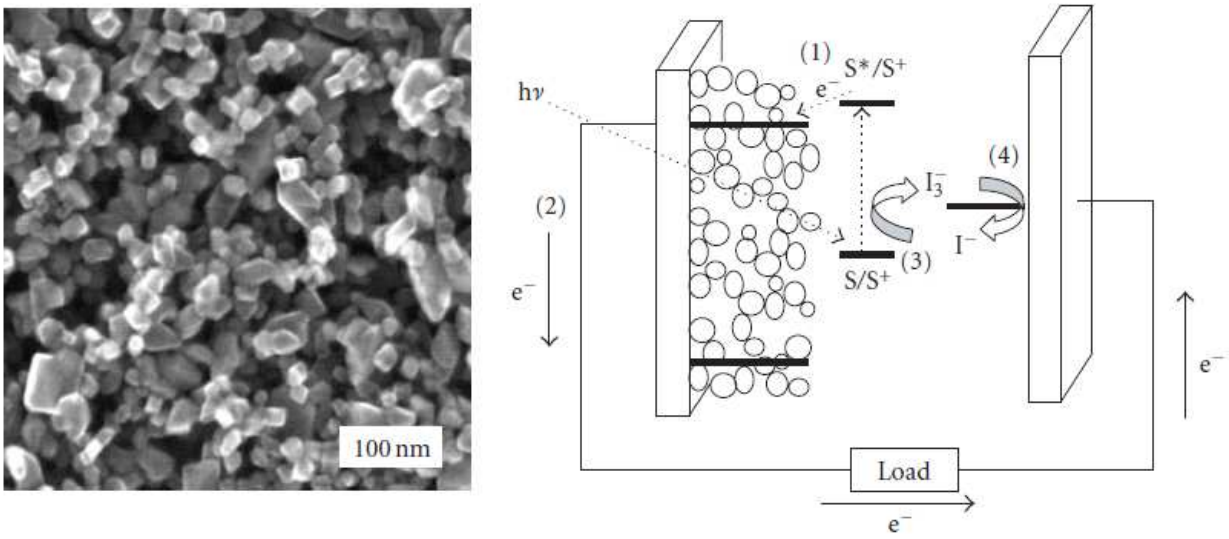

Figure 6. SEM micrograph of a nanocrystalline TiO2 film and schematic structure of a DSSC [6].

Electron transport is a limiting factor in the performance of these nanoporous nanocrystalline electrodes, hindering the progress in achieving higher efficiencies. The slow percolation of electrons through a random polycrystalline network and the poor absorption of low energy photons by available dyes are two of the major factors limiting the further improvement in the photoconversion efficiencies achievable using nanocrystalline dye-sensitized solar cells . A desirable film morphology would have the mesoporous channels aligned parallel to each other, vertically oriented with respect to the TCO glass current collector. The arrangement of the highly ordered TiO2 nanotube arrays perpendicular to the surface permits directed charge transfer along the length of the nanotubes from the solution to the conductive substrate, thereby reducing the losses incurred by charge-hopping across the nanoparticle grain boundaries. Easier access to the surface, as well as better control of the interface makes this morphology desirable for DSSCs. The enhancement in charge transport allows for improved light harvesting as thicker films can be used to increase the optical density, thus, improving the absorption of low energy photons in the red and

infrared regions without losing the additionally harvested charge carriers to recombination. On the other hand, TiO2 nanotube arrays can be self-organized on Ti foil as well as on conducting FTO glass [5].

1.4.2 Operating principles.

The operating principle of a DSSC based in titania nanotubes is shown schematically in figure 7, the surface of which is sensitized of, typically, a ruthenium complex dye, for example, N719, N3 or Black dye, anchored to the TiO2 surface by a carboxylated bipyridyl ligand. The visible light absorption of these types of complexes is based on a metal-to-ligand charge transfer. The carboxylate groups are directly coordinated to the surface titanium ions producing intimate electronic contact between the sensitizer and the semiconductor. Photo-excited dye molecules inject electrons into the TiO2 conduction band, and redox species such as the iodide/triiodide couple in the electrolyte reduce the oxidized dye molecules back to their original state. Dye regeneration by the iodide happens through the thiocyanate group and, thereby, intercepts the recapture of the conduction band electron by the oxidized dye. In turn, the iodide is regenerated by the reduction of triiodide at the counterelectrode, with the circuit completed via electron migration through the external load. The value of the redox potential is the formal potential in the solution, whereas the value of the oxidation potential of the dye is the standard potential. The absorption threshold for Ru dye adsorbed on TiO2 is about 750 nm, corresponding to a potential of 1.7 V, which added to the dye oxidation potential gives a reduction potential of −0.85 V vs. SCE. The voltage generated under illumination corresponds to the difference between the Fermi level of the electron in the solid and the redox potential of the electrolyte. About 0.4 V is lost in the reduction of the photoexcited dye by iodide, but so far

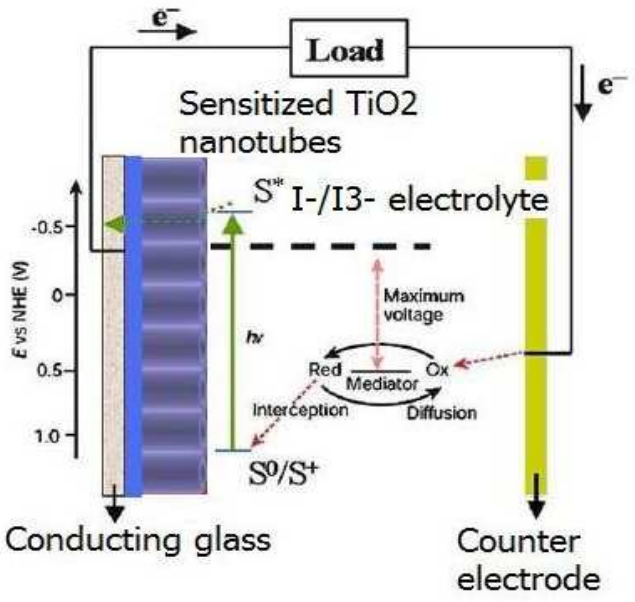

Figure 7. Operation principles.

no other candidates have been as efficient as the I-/I_3- couple when it comes to the kinetics of dye interception and electron uptake at the counter electrode[5].

1.4.3 Kinetics of the process.

Fortunately, for the transition metal complexes, the ratio of injection over recapture rate is greater than 10^3. The carbxylate groups interact directly with the surface Ti(IV) ions resulting in good electronic coupling of the wave function of the carboxylated bipyridyl ligand with the 3d orbital manifold of the conduction band of the TiO2. As a result, electron injection from the excited sensitizer into the semiconductor is an extremely rapid process occurring on a femtosecond scale. By contrast, electron back-reactions with the oxidized ruthenium complex involves a d orbital localized on the ruthenium metal whose electronic overlap with the TiO2 conduction band is small. The spatial contraction of the wave function upon oxidation of the Ru(II) to the Ru(III) state further reduces this electronic coupling causing relatively slow backward electron transfer which, typically, is on the order of microseconds. The oxidized dye is restored by electron donation from the organic solvent-based electrolyte containing iodide/tri-iodide redox couple. The rate constant is about 10^7 per second. As a consequence, the presence of a local electrostatic field is not required to achieve good efficiencies for the process[5].

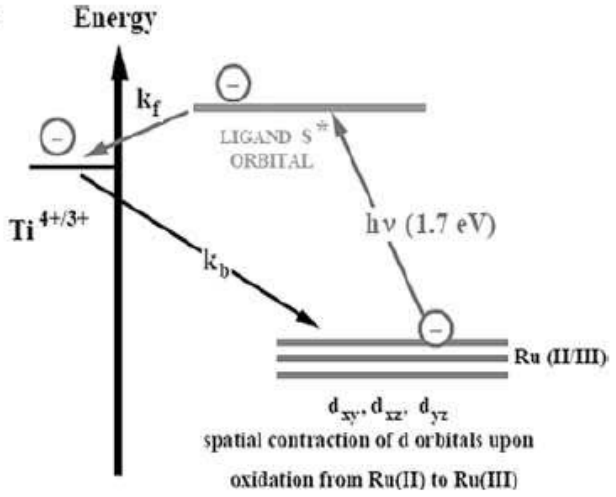

Figure 8. Molecular orbital diagram for ruthenium complexes anchored to the TiO2 surface by acarboxylated bipyridyl ligand

2. Materials and methods.

2.1 DSSC in detail.

Main components of Dye-sensitized solar cell with titania nanotubes as metal base can be distinguished as follows:

- Conductive glass.
- Dye-sensitized titania nanotubes.
- Electrolyte.
- Counter electrode.

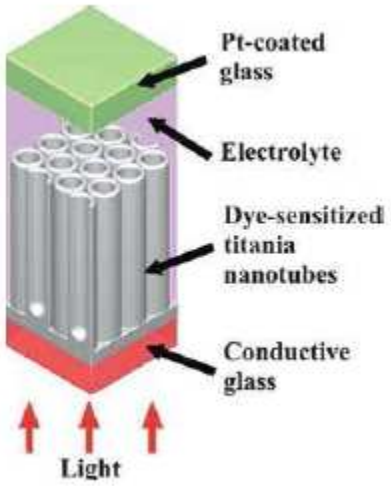

Figure 9. Ilustrative drawing of the TiO2 DSSC

2.1.1 Conductive glass.

The glass must meet two fundamental properties for the proper functioning of the cell; electrical conductivity and transparency in the visible spectrum. The most used is the ITO glass with a transparent glass with a thin layer of indium oxide" In_2O_3" placed upon one side doped with "Sn". It guarantees a transmittance about 80% and a low electrical resistivity. Concretely, there are also other interesting technology about conductive glass such as fluorine doped tin oxide (FTO) and zircon doped tin oxide[7].

2.1.1.1 Conductive glass production.

During the experimental part we have been working with FTO and ITO glass which is prepared depositing a mix of 80% In_2O_3 and SnO_2 99.99% pure on a layer of sodic-lime glass, washed with detergent solution and then with acetone using ultrasound.

The deposition process is carried out by evaporation of pellets sintered in the mix vacuum chamber ($5*10^{-5}$) subjected to a voltage of 6 kV and driving a current of 10-15 mA. This produces thickness deposited approximately 13-15 nm per minute. Then, substrate is sintered and grabbed on the glass thanks to a heat treatment at 350 ° C for 30 minutes.

2.1.1.2 Optimization of electrical conductivity.

The first major purpose of the ITO glass is conducting electricity, however the chemical composition of the mix used must be in relative percentage of 80% 20% In2O3 and SnO2 to achieve the optimal conditions as shown figure 10.

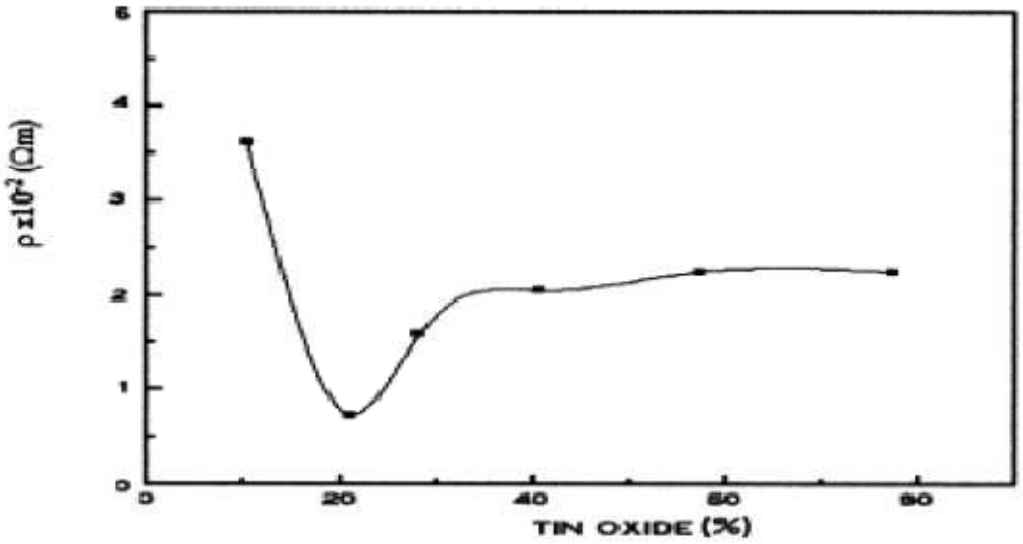

Figure 10. Resistivity in function of tin oxide percent.

Other important phenomenon in relation with the conductivity is the diffusion effect of the oxides in the glass. It has been tested that the resistivity of ITO, when is exposed at 200ºC, results lower than $7.6*10^{-3}$ Ωm that is the experimentally achieved for the composition described. On the another hand, is important to note that glass subjected to heat treatment for long periods or high temperatures loses the electrical conducting behavior as shown in figure 11.

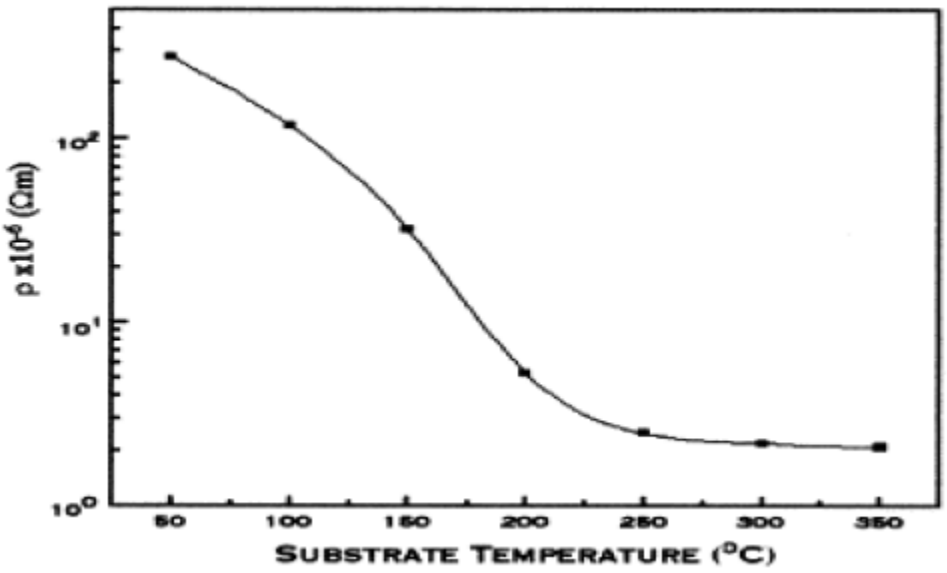

Figure 11. Resistivity increasing.

2.1.1.3 Transmittance optimization.

By the other side of the glass is necessary to guarantee the transparency because the radiant power must reach sensitized nanotubes. However, 20 % of tin oxide in ITO glass is not enough to ensure a perfect transparency, which is in function of the temperature as we can see in figure 12.

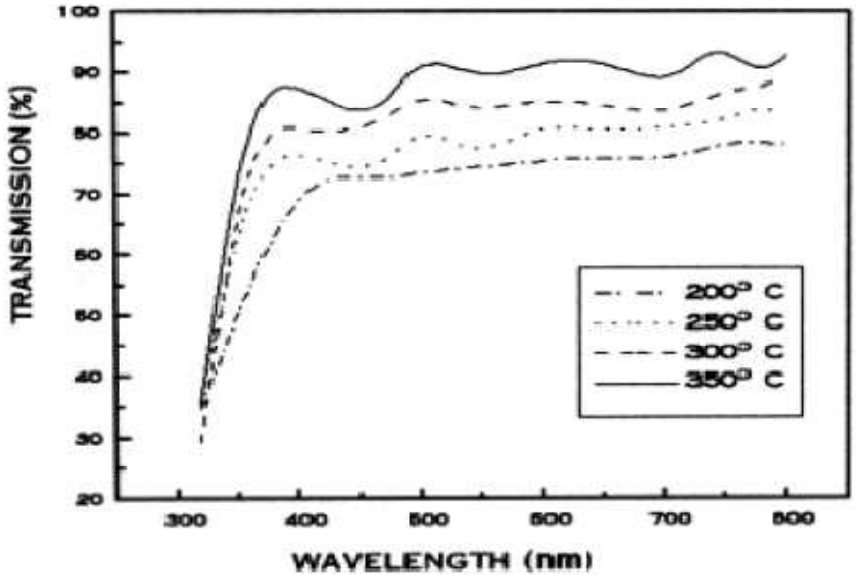

Figure 12. Transmission depending on wavelength.

It is already proved that is impossible to obtain a substrate with low resistance and high transmitivity. Therefore, is important to assume a compromise between them, taking care about the optimization of the cell we are building.

2.1.2 Titania nanotubes for Dye-sensitized solar cells.

DSSC fabricated using titania nanotube arrays grown on titanium foil, have charge-collectionand light harvesting efficiencies 25 and 20% higher, respectively, than corresponding nanoparticle-based DSSC. The higher light harvesting efficiency has been attributed to the enhanced light-scattering properties of the titania nanotubes. Recent works have estimated the electron diffusion length in tiania nanotubes on titanium foil by considering the electron diffusion coefficient and lifetime as a function of electron quasi Fermi level and obtained a value of 100μm, which is a three times better than that in nanoparticle flim-based DSSC. Thus, titania nanotube-based DSSC can afford much higher thicknesses, thereby enable harvesting of low-energy photons using either a single dye, or different dyes covering different regions of the nanotube length. Transparent titania nanotube films offer a tremendous opportunity to make use of the near-infrared region of the solar spectrum, thereby increasing the overall efficiency of the DSSCs [9].

Micrometre-length titania nanotubes are commonly grown on opaque titanium foils or sheets, but these are not suitable for achieving high-efficiency DSSC because light must past through the counter-electrode and light absorbing electrolyte, resulting in a loss of ~25% of the incident solar energy. A hybrid technology that involves fixing titania nanotube membranes on glass coated with fluorine-doped tin oxide using a layer of titanium alkoxide solution or titania nanoparticle paste has been used in an effort to take advantage of the front ilumination geometry. A problem inherent to this technique is macro/micro-crack formation in the nanotube films, resulting in some cases in the destruction of the nanotubes, when the volatiles scapes during heat treatment.

Efforts to fabricate transparent nanotube arrays for DSSC applications have been limited to short nanotube arrays using titanium thin films deposited at high temperatures (400ºC). Although transparent nanotube arrays of extended length (comparable to or greater than the nanoparticle film thicknesses used in high-efficiency DSSC) have been highly sought after,

the ability to fabricate such films has remained, until now, an unsolved technological challenge.

There have been three major challenges in the fabrication of transparent nanotube array films of extended length possessing the high optical transparency and superior electrical properties needed for efficient DSC.

1) Formation of uniform, nonporous titanium films tens of micrometers thick on FTO glass with sufficient adhesion to the FTO layer to withstand the stresses associated with the anodization process and the different thermal and surface treatments inherents to DSSC fabrication.

2) Anodization of these thick titanium films until uniform optical transparency is achieved. During normal anodization conditions the region of the titanium film at the solution-air interface is anodized faster than the rest of the film, exposing the FTO layer to the electrolyte and thereby short-circuting the anodization and leaving the rest of the film opaque.

3) Fabrication of titania nanotubes of great length using fluorine-containing non-aqueous organic anodization electrolytes needs to be achieved without debris of clumping of the nanotubes. It has been demonstrated that such 'crumpled' nanotube arrays films have longer transport time constants and hence are less appropriate for DSSC applications. Moreover, the surface debris on the nanotubes associated with the low titania dissolution rate, significantly reduces the transmittance, resulting in inferior solar cells characteristics.

Building in detail of titania nanotubes will be properly discussed in Chapter 3.

2.1.3 Dye loading.

Three dyes can be considered as the backbone of currently applied sensitizers in DSC. All of these dyes are ruthenium based metal-organic complexes with the general formula $RuL_xL'_ySCN_z$, where L and L' are polypyridyl ligands; they are readily available commercially and show excellent efficiency levels up to 11%. The molecular structures of these dyes are shown in Figure 13. Because of the complex chemical nomenclature, they are most often referred to with trivial names as indicated below (N-3 and N-749, which are commonly also called red and black dyes and Z-907). There is a widely used variant of the

N-3 dye, which differs from it only in the degree of protonation (trivial name: N-719). The black dye shows the broadest absorption range up to 900 nm[6].

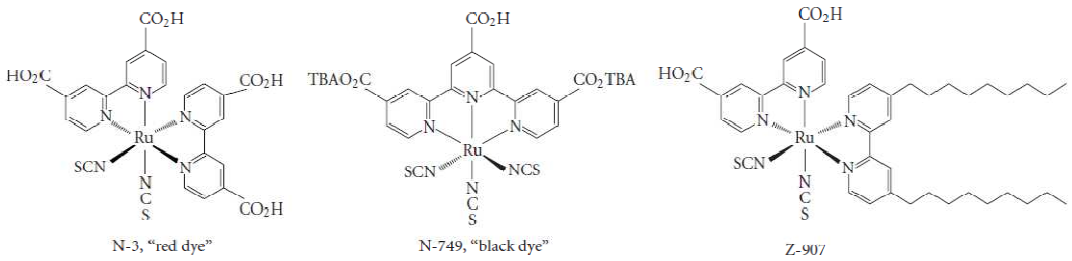

Figure 13. The three most frequently applied ruthenium polypyridyl complexes.

The primary goal of ruthenium based dyes on sensitizers is further progress in efficiency. Issues with respect to robustness, sustainability, and cost are also of relevance, though. For improvements in current output, an extension of the absorption range of DSSCs towards longer wavelengths from currently 800–900nm to 900–1000nm is required. Moreover, dyes with enhanced molar absorption coefficients are attractive for efficient light harvesting with thinner TiO2 layers. This can lead to an efficiency boost of DSSC concepts, which depends so far on such thin layers (particularly solid state- but also ionic liquid-based systems) and generally to improved V_{OC} independent of the type of system. With regard to sustainability and cost, organic dyes may be advantageous.

An impressive number of new sensitizers are being developed in recent years. Many of the new dyes are derivatives of the N-3 molecule with various chemical modifications on one of its two bipyridyl moieties while leaving the rest of the molecule unchanged. This work has lead to sensitizers with improved molar absorption coefficients, referred to in the literature as the "K-series", as well as to the discovery that hydrophobic side chains (like in Z-907) can be beneficial for long-term stability. This latter effect is assigned to the inhibition of H2O adsorption to the TiO2 surface. Dyes in which the carboxylic acid functions are replaced by phosphonic acid functions may also be advantageous for long-term stability because of the stronger adsorption of these groups to the TiO2 surface.

On the other hand, efforts to further extend the spectral absorption range of the sensitizer beyond that of the "black dye," published for the first time in 1997, have not been successful yet, which is why record efficiencies have remained unaffected by this research thus far. The coadsorption of several dyes in "dye cocktails," following this same goal, has

shown to be conceptually applicable, but it needs further elaboration. The development of tandem concepts is another promising route. A significantly enhanced absorption range and improved efficiency (15%) could be achieved by the combination of a DSSC top cell with a CIGS bottom cell —approaches based on DSSCs exclusively are under development.

Next to the systematic development of improved ruthenium complexes, there is also a significant number of publications on purely organic dyes with increasingly good photovoltaic performance. This trend is driven among others by the argument of potentially lower cost. The best results thus far have been obtained with the indoline dye D-149. Such dyes may become a viable alternative to ruthenium complexes in case further favorable characteristics, also on long-term stability, can be achieved.

Rather, a sideline of current research but with potential significance for new markets (decorative applications) is the development of sensitizers with different colors, such as green Zn phthalocyanine complexes.

Another innovative research line is the replacement of molecular sensitizers by semiconductor quantum dots, for example, PbS. This approach, which is still in its infancy, may profit from the very high absorption cross-sections of quantum dots as well as from the recently discovered phenomenon of impact ionization (creation of multiple excitons by excitation with a single photon when the photon energy is three times higher than the bandgap). To date, reaching competitive levels of overall conversion efficiency by sensitization with quantum dots has remained a major challenge though. A notable exception is a related approach based on a nanocomposite structure consisting only of TiO2 and CuInS2. Here, the CuInS2 assumes the functions of sensitizer and hole conducting medium at the same time, and an overall efficiency of up to 5% has been published for this all solid-state approach.

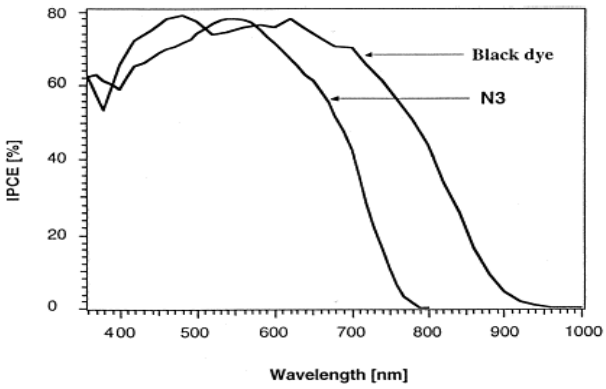

Figure 14. The incident photon to current conversion for Black dye and N3.

Ruthenium bipyridyl dye, N719, which absorbs light in the wavelength range up to ~750nm is used in the project for sensitizing the nanotubes. The amount of dye adsorbed on the nanotube surface depends upon its surface area and density of the dye-binding states. The difference in behavior is believed to be primarily due to the type of surface states present in nanotubes fabricated in different electrolytes.

Is important to note that, the potential future increases in DSSC efficiency relies largely on the invention of new dyes that absorb both high-and low-energy solar spectrum photons, and on the development of highly ordered material architectures offering longer electron diffusion lengths and shorter electron transport time constants than those in conventional randomly oriented nanoparticles films.[9]

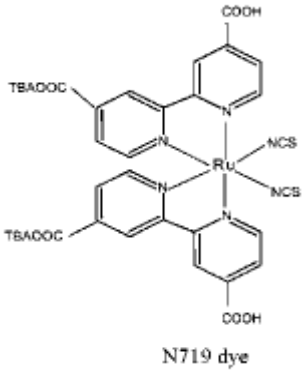

Figure 15. N719 dye.

2.1.4 Electrolyte.

Between the TiO2 electrode and the counter electrode is the electrolyte. The electrolyte consists of the redox couple I-/I_3- in charge of make possible the durable photogeneration of the electron-holes created in the dye. This particular solution is an oxide-reducing agent that has easy-donating electron properties when is reduced and vice versa, when is being oxidized, yields electron, reducing itself.

The record conversion efficiencies up to 11% are typically achieved with liquid electrolytes based on acetonitrile—a low-viscosity volatile solvent—and by using comparatively low iodine concentration. These high efficiency electrolytes are not at the same time optimized for achieving the best long-term stability characteristics, for which other electrolyte formulations with less volatile solvents or ionic liquids as well as higher iodine concentrations are more appropriate. These latter electrolytes are often referred to as robust electrolytes in the literature and their application leads to a lower-efficiency output in the range of 7–9%. Next to the redox-active species and solvents, the electrolytes contain typically some additives. The function of these additives is in most cases to reduce the dark current by coordination to the TiO2 surface, thus improving the V_{OC} of the solar cells.

The predominant technological drivers for the current work on electrolytes are aspects related to robustness, environmental sustainability, and processability for module concepts. As an example of processability, the replacement of the corrosive iodine-based electrolyte could facilitate module production on larger areas by avoiding the necessity to apply protective coatings to metallic current collector grids. Concerning system robustness and sustainability, the replacement of volatile solvents is expected to be beneficial. Full solid-state versions in which the electrolyte is completely replaced by a solid material will have clear advantages for interconnection schemes on the level of module fabrication.

Furthermore, the goal to further improve the efficiency is also an important motivation for the work on electrolytes, for instance, by the search for new additives for the suppression of interfacial recombination. This could lead to gains in V_{OC}.

One current research direction is the development of noncorrosive electrolytes. The most promising results so far have been obtained with the Co(II)/Co(III) redox couple with external quantum efficiency values up to 80% and overall efficiencies up to 4% at full sun illumination and 8% at 1/10 sun illumination. The amount of research going on in this direction is surprisingly limited considering the obvious benefits which could be achieved. This may in part be explained by the impeccable functioning of the I-/I_3- couple, in which a negatively charged ion carries the positive electrical charge. The resulting electrostatic repulsion between the electron in the TiO2 and the hole on the I_3-ionmay be advantageous for the slow interfacial recombination kinetics (in the millisecond time domain). A further probable factor in the context of these favorably slow kinetics is the involvement of two electrons in the recombination reaction (I_3-+ 2e− 2e-TiO2 →3 I^-).

Several research groups currently investigate the use of ionic liquids instead of organic solvents in liquid electrolytes. Ionic liquids are a new class of materials with a number of attractive properties for application in DSSCs, such as high stability, negligible vapor pressure, nonflammability, as well as excellent environmental compatibility. On the other hand, overall power conversion efficiencies obtained with ionic liquids are so far considerably lower than those obtained with organic solvent electrolytes, typically in the range of 4–7.5% (on device areas < 1 cm2). This is due to diffusion limited current output in these systems caused by their more viscous nature. Viscosity values are higher by a factor of 10– 100 than in acetonitrile-based electrolytes. If these limitations can be overcome, ionic liquids may well turn out to be an attractive alternative to the liquid

electrolytes based on volatile solvents. The most frequently studied class of ionic liquid materials is 1-methyl-3alkylimidazolium iodide.

An alternative approach for the replacement of volatile electrolytes is the addition of gelators to solvent-based electrolytes, leading to the formation of quasisolid gel electrolytes. A considerable number of articles have appeared on this topic in recent years. Systems with efficiencies in the range of 4–6% have been published, with some including promising stability data. A more "radical" and fundamentally different approach is the replacement of the electrolyte by a solid-state mediator. Practical preparation issues are substantially more challenging than for all liquid-based approaches though. It is not evident to fill all the nm-sized pores of the TiO2 films with another solid and to achieve a similarly quantitative and intimate interfacial contact with the dye molecules as can be achieved with a liquid. This is one of the reasons why rather thin TiO2 layers of only 2–3 μm are typically employed in solid-state devices leading to limitations in light absorption. Next to this, the interfacial charge recombination dynamics—for electrons in the TiO2 with holes in the mediator—are reported to be faster by a factor of about 10 compared with liquid electrolytes. Special attention to interface engineering is thus required, a topic which has only been addressed in a preliminary fashion so far. Considering these two major challenges, pore filling and recombination kinetics, the results obtained in various groups with efficiencies up to >4% are promising. The best material so far investigated is the amorphous organic hole conductor spiro-OMeTAD followed by crystalline Cu(I) compounds, CuSCN and CuI. The amorphous state seems clearly to be more appropriate for the pore-filling requirements, which is also consistent with the observation of improved device performance by the addition of a crystal inhibitor in systems based on crystalline CuI as mediator. In terms of pore-filling, the development of more sophisticated deposition techniques is desirable; the methods applied so far, spin-coating and "solution-casting," are not suited well enough. Self-assembly concepts—similar to the one successfully applied ever since for the monolayer formation of the dye molecules on the TiO2 surface—could prove to be helpful in this context[6].

2.1.5 Counter electrode.

The function of the counter electrode is the reduction of triiode to iodide. Nevertheless, the reduction reaction of I_3^- ion kinetically needs long time and thermodynamically requires a discrete energy of activation.

Therefore, the counter electrode must have some main competencies such as good electrical conductivity in mode to facilitate electron transport in the contact with ITO glass. Is also important, a high contact surface to arrive as many possible reduction sites for fast restoration of ion I^- (this does not involve improved kinetic reductive but an increase in the number of sites reactions) and must catalyze the reduction reaction in order to keep the equilibrium in the electrolyte in fast times (this results in an improvement of kinetic and thermodynamic reduction times). Moreover, the counter electrode, is intimately linked to the redox reaction and is responsible of the cell voltage behavior when load circuit changes.

In practice, the counter electrode is mainly composed of graphite powder, carbon black and titanium; all in form of nanoscale grains. Graphite has the important task of ensuring good conductive layer as well as to have low resistivity. Titanium is used as a combination of the first two species and carbon black serves as a catalyst for the oxidation reaction. As regards the composition, is sometimes added platinum, excellent catalyst but very expensive, to help in his task to the carbon black [8].

2.1.6 Titania nanotubes.

One-dimensional (1-D) nanowire and nanotube systems with high surface- to-volume ratios have been found to possess significant, useful, and unique properties. The synthesis of highly ordered 1-D materials using localized chemical dissolution with controlled, field-assisted oxidation and dissolution reactions is particularly noteworthy for it permits achievement of a precisely ordered, nanoscale self-assembly. Comparative studies show that ordered arrays of TiO2 outperform colloidal TiO2 for photocatalytic applications, sensing, photoelectrolysis , polymer-based bulk heterojunction photovoltaics, dye-senstized solar cells, biofluids filtration, drug delivery and other biomedical application. Initial investigations indicate that they also may be useful for energy storage devices such as Li-ion batteries and supercapacitors.

TiO2 nanotubes and arrays thereof have been produced by a number of methods. These include: using a template of nanoporous alumina, sol-gel transcription processes using organo-gelator templates, seeded growth mechanisms, and hydrothermal techniques. None of these methods, however, offer superior control over the nanotube dimensions than does the anodization of titanium in a fluoride-based electrolyte.

In 1999, Zwilling and co-workers achieved self-organized porous TiO2 by anodizing a Ti-based alloy in an acidic, fluoride-based electrolyte. In 2001, Gong and co-workers fabricated self-organized, highly uniform TiO2 nanotube arrays by anodizing Ti in an aqueous dilute HF electrolyte. Maximum nanotube lengths in this first synthesis generation were approximately 500 nm. In subsequent work, the second-generation, the nanotube array length was increased to approximately 7mm by proper control of the anodization electrolyte pH thereby reducing the chemical dissolution of TiO2 during anodization; the pH should be high but remain acidic. In later work, the third-generation, TiO2 nanotubearrays with lengths of up to approximately 1000mm were achieved using a non-aqueous, polar organic electrolyte such as formamide, dimethylsulfoxide, ethylene glycol or diethylene glycol. Fourth synthesis generation is suggested as non-fluoride-based anodization chemistries [5].

2.2 The electrochemical anodization process.

Anodization is an electrolytic process that creates a protective or decorative oxide film over a metallic surface. Anodization typically increases both the thickness and density of the oxide layer that forms on any metal surface exposed to the earth's atmosphere. To accomplish it, the conducting piece undergoing anodization is connected to the positive terminal of a dc power supply and placed in an electrolytic bath where it serves as the anode. The cathode is commonly a plate or rod of platinum, although materials such as carbon are sometimes used. When power is applied electrons are forced from the electrolyte to the positive anode. The process leaves surface metal atoms exposed to oxygen ions within the electrolyte. The atoms react and become an in situ integral part of the oxide layer. The electrons travel through the power source and return to the cathode where, if an appropriate electrolyte pH is present, they react with hydrogen ions and the combination bubbles off as hydrogen gas.

Since the metal oxide partially dissolves in any electrolyte, it is necessary to use only those electrolytes for which the oxide forms more rapidly than it dissolves. The electrolyte composition is also the primary determinant of whether the oxide film is porous or if it forms a barrier layer. Oxide barrier layers grow in those neutral or slightly alkaline solutions in which titanium dioxide is largely insoluble. Porous oxide layers grow in acidic

electrolytes with fluoride or chloride ions in which oxide forms and then rapidly dissolves. The acid cations also affect the resulting nanotube array structures. A depiction of an electrochemical anodization cell is shown in figure 10.

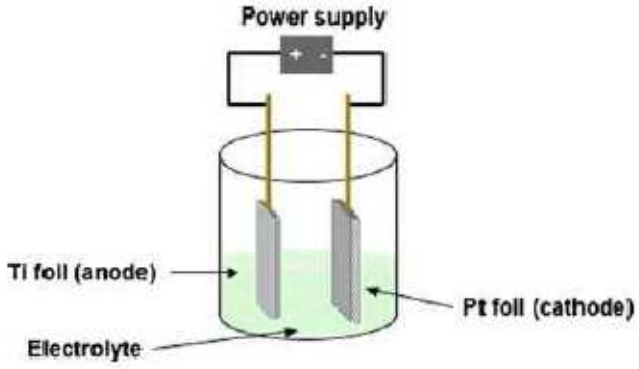

Figure 16. Depiction of aelectrochemical cell in which the Ti samples are anodized.

With a titanium anode and a platinum cathode immersed in an aqueous electrolyte of dilute acid to which a small dc voltage is applied the surface layer is sufficiently resistive to prevent current flow. Increasing the applied voltage produces no additional current flow until a threshold level is reached where the electric field intensity within the barrier is sufficient to force oxygen ions to diffuse across it, producing anionic current. These oxygen ions react with the metal and increase the thickness and/or density of the oxide barrier. This process of high-field ionic conduction is central to anodization. Of course, the same process liberates hydrogen gas from the cathode. Since the electric resistance of the layer increases in proportion to its thickness and since the rate of oxide growth is proportional to the current density, the thinner portions of the layer carry more current than the thicker ones. Hence, a thin section grows faster than a thick one, creating an even more uniform layer. As the layer thickens the applied voltage necessary to maintain a constant current increases. The process continues until, for each bath composition and temperature, a maximum applied voltage is reached above which other, non-desired reactions become manifest, for example: oxygen evolution, solute oxidation, or sparking due to electron avalanche through the oxide [5].

2.2.1 Nanotubes formation.

The key processes responsible for anodic formation of nanoporous alumina and TiO2 appear to be the same, and are fundamental to the formation of TiO2 nanotube arrays. The key processes are:

1. Oxide growth at the metal surface due to interaction of the metal with O^{2-}or OH^- ions. After the formation of an initial oxide layer, these anions migrate through the oxide layer reaching the metal/oxide interface where they react with the metal.

2. Metal ion (Ti^{4+}) migration from the metal at the metal/oxide interface; Ti^{4+} cations will be ejected from the metal/oxide interface under application of an electric field that move toward the oxide/electrolyte interface.

3. Field-assisted dissolution of the oxide at the oxide/electrolyte interface. Due to the applied electric field the Ti–O bond undergoes polarization and is weakened promoting dissolution of the metal cations. Ti^{4+} cations dissolve into the electrolyte, and the free O^{2-} anions migrate toward the metal/oxide interface, process 1, to interact with the metal.
4. Chemical dissolution of the metal, or oxide, by the acidic electrolyte. Chemical dissolution of TiO2 in the HF electrolyte plays a key role in the formation of nanotubes rather than simple nanoporous structures.

To help understand the process of nanotube formation, FESEM images of the surface of the samples anodized at 20 V for different durations were taken and analyzed. As the anodization started, the initial oxide layer, formed due to interaction of the surface Ti^{4+} ions with oxygen ions (O^{2-}) in the electrolyte, can be seen to uniformly spread across the surface. At the anode oxidation of the metal releases Ti^{4+} ions and electrons, shown as:

$$Ti + H_2O = TiO_2 + 2H^+ + 4e^-$$

At the cathode hydrogen evolution occurs:

$$8H^+ + 8e^- \rightarrow 4H_2$$

The overall process of oxide formation is given by:

$$Ti + \ 2H_2O \ \rightarrow TiO_2 + \ 2H_2$$

Fluorine ions can attack the oxide and hydrated layer; or, the ions being mobile in the anodic layer under the applied electric field, react with Ti^{4+} as described by:

$$TiO_2 + \ 6F^- + \ 4H^+ \ \rightarrow TiF_6^{2-} + \ 2H_2O$$

$$Ti(OH)_4 + \ 6F^- \ \rightarrow TiF_6^{2-} + \ 4OH^-$$

$$Ti^{4+} + \ 6F^- \ \rightarrow TiF_6^{2-}$$

In the initial stages of the anodization process field-assisted dissolution dominates chemical dissolution due to the relatively large electric field across the thin oxide layer. Small pits formed due to the localized dissolution of the oxide; act as pore forming centers, after which these pits convert into pores with increasing pore density, uniformly, over the surface. The pore growth occurs due to the inward movement of the oxide layer at the pore bottom (barrier layer). The Ti^{4+} ions migrating from the metal to the oxide/electrolyte interface dissolve in the HF electrolyte. The rate of oxide growth at the metal/oxide interface and the rate of oxide dissolution at the pore bottom/electrolyte interface ultimately become equal, thereafter the thickness of the barrier layer remains unchanged although it moves further into the metal increasing the pore depth. FESEM images show the formation of small pits in the inter-pore regions, which eventually lead to pore-separation and tube formation. The thickness of the tubular structure ceases to increase when the chemical dissolution rate of the oxide at the mouth of the tube (nanotube array surface) becomes equal to the rate of inward movement of the metal/oxide boundary at the base of the tube. Higher anodization voltages increase the oxidation and field-assisted dissolution and hence, a greater nanotube layer thickness can be achieved before equilibrating with chemical dissolution.

With anodization onset a thin layer of oxide forms on the titanium surface, figure. 17a. Small pits originate in this oxide layer due to the localized dissolution of the oxide figure 17b making the barrier layer at the bottom of the pits relatively thin which, in turn,

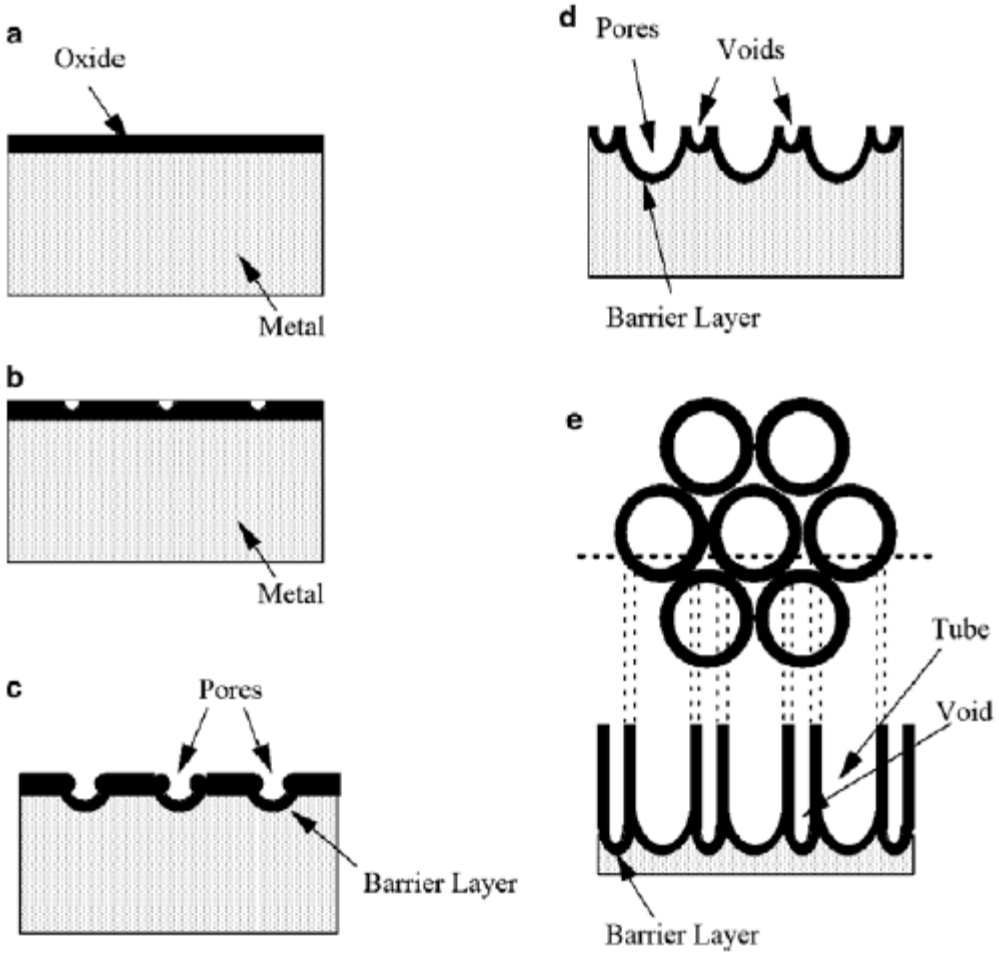

Figure 17. Schematic diagram of nanotube evolution at constant anodization voltage: (a) Oxide layer formation, (b) pit formation on the oxide layer, (c) growth of the pit into scallop shaped pores, (d) the metallic region between the pores undergoes oxidation and field assisted dissolution,(e) fully developed nanotubes with a corresponding top view

increases the electric field intensity across the remaining barrier layer resulting in further pore growth, figure 17c. The pore entrance is not affected by electric field assisted dissolution and hence remains relatively narrow, while the electric field distribution in the curved bottom surface of the pore causes pore widening, as well as deepening of the pore. The result is a pore with a scallop shape. As the Ti–O bond energy is high (323 kJ/mol), in the case of TiO2 it is reasonable to assume that only pores having thin walls can be formed due to the relatively low ion mobility and relatively high chemical solubility of the oxide in the electrolyte, hence un-anodized metallic portions can initially exist between the pores. As the pores grow deeper the electric field in these protruded metallic regions increases, enhancing field assisted oxide growth and oxide dissolution, hence simultaneously with the pores well-defined inter-pore voids start forming figure 17d. Thereafter, both voids and tubes grow in equilibrium. The nanotube length increases until the electrochemical etch rate equals the chemical dissolution rate of the nanotube top surface. After this point is reached

the nanotube length will be independent of the anodization duration, as determined for a given electrolyte concentration and anodization potential.

Chemical dissolution, the key for self-organized formation of the nanotube arrays, reduces the thickness of the oxide layer (barrier layer) keeping the electro- chemical etching (field assisted oxidation and dissolution) process active. No nanotubes can be formed if the chemical dissolution is too high or too low. The electrochemical etch rate depends upon anodization potential as well as electrolyte concentrations. If the electrochemical etch proceeds faster than chemical dissolution the thickness of the barrier layer increases, which in turn reduces the electro- chemical etching process to the rate determined by chemical dissolution. The chemical dissolution rate is determined by the F^- concentration and solution pH. With increasing F^- and H^+ concentrations chemical dissolution increases. Investigations have shown that for aqueous electrolytes only in a certain F^- concentration range can nanotube arrays be achieved. The anodic potential at which nanotubes are formed is related to the F^- concentration, with higher potentials requiring electrolytes of higher F^- concentration[5].

2.3 Sputter deposition.

Sputter deposition is the deposition of particles vaporized from a surface ("target"), by the physical sputtering process. Physical sputtering is a non-thermal vaporization process where surface atoms are physically ejected from a solid surface by momentum transfer from an atomic-sized energetic bombarding particle which is usually a gaseous ion accelerated from a plasma. Generally the source-to-substrate distance is short compared to vacuum deposition. Sputter deposition can be performed by energetic ion bombardment of a solid surface (sputtering target) in a vacuum using a ion gun or low pressure plasma (<5 mTorr) where the sputters particles suffer few or no gas phase collisions in the space between the target and the substrate. The sputtering source can be an element, alloy, mixture, or a compound and the material is vaporized with the bulk composition of the target. The sputtering target provides a long-lived vaporization source that can be mounted so as to vaporized in any direction. Compound materials such as titanium nitride (TiN) and zirconium nitride (ZrN) are commonly reactively sputter deposited by using a reactive gas in the plasma. The presence of the plasma "activates" the reactive gas ("plasma activation") making it more chemically reactive.

Sputter deposition is widely used to deposit thin film metallization on semiconductor material, coatings in architectural glass, reflective coatings on compact discs, magnetic films, dry lubricants and decorative coatings.

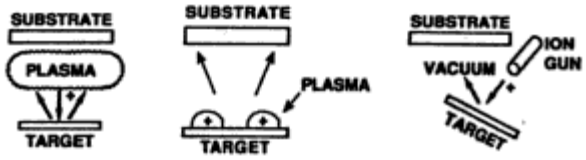

Figure 18. Sputter depositions

2.3.1 Radio frequency Sputtering.

At frequencies above 50 kHz, the ions do not have enough mobility to allow establishing a DC diode-like discharge and the applied potential is felt throughout the space between the electrodes. The electrons acquire sufficient energy to cause ionizing collisions in the space between the electrodes and thus the plasma generation takes place throughout the space between the electrodes. When an rf potential, with a large peak-to-peak voltage, is capacitively coupled to an electrode, an alternating positive/negative potential appears on the surface. During part of each half-cycle, the potential is such that ions are accelerated to the surface with enough energy to cause sputtering while on alternate half-cycles, electrons reach the surface to prevent any charge buildup. Rf frequencies used for sputter deposition are in the range of 0.5-30 MHz with a 13.56 MHz being a commercial frequency that is often used. Rf sputtering can be performed at low gas pressures (<1 mTorr).

Since the target is capacitively coupled to the plasma it makes no difference whether the target surface is electrically conductive or insulating although there will be some dielectric loss if the target is an insulator. If an insulating target material, blacked by a metal electrode is used, the insulator should cover the whole of the metal surface since exposed metal will tend to short-out the capacitance formed by the metal-insulator-sheath-plasma.

Rf sputtering can be used to sputter electrically insulating materials although the sputtering rate is low. A major disadvantage in rf sputtering of dielectric targets, is that most

electrically insulating materials have poor thermal conductivity, high coefficients of thermal expansion, and are usually brittle materials. Since most of the bombarding energy produces heat, this means that large thermal gradients can be generated that result in fracturing the target if high power levels are used. High rate rf sputtering is generally limited to the sputter deposition from targets of silicon diozide (SiO2) which has low coefficient of thermal expansion and thus is not very susceptible to thermal shock. In some cases, 48 hours is used to rf sputter-deposit a film of SiO2 several microns thick.

2.3.2 Magnetron sputtering.

In DC diode sputtering, the electrons that are injected from the cathode are accelerated away from the cathode and are not efficiently used for sustaining the discharge. By the suitable of a magnetic field, the electrons can be deflected to stay near the target surface and by an appropriate arrangement of the magnets, the electrons can be made to circulate on a closed path on the target surface. This high flux of electrons creates a high density plasma from which ions can be extracted to sputter the target material producing a magnetron sputtering configuration.

The most common magnetron source is the planar magnetron where the sputter-erosion path is a closed circle or elongated circle on a flat surface. A closed circulating path can easily be generated on any surface of revolution such as post or spool, inside of a hollow cylinder, a conical section, or a hemispherical section. In the case of the post-cathode and hollow-cylinder cathode a flange at the ends at a negative potential can be used to electrostatilly contain electrons that would be lost from the cathode. Figure 19 shows some magnetron configurations.

The planar magnetron configuration forms a vaporization source that consists of two parallel lines that can be of almost any length. The post cathode source allows deposition on the inside of a cylinder or cylindrical fixture. This arrangement was first used over 25 years ago for depositing films on the edges of razor blades that were stacked around the post cathode. Many razor blades are still coater the same way. The hollow cylindrical cathode is useful for coating three-dimensional parts since flux comes from all directions. A substrate, such as a fiber, can be passed up the axis of the cylinder and continuously coated. The hollow cylinder has the added advantage that the material that is not deposited on the part is

deposited on the target and re-sputtered, giving good target material utilization. The conical target produces a very dispersed flux and is useful for coating large areas. The S-gun configuration can prevent the "disappearing anode effect" problem by continuously

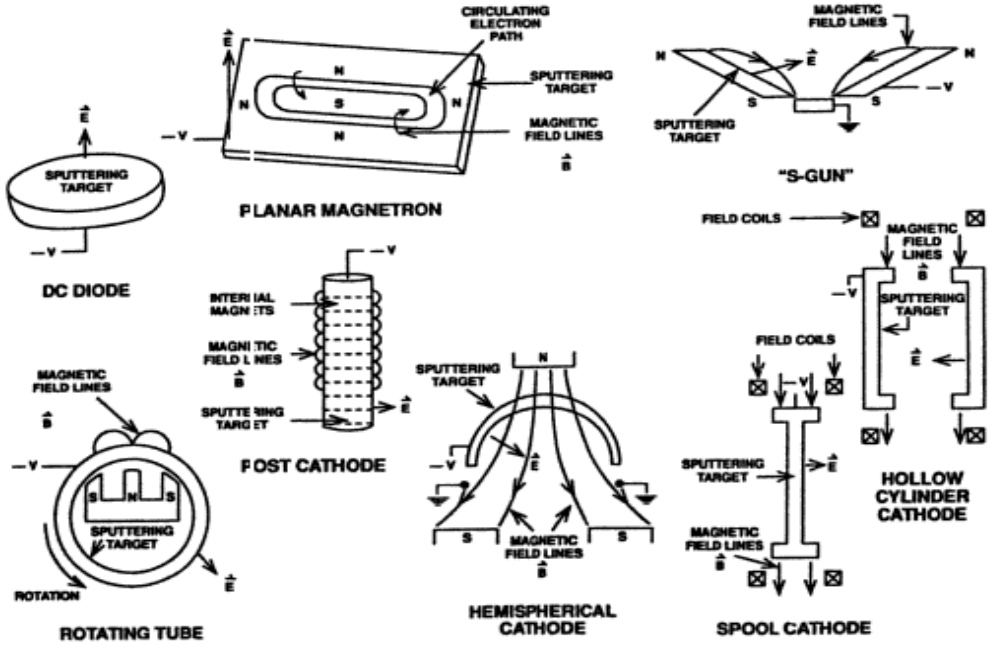

Figure 19. Some magnetron configurations

depositing pure metal on a shielded anode. The hemispherical target is an example of a conformal target is used in coating a hemispherical substrate.

The principal advantage to the magnetron sputtering configuration is that a dense plasma can be formed near the cathode at low pressures so that ions can be accelerated from the plasma to the cathode without loss of energy due to physical and charge-exchange collisions. This allows a high sputtering rate with a lower potential in the target than with the DC diode configuration. This configuration allows the sputtering at low pressures (<5 mTorr), where there is no thermalization of particles from the cathode, as well as at higher pressures (>5mTorr) where the thermalization occurs.

One disadvantage of the planar magnetron configuration is that the plasma is not uniform over the target surface. Therefore the deposition pattern is dependent on the position of the substrate with respect to the target. This means that various types of fixturing must be used to establish position equivalency for the substrate. The non-uniform plasma also means that target utilization is non-uniform, sometimes with only 10-30% of the target material being used before the target is scrapped. A great deal of effort has been put forth to improve utilization of the target material.

2.4 Experimental procedure.

Once fully explained the operational principles of the photovoltaic cell and its components, is the time to detail the steps which have allowed us to build a dye-sensitized solar cell with titania nanotubes.

Within the experimental procedure can be distinguished several key parts as:

1. Synthesis of titania nanotubes on titanium plates.

2. Sputtering titanium on FTO glass.

3. Anodization of sputtered titanium.

4. Preparation of DSSC device.

2.4.1 Synthesis of titania nanotubes on titanium foil.

Before starting the synthesis of titania nanotubes under controlled conditions, we were trying some samples that we had achieved with sputtering titanium, however, we saw that was really hard to control the reaction before it separates the titanium from ITO glass and we realized that we needed to control the context where nanotubes "emerged" during the anodization before trying sputtered films. Is also important to note that for us, due to problems related to availability of equipment, was quite difficult to get sputtering samples at the same time we needed it and therefore we took care with each one of the sputtering samples we had.

2.4.2 Samples of titanium foil.

During the experimental part, we were working with two types of titanium samples 99.99% pure. The first, was shaped as a cylindrical button with an 1 mm. thickness and 6 mm. diameter and was used until NNT18 test. Since that time, we had available titanium

square plates of 2.5 cm. side and 1 mm. thickness that were used in the rest of the experiments.

Figure 20. Buttton and square titanium plates.

2.4.3 Anode and cathode preparation.

Before anodizing was necessary to clean the samples. For this, we used a brush with diamond dust in order to remove traces of rust and to polish properly the metal surface. After this, samples were firstly washed with detergent and water, and then with ethylenglicol. Later, samples were submerged in an ultrasound bath for 10 minutes and finally were maintained in plasma for 15 seconds at 120 W. In this way, the surface of the samples was ready for anodization process.

2.4.4 Anodization.

The anodization process was explained above though were not always used the same geometric arrangements and materials for the experiments. This was due to the attempts made to achieve the optimum conditions for growth of nanotubes, specially to reduce the effects of electric field concentration and solve the leakage problems when titanium cylindrical samples were used.

In the same way, all experiments had not in common the container where cathode and anode were immersed, as well as the solution and the magnetic stirrer; the power supply providing the potential difference necessary for the reaction happens and voltmeter and ammeter with which we controlled the main parameters. Sometimes we also used a thermal

bath that kept the reaction container at a temperature ranging in order to vary the nanotube growth conditions.

It could be distinguished several parts to be carried out in the anodization as cleaning of samples, preparation of the solution, installation of the device where we were going to anodizate (this involved the cathode and anode connection and development of temperature if it was necessary), solution discharge, voltage application, current monitoring, end of the experiment (voltage off), device removal and oxidized sample conservation.

2.4.5 Electrolytes used.

During the experiments, electrolytes of water with 0.4 and 0.5 weight% Hydrofluoric acid (HF) were normally used. Similarly, also were used in specific cases an electrolyte of fluorinated dimethyl sulfoxide (DMSO) with 0.5 weight% HF and adding acetic acid to the 0.5% HF electrolyte mentioned before, in a 1:7 ratio. Is important note that electrolyte was change with every new experiment carried out.

2.4.6 Solution containers.

Due to use of HF, glass was banned as a material for containers for safety reasons in tests. Thus, we had to choose containers with an adequate shape, transparent, but mostly made of a material to endure the presence of acid.

First tests were done with a properly cut piece of silicon where all the elements for anodizing were housed. However, seal was very diffcult to maintain and was not possible to increase the reaction temperature due to the material. Consequently, it was rule out after first tests.

Figure 21. Silicon container.

Next container used was composed of two plastic tubes in which the outer diameter of the inner tube coincided with the inside diameter of the outer tube, the cathode and anode were placed at each end and were made two radial-direction holes in the middle of the tubes, one to introduce the solution and other to allow entry and exit of gases. Length of inside tube was just 1 cm (distance used for anodization) and related problem with sealing were not still solved.

Last container for titanium plate experiments was a small Teflon vessel located within a metal container. Inside the metal part there was circulating water at given temperature to maintain the reaction conditions and normally the whole equipment was placed on the base of a magnetic stirring. Finally, seal problems were solved changing the geometry of the process or with the square plates.

Figure 22. Teflon receptacle.

Is important to take in consideration that each one of these containers were properly washed, before and after of each experiments carried out with them.

2.4.7 Geometric arrangement.

When we talk about the geometric arrangement we mean the location of the cathode and the anode in the experiment as well as the form how they were introduced in the electrolyte. Actually the discussion of this factor is due to the technical difficulty that supposed to work with samples of titanium did not reach one centimeter in diameter. Once we had at disposal the square plates we could standardize the experiments and not depend on the geometry as a parameter.

The main problem we found was that the sample of titanium surface we wanted oxidize should remain in the solution while on the other side we had to keep attached the copper that helped holding the potential difference. In order to resolve this handicap, we devised a piece of plastic tube which kept one face of the sample isolated of the electrolyte. In this manner, it was possible to submerge the device in the solution maintaining the electrical contact dry between the wire and the titanium. The platinum cathode was easier to maintain because from the beginning were ready square plates 2.5 cm side.

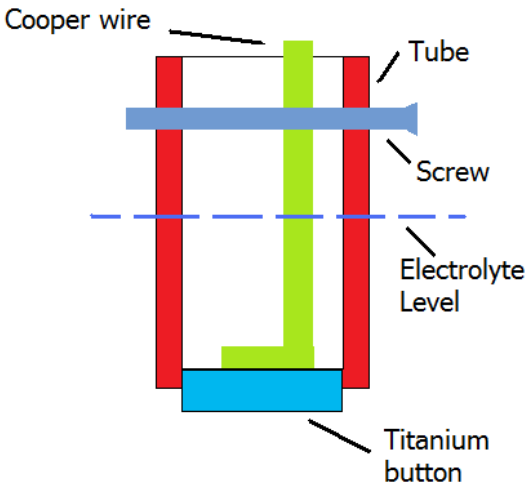

Figure 23. Button titanium schema.

Another problem was related to the electric field distribution within the solution, because depending on how we put the cathode, was produced a concentration of electric field in certain areas of the sample, accelerating the reaction and resulting no-nanotubes.

First tests we did with a silicone container did not give good results because of the poor sealing between the tube containing the titanium and material of the container. Different geometries were used to improve the results, but were not enough to keep using silicone recipient. It is important to mention that in those experiments the plastic tube was always introduced in a horizontal position.

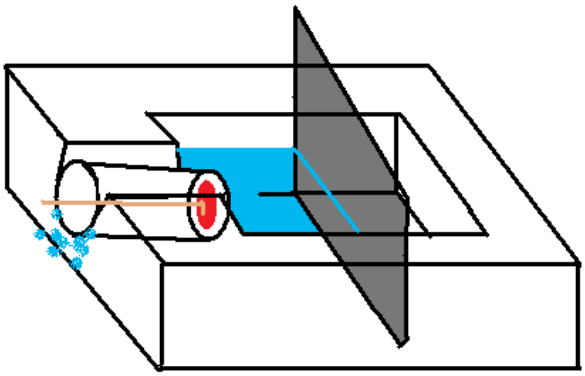

Figure 24. Silicon arrangment.

Next geometry was chosen mainly because we wanted to use for the experiment, another titanium sample as cathode. Thus, there were two areas we needed to keep in the solution and another pair attached to copper wire. The only possible way foe that was using the double-tube described idea.

Figure 25. Double tube.

With the last container were used two different arrangements. This was, because after the microscope analysis, it was possible to note that the oxidized surfaces on the samples were not homogeneous. The main objective of the new geometry used in this recipient was to reduce the impact of electric field concentration.

In the original geometry, the plastic tube was introduced into the solution vertically with the anode at the bottom, otherwise the aluminum plate was bent to be able to maintain parallelism between the anode and cathode, allowing one end outside the solution could be attached.

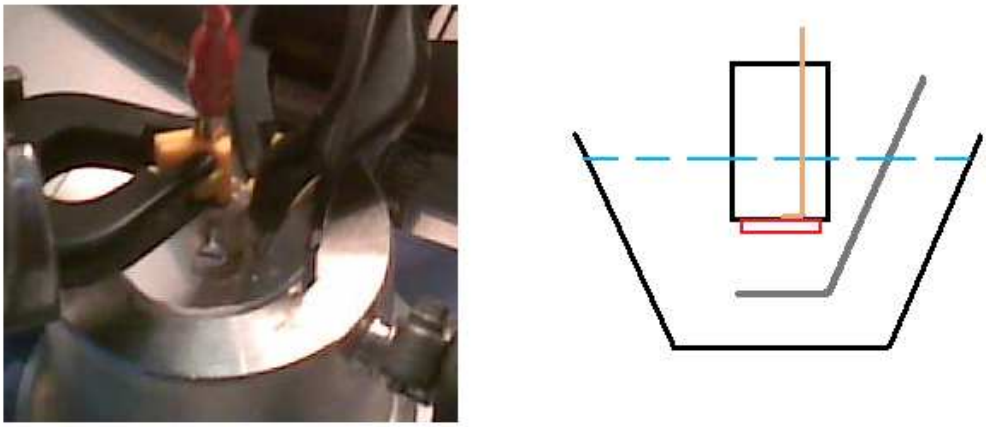

Figure 26. Original geometry for Teflon container.

According to literature [12] there is a concentration of current density at the corner of the titanium sample that was located closer to the cathode surface. This made that oxidations were more intense in areas near the corner in mode of appreciate superficial differences [11].

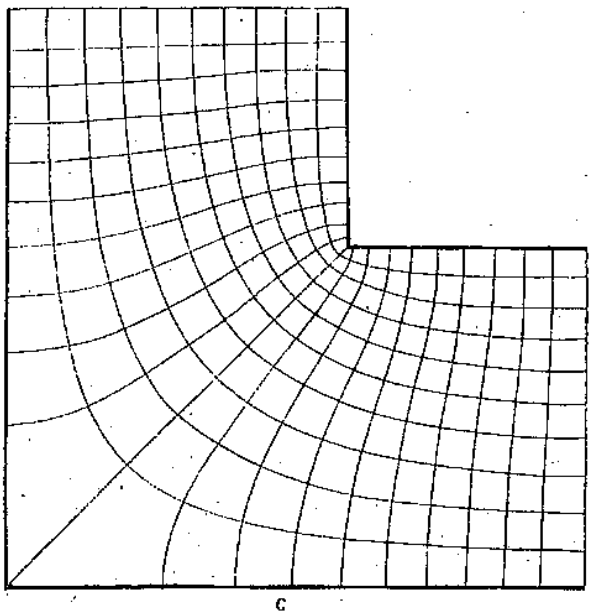

Fig. XIII.13 – Configurazione del campo fra due elettrodi piegati ad angolo retto.

Figure 27. Field concentration area. Visible non-homogeneous surface.

Because of this, we searched one way to reduce the local increase of the field density. The solution adopted was changing the position of the anode and the cathode inside the Teflon vessel, resulting an oblique arrangement that allowed to keep the parallelism with no field concentration.

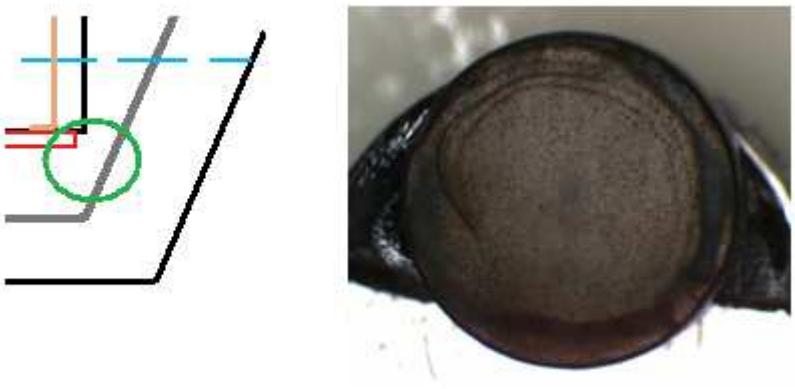

Figure 28. Concentration of current density for two right-angle electrodes

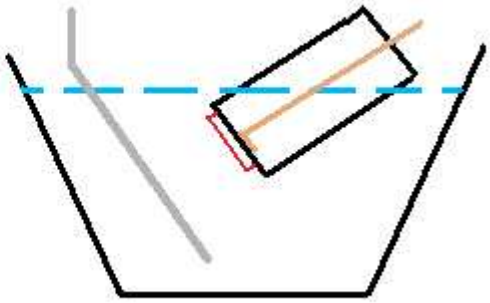

Figure 29.New arrangment.

Once we had at our disposal titanium square plates, parallel problem was finally resolved and during the rest of the experiments we used a plastic base that kept the anode and the cathode at the precise distance with a small hole that allowed the presence of magnetic stirring between them. At the top, out of the solution, were locate the electrical connections.

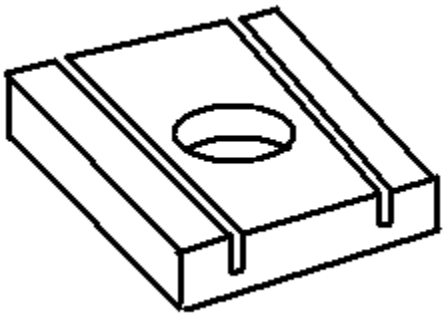

Figure 30. Plastic base

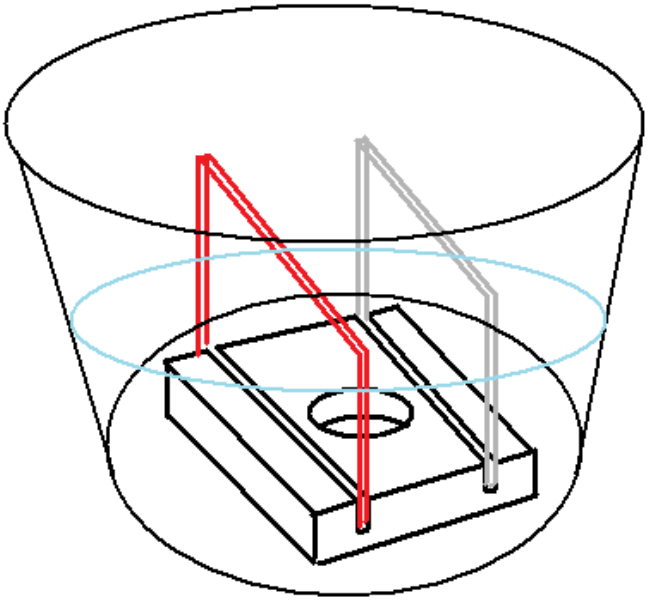

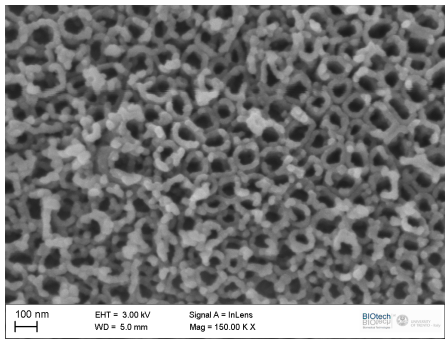

Figure 31. Teflon container disposition with the plastic base holding electrodes and electrolyte level. Exaample of nanotubes on titanium plates.

After anodization were made, we move to ESEM “Gemini Supra 40 (ZEISS)” microscope located in Mattarello for the surface analysis. This was one of the most important parts of the synthesis because we should accurately determine exact areas where the nanotubes have grown in relation with geometry, anodization used time, voltage used, temperature, and type of used solution. Based on these results, we chose the path we thought desirable to improve conditions to facilitate the nanotube growth.

2.5 Sputtering titanium on ITO glass.

First attempts were carried out in the laboratory of materials in the University of Trento. Specifically, the device used, was "laboratory LEYBOLD Z400 sputtering system.", Fergutec brand; this device worked using RF sputtering technology. Is important to note that, these samples were sputtered with a deposition rate around 20 nm/min, because of this, titanium film on the sample did not remain attached to the glass and quickly was detached as soon as was applied the voltage during anodization.

Despite of related problems with the high deposition rate, as is described above, there were some availability problems with the equipment in Trento. Thus, we had to search another way to obtain sputtering samples enough to keep working once ended the synthesis of titania nanotube part.

At this time, our Tutor contacted with professor Maggioni working at “Laboratorio Nazionali di Legnaro” belonging to “Istituto Nazionale di Fisica Nucleare” in the city of Padova. Maggioni’s area includes sputtering using magnetron and radio frequency technology and surface characterization through Rutherford Backscattering Spectrometry (RBS) using a particle accelerator. Hence, Maggioni’s collaboration was key in our project to continue with the experimental part.

Figure 32. RF and Magnetron sputtering machines from Padova.

In first visit, we agreed to make the titanium deposition of 1000 nm. thickness on four FTO glass samples using RF sputtering, as well as 500 nm. deposition thickness in this case using magnetron sputtering for eight samples. Once all the terms were specified in this first visit to Padova with Maggioni, we made a four-day trip in order to obtain new samples of titanium sputtering next week. We also left in Padova a dozen samples with which professor Maggioni would try to make depositions according to his availability in the week between visits.

Before the second visit, 20 samples of FTO glass were properly cut with dimensions determinated for the correct cell geometry and washed using detergent, ethylenglicol and ultrasonic bath. Afterwards, each one was introduced in an individual plastic receptacle to transport and identify it.

When we arrived to Padova second time, we could see that Maggioni had done 250 nm. deposition on six samples of the dozen we left at the beginning on his own account. The impression we had with these samples were good because of titanium on the glass seems much more homogeneous and compact than Trento-sputtered samples.

However, first day was dedicated to calibrate the deposition rate of RF-sputtering equipment. To this end, we made the vacuum in deposition chamber with a sample inside leaving all the night to achieve working pressure (10^{-5} mbar).

Second day, always working with RF device and after checking the correct pressure, we put one silicon target and the sample was sputtered for 30 minutes. Then, silicon-sputtering sample was removed and were inserted four ITO glass samples. Same process to make vacuum was carried out and we waited until next day to sputtering. Parallelly, we could see how particle accelerator works following Maggioni's indications to measure the amount of silicon deposited on the sample. Eventually, we calculated 1.2 nm/min deposition rate.

Figure 33. Samples just after sputtering.

In that moment, we discussed about the depositions because magnetron machine was full-time working, and we wanted to realize at least one long deposition to arrive 1000 nm of titanium thickness, finally adopted solution was to stop the RF machine during the night between third and fourth day maintain the vacuum in the chamber; to sputter the samples during the day when we were with the machine. In this moment we got to set another deposition in magnetron machine, for fourth day, to achieve 500 nm thickness using this method.

Third day, we arrived to the laboratory and we started to sputtering the samples with a titanium target in RF device. The machine was stopped one hour for lunch and was working 6 hours during the day. At the same time we had to prepare the samples for magnetron sputtering and let it inside the machine, vacuum-pump was turned on to sputtering samples at correct pressure next day.

Is important to note that, magnetron sputtering machine was a semi-industrial equipment giving us the advantage of sputtering 12 samples each time with, 5 nm/min. as deposition rate. Hence, we only needed two hours sputtering to achieve 500 nm titanium thickness.

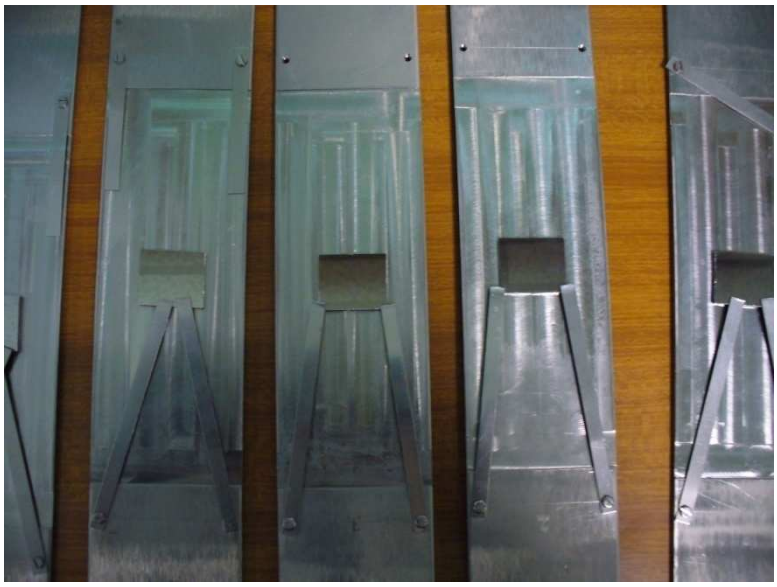

Figure 34. Sputtering samples in detail.

Fourth day, RF sputtering was restarted during 8 hours, with no interruptions. Regarding to magnetron machine was sputtering two hours as is commented above. Afterwards, all equipments were turned off and samples were prepared for transport. We used a plastic container immersed in an argon atmosphere for this purpose driving to Trento laboratory two hours approximately.

One of associated problems with titanium sputtering was that before anodization we could not clean the surface as we have done with the plates during the synthesis. This was mainly because of the sputtering surface was much more delicate and there was a high risk of separating the film from conductive glass. In this way, samples were kept in vacuum or inert atmosphere until the anodization moment arrived. Is for this reason that we took extra cares with the samples once they were out of the machines in Padova.

Figure 35. Trasport container

Summarizing, we had got 6 samples of 250 nm. sputtering-titanium thickness, 12 of 500 nm. all of them made using magnetron sputtering and 4 samples of 1000 nm made in RF sputtering. In total 22 samples to anodizate in Trento.

2.6 Anodization of sputtering titanium.

Once all samples were at our disposal in Trento laboratories we were in grade to continue the experimental procedure. The idea was anodizing the samples obtained in Padova with good conditions achieved in the synthesis of nanotubes on plates to grow titania nanotubes on the sputtering metal films.

In this case, as is mentioned above, was not made any washing with the samples. Thus, each one was directly driven from vacuum container to the anodization receptacle.

Anodization of sputtering titanium was carried out in another new container because the first one, was not big enough to keep inside the ITO glass (3 cm x 2.5 cm) and platinum cathode.

This time was chosen a plastic, being transparency the main factor. The reason was, as we could see after, that the reaction with sputtering titanium was much more quick compared with titanium plates. However, continued banned any material that does not endure the acid attack such as glasses. Similarly, a plastic base shown in figure 30 continued being our method to achieve parallelism between samples leaving place for magnetic stirring in the middle.

In this mode, it was necessary to keep looking titanium surface during anodization due to pitting occurred in the metal film. When pitting occurred usually we stopped the reaction turning off power supply and removing current sample from the solution bath to another distilled-water bath to stop definitely the reaction.

Regarding temperature control, that was used in titanium plates, is important to note that this time was never present in sputtering-titanium experiments.

Power supply, ammeters and voltmeters used in this part were the same that used for titanium plates, as well as platinum plate as cathode.

About the electrolyte, one more time was used 0.5 weight% hydrofluoric acid and adding acetic acid to 0.5 weight% hydrofluoric acid electrolyte, in a 1:7 ratio.

Washing methods of related elements with the experimental part, cathode and container, are as described ones for titanium plates.

It should be noted that, due to first non-good results with anodization and limited number of samples, we decided to carry out two anodization per sample keeping first in the electrolyte only half part of the metal film and then the other one. Anodizations in this manner were done in a short period between experiments. Often, the only change we did was applied voltage, introducing new value in power supply. Being time between anodizations: the necessary to remove the sample, stop the reaction in distilled-water bath and introduce again in the electrolyte. These times, unlike titanium-plates experiments, electrolyte was changed every two anodization instead of every one.

Is important to note that, once achieved anodization conditions for sputtering samples, completed samples were immersed with the purpose of make up of the cell.

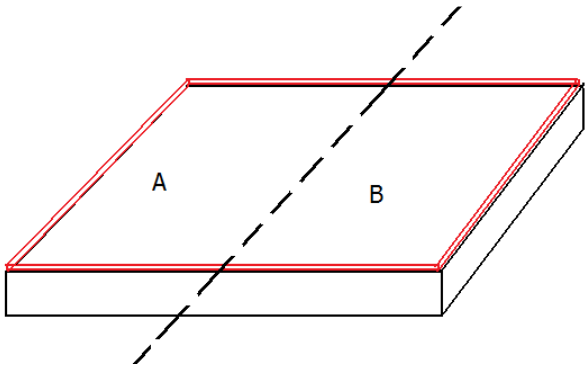

Figure 36. How samples were divided.

After anodization, samples were preparated for transport and carefully transferred to ESEM to analyze the surface. Normally we performed experiments just before we had made an appointment in Mattarello facilities. Thus, samples were preserved from external agents when they were in the microscope.

We can summarize the process of sputtering samples anodization in following steps: platinum cathode and receptacle preparation, make electrolyte mix, choose the sample and introduce anode and cathode in solution container, prepare power supply, voltmeter ammeter and wires, pour the electrolyte and turn on the power supply with determinated voltage during planned time. Once experiments were finished samples were immersed in a distilled-water bath and kept them later in an individual plastic tube for transport and identification.

2.7 Preparation of DSSC device.

In this part it will be explained how different of the solar cells elements were done while related experiments were carried out..

Is important mention that for this project have been used results and methods achieved by Massimo Sebastiani in his thesis "Costruzione e caratterizzazione di un dispositivo fotovoltaico a colorante organico" in polymers and composites laboratory, Trento's university, to prepare the counter electrode, electrolyte and device assembly [8].

2.7.1 Conductive glass preparation.

In all DSSC devices designed was used as substrate and the collector charge ITO glass with the properties outlined above. Such material, however, creates considerable limitations in the performance of both cells processes that are subject to the layers deposited on it.

As is reported in recent research, fluorine doped tin oxide (FTO) is used for all groups such as usual DSSC building glass devices.

Regarding the geometry, it is noteworthy that the main parameters in their choice were: the dimensions of the devices we used during the anodization and sputtering, and the machine that kept the separation between the electrodes during the assembly of the cell

Thereby, dimensions to cut the glass before sputtering and making counter electrode were defined as 3 cm per 2.5 cm. Nevertheless, as it is mentioned in bibliography record efficiencies are achieved on small device areas [6].

2.7.2 Sputtering titanium film preparation.

Once the sputtering titanium samples were anodized and surfaces were analyzed, the films were annealed in oxigen at 450ºC for 1 hour. The reason for doing that is to crystallize the nanotubes and oxidize residual metal regions on the film. Later, the samples were kept in the oven until they reach free room temperature in order to avoid residual stress in the anodized metal.

Before DSSC fabrication, was not realized any more treatments with the samples. However is reported in literature a $TiCl_4$ solution in ice water applied to the TiO_2 film and thereafter sintered. The newly applied TiO_2 molecules improve the necking of the adjacent nanocrystals, thus enhancing the percolation [10].

2.7.3 Dye adsorption.

In this work, the only dye used was sensitive ruthenium535bistba obtained from the (Solaronix) as indicated in literature; this dye is the product that provides the best performance in sensitization of titanium oxide.

Figure 37 Water bath machine.

Dye was dissolved in ethanol in order to achieve M = $3*10^{-4}$ mol/l. solution. Adsorption on the nanotube layer is carried out by immersion of sintered samples for a time of 24 hours keeping 65ºC in a water bath.

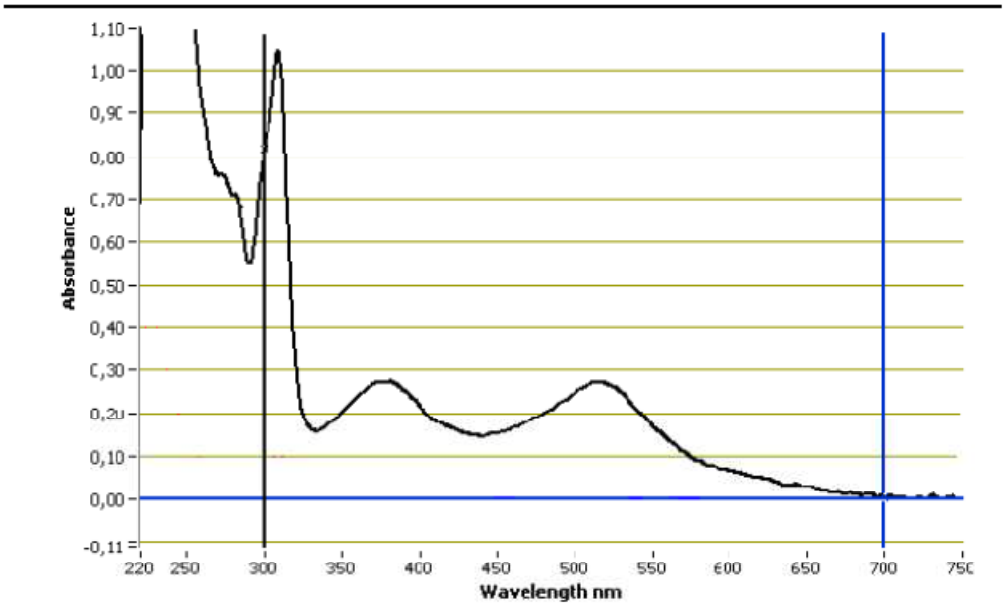

Figure 38. Absorbance spectrum of 3*10-4 M di ruthenium535bistba.

2.7.4 Counter electrode preparation.

The basic substances used to prepare the counter electrode were graphite, excellent conductor, and carbon black reaction catalyst to restore the I^-.

In the realization of devices we tried to obtain a layer deposed about ten microns using tape-casting technique. Preparation for this technique was covering with tape following long sides of future cell. Afterwards, conductive glass were "painted" with solution mix using a paintbrush and one glass blade was passed over the "painted" surface with an angle about

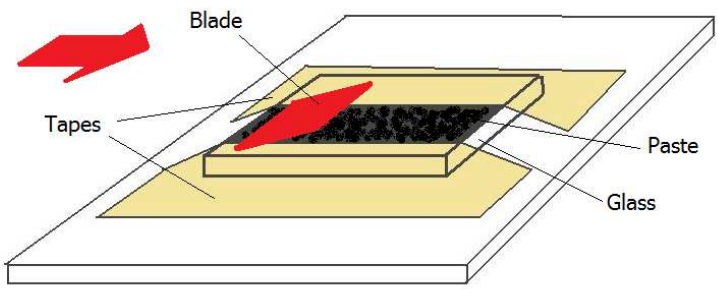

Figure 39. Schematic representation of blading method.

30º. In this mode only non-taped part of the ITO glass was covered by the material.

Then, counter electrode was subjected to heat treatment keeping the samples for 1 hour in the oven at 450ºC. Using this technique, a film about 10-15 μm thick was obtained and its thickness measured using an optical microscope focusing glass and film surface.

2.7.5 Electrode and counter electrode distancing.

For precision distancing between the electrode and the counter electrode has been used a device consisting of a platform where binding elements of the samples were placed. These elements were positioned to move in the XY directions. In the angular component the error guaranteed by the manufacturer was lower than 5 μrad; in this way, the compact structure guaranteed high precision in the parallelism between the surfaces and the device was able to obtain a few microns distance between electrodes without causing internal short-circuit.

On the other hand, the servo dynamic actuator (PT1/M-Z612, Thorlabs brend) used for the approach, had a sensitivity of 0.1 nm. The adhesion of the samples to the support was ensured by a pressure gap produced by a membrane pump. This vacuum was applied between the samples and their supports that had a hole for this purpose.

All operation and controlled approach was followed by an easy to use software which calibrating the device, and determined the separation distance between the supports.

It should be mentioned, that to well evaluate the distance it was necessary to estimate the thickness of the glass of the two samples, as well as the thickness of the layer deposited on each of them to know exactly the distance to enter.

The thickness of the glass was evaluated through a micrometer, while an optical microscope has been used for the counter electrode layer and the titania film , as mentioned above.

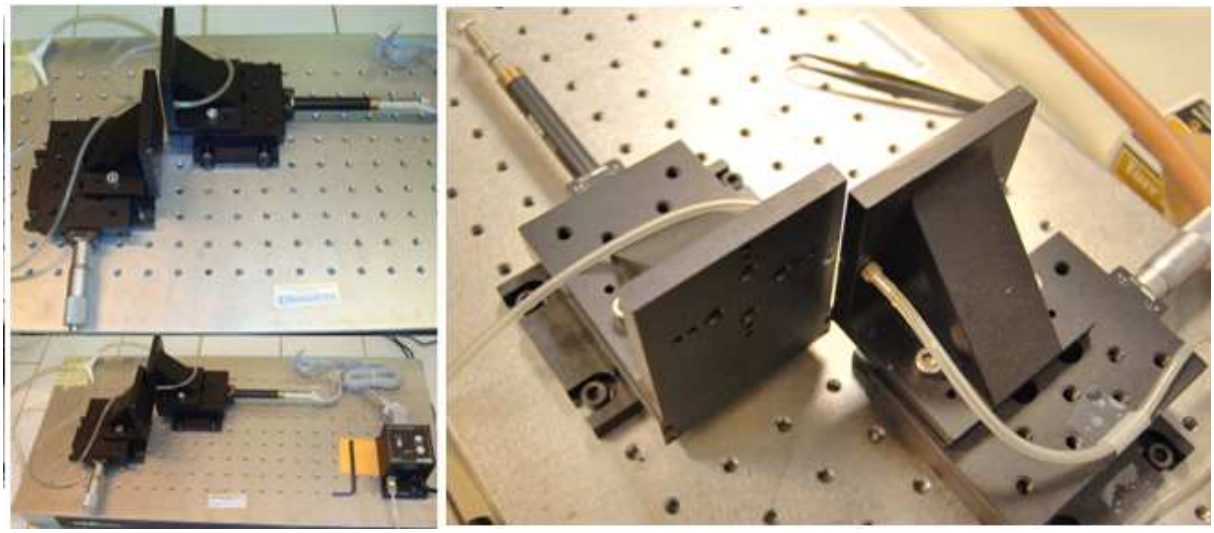

Figure 40. Distancing device.

2.7.6 Electolyte.

From the beginning it was used a solution of 0.5M LiI (lithium iodide) in acetonitrile. This electrolyte has proved particularly effective as a solvent, although its handling is toxic and dangerous to handle, has excellent characteristics for the purpose of our electrolyte.

The process of filling the space between electrodes was carried out by capillarity leaving in a first stage two sides without sealing. Thus, electrodes were held vertically until electrolyte filled the cavity as shown figure 41. Filling time depends on separation between surfaces, roughly following Washburn's equation i.e.: narrow separations lower times and vice versa.

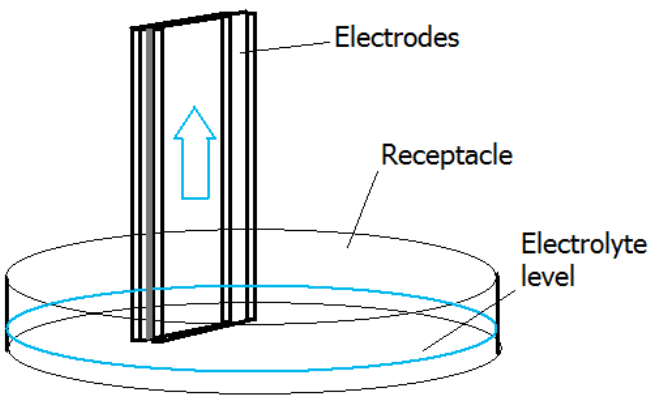

Figure 41.Cell filling procces.

2.7.7 Sealing.

Torr Seal®, an epoxy resin, chosen by the optimal correspondence with the requirements needed was used in sealing for cell fabrication.

A drying period of 2 hours was able to guarantee the mechanical properties required for assembly, especially good resistance to corrosion and solubilization caused by the use of acetonitrile in the electrolyte.

2.7.8 Collector preparation.

An epoxy-silver-containing paste has been used on the voltmeter connection zone of cell to reduce the electrical resistance of ITO glass, due to its low but significant resistivity.

2.8 Components analysis.

2.8.1 Performance test and fill factor.

A photovoltaic cells has the aim of converting the sun radiant energy into electrical energy. The operation of a photovoltaic cell under illumination but subjected to the variation of the external circuit load is shown below.

2.8.1.1 Voltage-Current curve:

The most immediate and complete method for testing a photovoltaic device is to determine the current-voltage curve. This analysis can be performed using the device as a current generator in an electrical circuit with a variable resistance. In this way, we obtain values of the voltage depending on different resistances applied in the circuit.

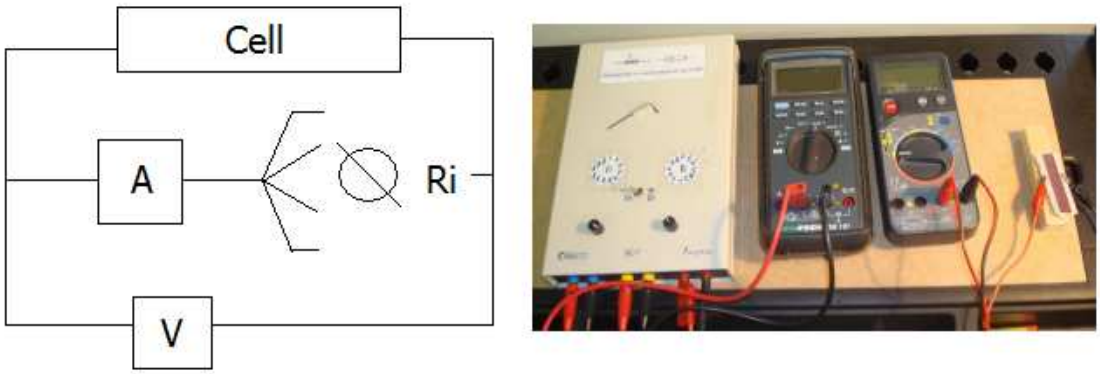

Figure 42. Circuit used for obtain Voltage-current graph.

For this work have been used 24 resistors, which gave sufficiently precise curves between , displaying cell behavior between open circuit and short-circuit state. Resistor values used are as follows: 0, 10, 56, 100, 180, 328, 561, 815, 1000 Ω and 1.50, 1.80, 2.20, 2.60, 3.80, 4.60, 5.45, 6.60, 8.00, 14.0, 29.0, 45.0, 147.0, 237.0 kΩ.

For the simultaneous reading of the current and voltage, a voltmeter was introduced in parallel and an ammeter in series with the applied resistance.

From a performance point of view, the most important parameters of study are the point of maximum current and open circuit voltage determined in terms of short circuit (Isc) and null current conditions (Voc). The product of these two factors gives us an ideal value of the power that could achieve our cell.

However, in the curve obtained from the experimental data, we can see that the maximum value of the ideal power is not reached for the current tension value pairs:

$$P_i = V_i * I_i$$

Here is possible to see that the photovoltaic cell does not behave like an ideal device, and follows the behavior of a diode and a current generator.

Now it is time to estimate the fill factor, which is a dimensionless number from 0 to 1 and represents the deviation from ideality of the representative curve obtained from the cell. Fill factor is defined as the relation between effective power and theoretical power obtainable.

$$FF = \frac{Vmpp * Impp}{Voc * Isc}$$

Rewriting the formula it is possible to express the maximum power produced as a function of the fill factor:

$$Pmax = Voc * Isc * FF$$

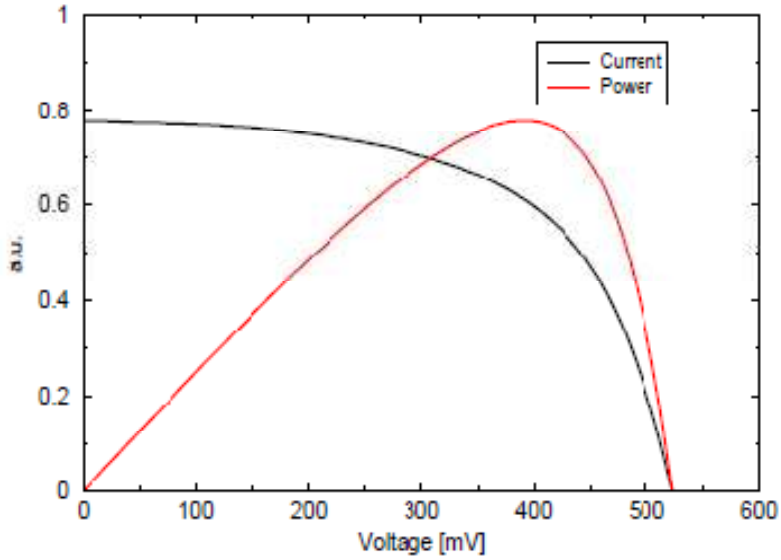

Figure 43. Voltage-current grapgh.

Similarly, the fill factor is directly related to performance, most important technological parameter.

Thus, performance is defined as the ratio of the output power of the cell and incident irradiance:

$$\eta = \frac{Pmax}{Pin}$$

The performance test is one of the best we can use to characterize solar devices, allowing us to compare different technologies independly on the applied technology. Nevertheless, this test has some drawbacks principally depending on environment analysis such as radiation spectrum, temperature, climate and intensity of incident light.

In order to obtain comparable results tests have been performed in standard conditions: temperature 25ºC, incident intensity 1000 W/m^2 and an spectrum distribution determinated AM1.5 spectrum representing standard conditions.

2.8.2 Sunlight analysis.

Testing was performed by exposing the cells to the sun without control of atmospheric conditions. In order to measure the incident radiation during the experiment, was used a traditional photovoltaic device whose sunlight behavior was previously known. Hence, incident power was measured from the open circuit of traditional device, before calibrated through a piranometer.

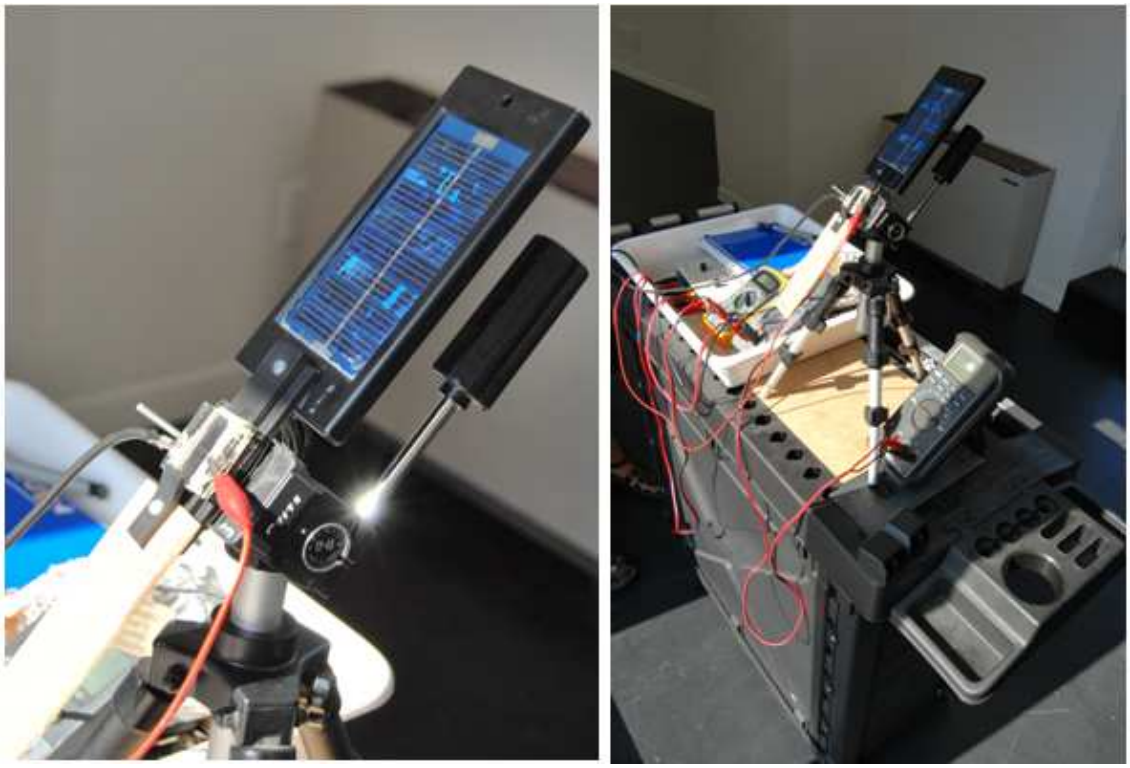

Figure 44. Device to measure incident radiation

2.8.3 Geometrical nanotube parameters.

During the synthesis, interesting areas were analyzed using an ESEM microscope. The photographs obtained were studied using an image processing software (ImageJ, by NIH) obtaining various parameters of the nanotubes such as the diameter, thickness and length.

The procedure carried out with the images, for diameter and thickness test, consisted on select one feature photo from the specific sample, applying a threshold filter and work over selected areas taking measures. The software itself had different options for choosing the measures depending on area selected with the cursor. For the analyzed photos were done 20 measures from different parts of the image to estimate a weighted result.

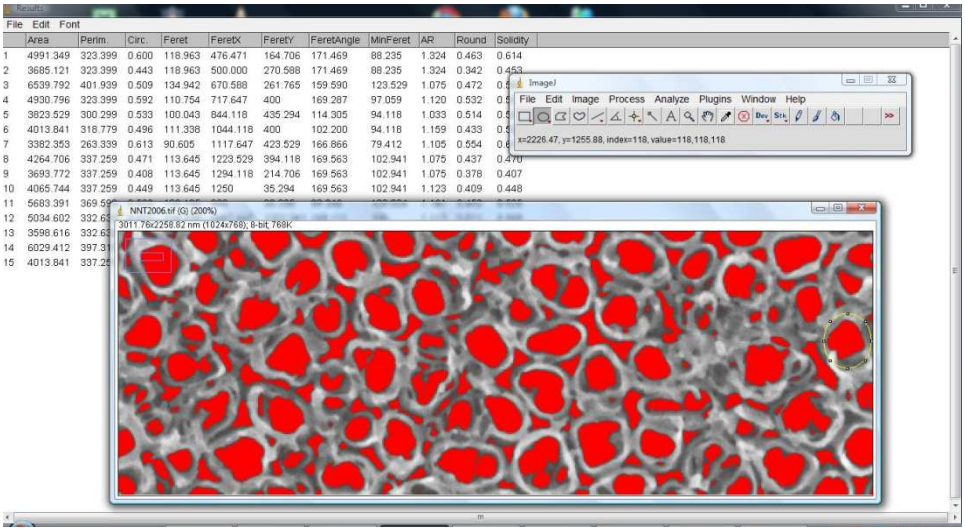

Figure 45. ImageJ screen

In case of length, were used photos taken from microscope with an angle apply to the samples taken advantage of fissures and superficial imperfections that permitted give us an idea of the lengths.

2.8.4 Post anodization film composition.

In order to verify the composition of sputtering metal film after anodization were carried out tests to determine its composition.

These tests were conducted in an SEM microscope located in the Facilities of Trento's university endowed with a technique which permitted to analyze the composing material on the surface.

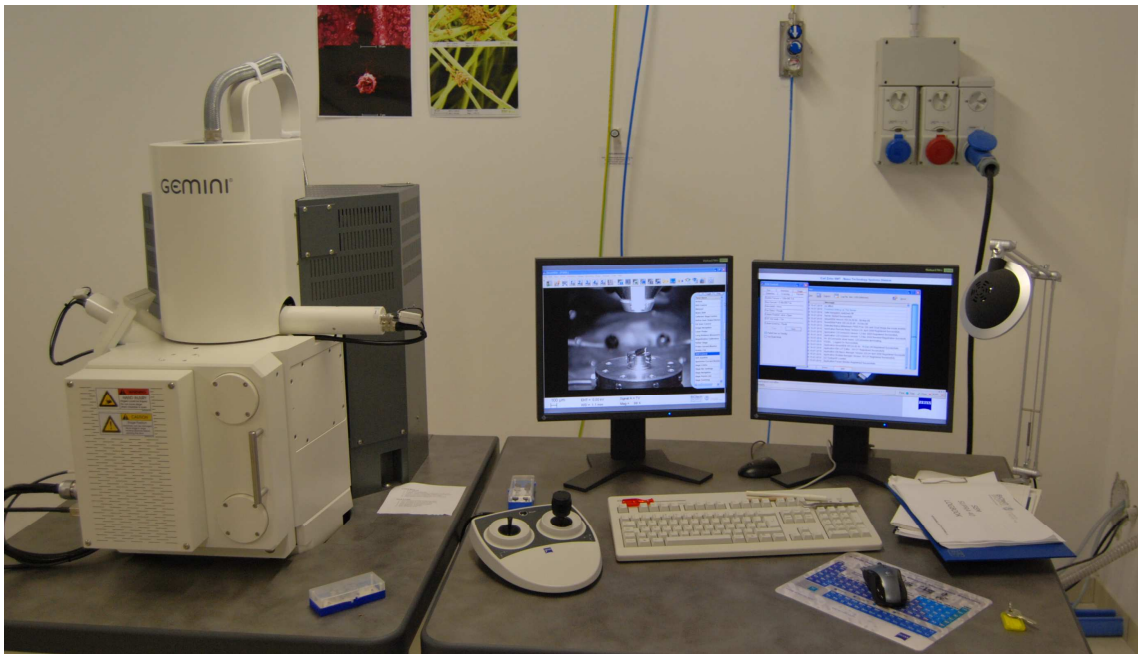

Figure 46. ESEM microscope.

3. Results and discussion.

In this part, results are exposed following two major developed groups in the project: synthesis of titania nanotubes and DSSC device fabrication with titania nanotubes as base material.

3.1 Synthesis of titania nanotubes.

Below, the results achieved in the work are presented chronological order. They were described depending on the parameters chosen to improve the nanotube-growth conditions or by the properties related with shape and robustness. Also, is important to distinguish two parts in this section, because at the beginning we failed achieving nanotubes. Thus, first part consists on searching main conditions to obtain nanotubes during anodization and the second to specify changing conditions were appreciated on surface images.

In the first anodizations, which were done with titanium button plates. Our idea was to anodizate directly sputtering titanium on FTO glass from the beginning but due to difficulties observed in these first experiments, we took the decision to work with titanium plates to understand what was happening with the nanotube growth.

Is important to note at this point that, our principal tools to evaluate the reactions and take further decisions were: current vs. time curve which will give us an idea of the electron flow between cathode and anode during experiments (speed reaction) and ESEM image analysis compared to the published results.

These experiments were realized using the silicon receptacle, with geometry indicated in figure 24. The electrolyte solution used was water with 0.4 weight% HF and platinum was placed as cathode of reaction. The distance between anode and cathode remained constant (1 cm) during all the experiments carried out in this project. Regarding temperature, reactions were carried out with no heating at laboratory conditions (25ºC). Process parameters are presented in table 1 and were chosen in function of experiments found in literature according to our purposes.

	Cathode	Time	Volt	Temperature	Stirring
NNT1	Pt	30 min	30 V	25°	NO
NNT2	Pt	15 min	30 V	25°	NO
NNT3	Pt	30 min	30 V	25°	NO
NNT4	Pt	15 min	30 V	25°	NO

Table 1. NNT1, NNT2, NNT4, NNT5 process parameters.

In this first attempts (NNT1, NNT2), measured currents were not satisfactory mainly because the geometric arrangement was incorrect and related problems of sealing were present. This caused the contact between the cooper wire, in charge to maintain the voltage difference, and the electrolyte solution. Current versus time for anodizations is shown below.

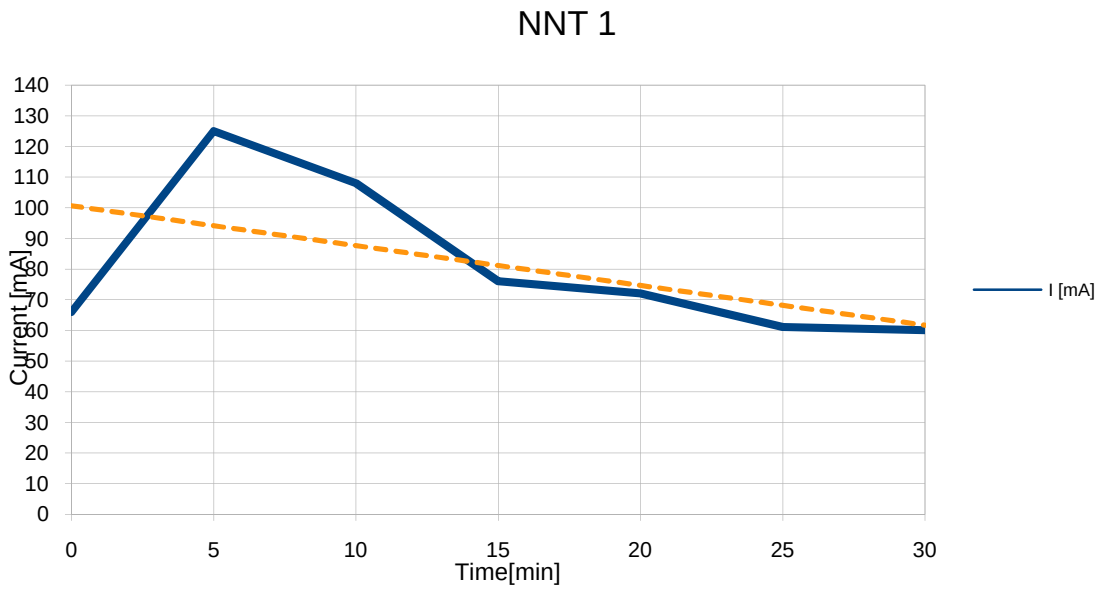

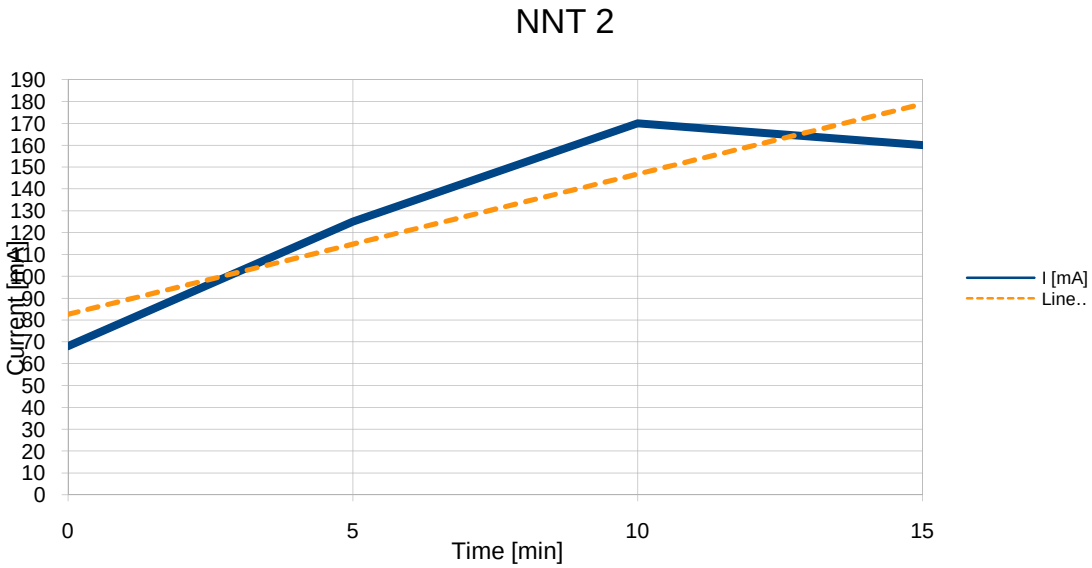

Main consequences, as we can see, were an increment of current flowing through the solution resulting one order of magnitude higher than using a normal sealing receptacle. For this reason, experiments were repeated taking more care to ensure no contact with the electrolyte.

For NNT3 NNT4, according to results found in literature, lower current intensities were achieved; however, when ESEM images of the surfaces were studied, we could distinguish similar nanotube structures but were not good enough. In figure 47 are shown these structures.

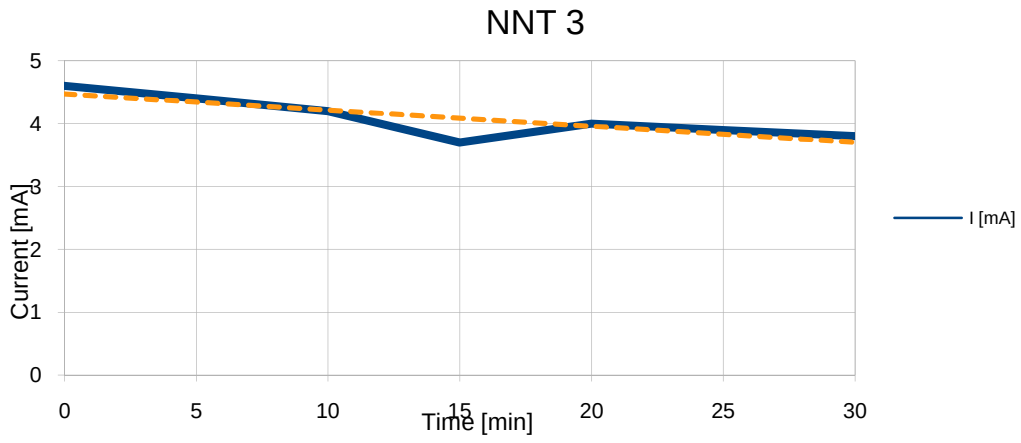

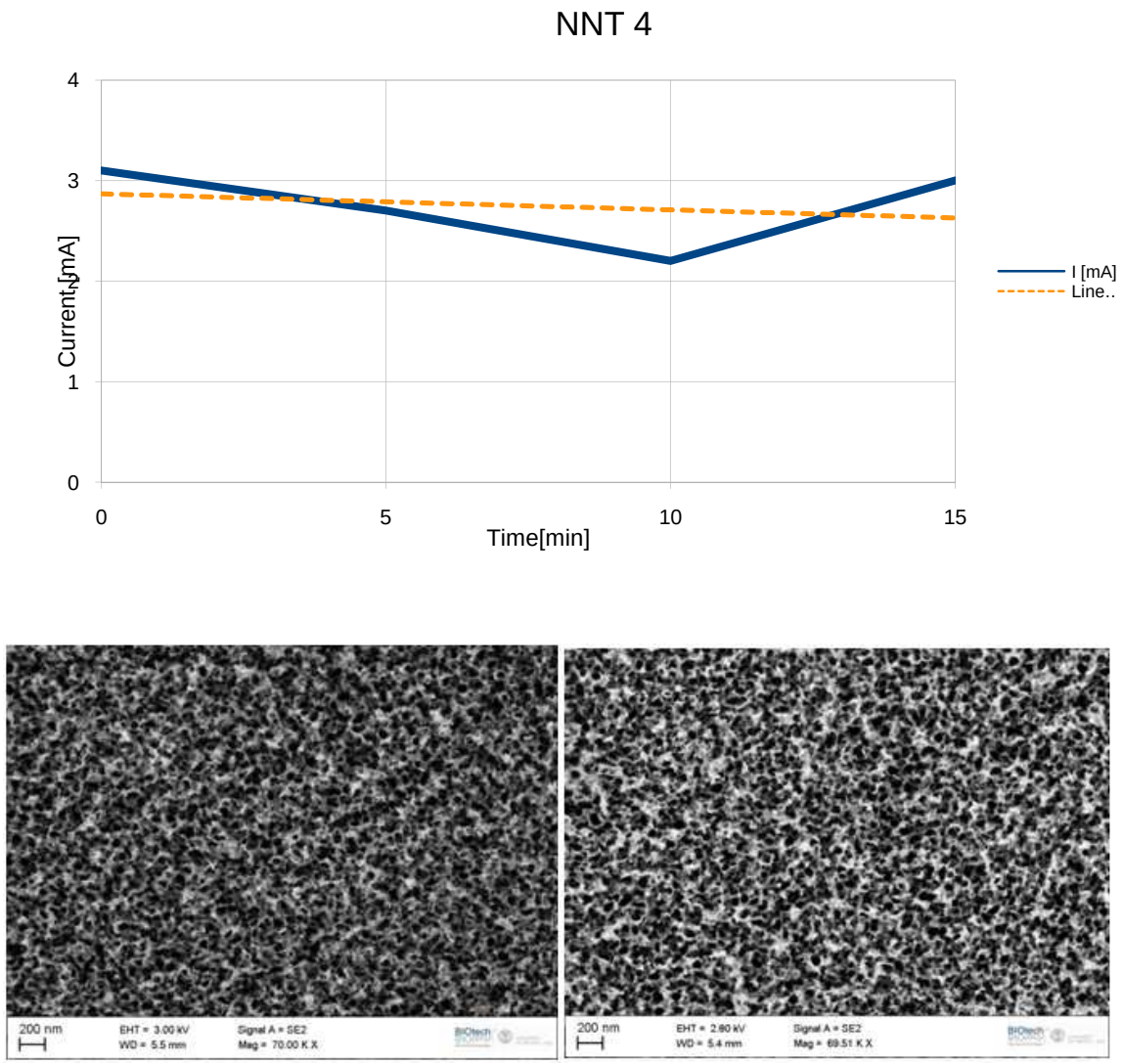

Figure 47. NNT3, NNT4 ESEM images.

As we could check, texture surface in NNT3/NNT4 matched with the optimal conditions published to achieve nanotubes adding an extra voltage during anodization. In this way, reducing the voltage and increasing the reaction time was the path to continue with the experiments.

Next anodizations were carried out for 45 min, decreasing voltage to 20 V. Following the geometry described in figure 23 a titanium button was used as a cathode in NNT5 while in NNT6 was used the platinum plate in the silicon receptacle. In the same way, no heating or stirring were presented in the reaction and electrolyte solution was unchanged. Process parameters and current depending on time are presented below.

	Cathode	Time	Volt	Temperature	Stirring
NNT5	Ti	45 min	20V	25°	NO
NNT6	Pt	45 min	20V	25°	NO
NNT7	Pt	45 min	20V	25°	YES

Table 2. NNT5, NNT6 y NNT7 process parameters.

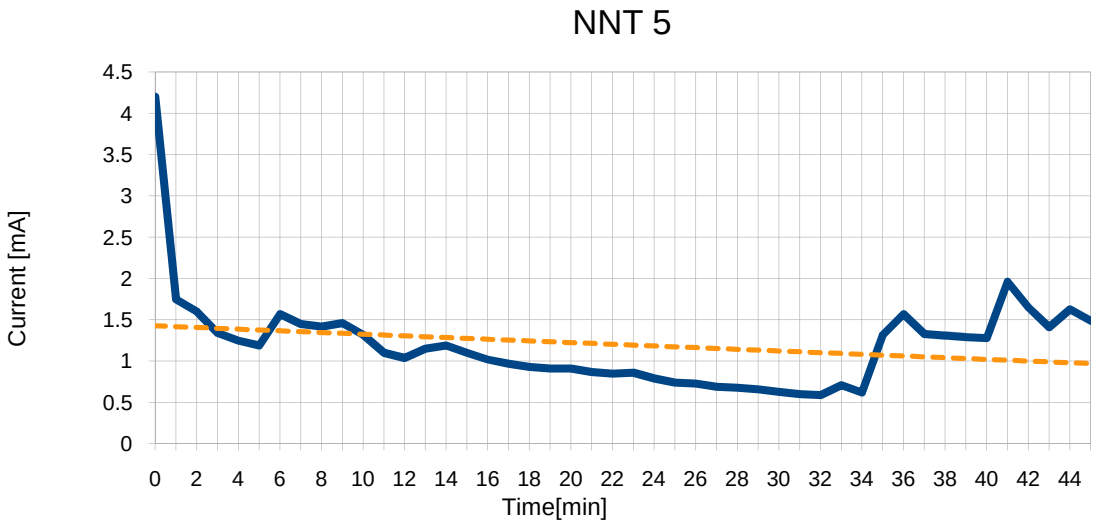

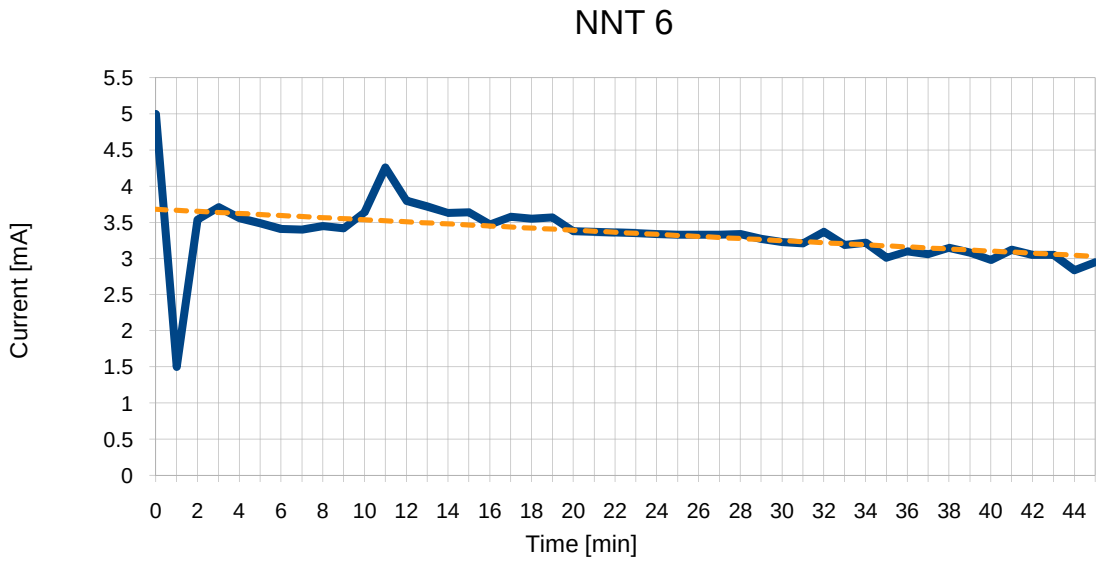

This time, intensities were lower than first tests. Also, we could observe a decreasing current behavior as is reported in literature for nanotubes growth as well as a high current during first seconds of experiment. Later we understood that it was common to have unnormal data at the beginning. Unlike the first experiments, time measures were taken

each minute to achieve accurate precisions in current evolutions. In this manner, we observed that during anodizations quick variations of current happened.

Once in Mattarello, analyzing surfaces on ESEM microscope, first nanotube structures were achieved in the project. The result was important but only several "islands" of less than 10 μm^2 in the total surface were found, as is shown in figure 50.

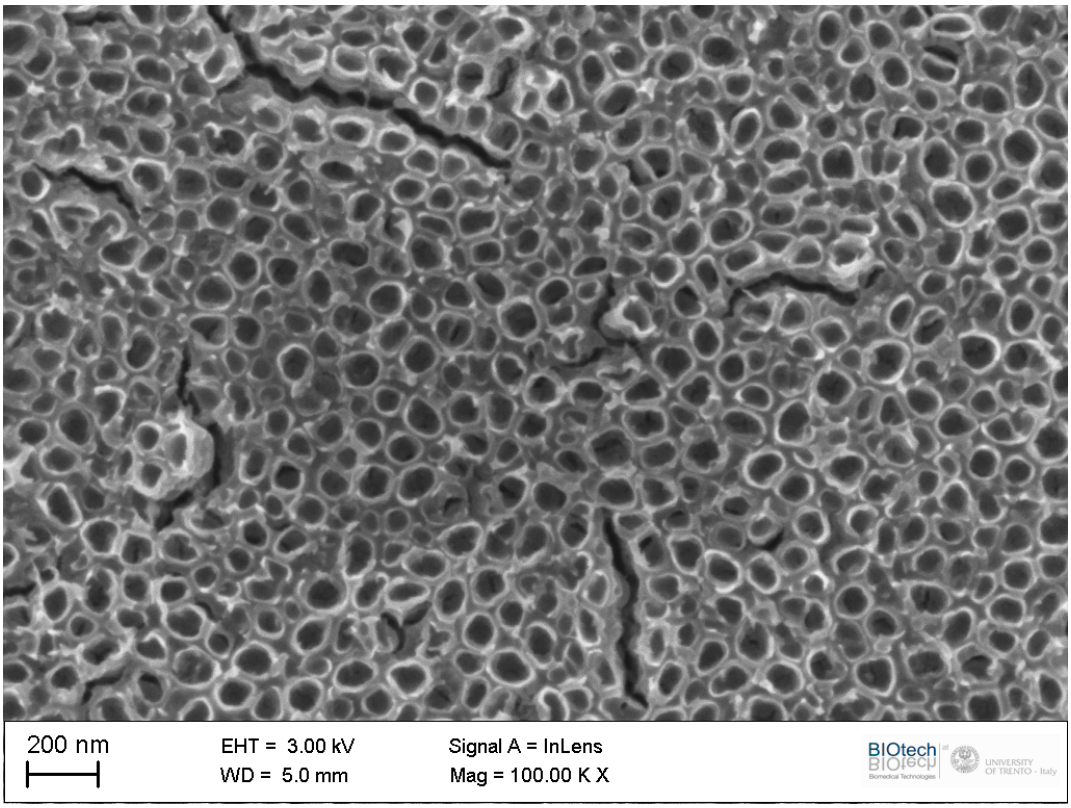

Figure 48. NNT5 image.

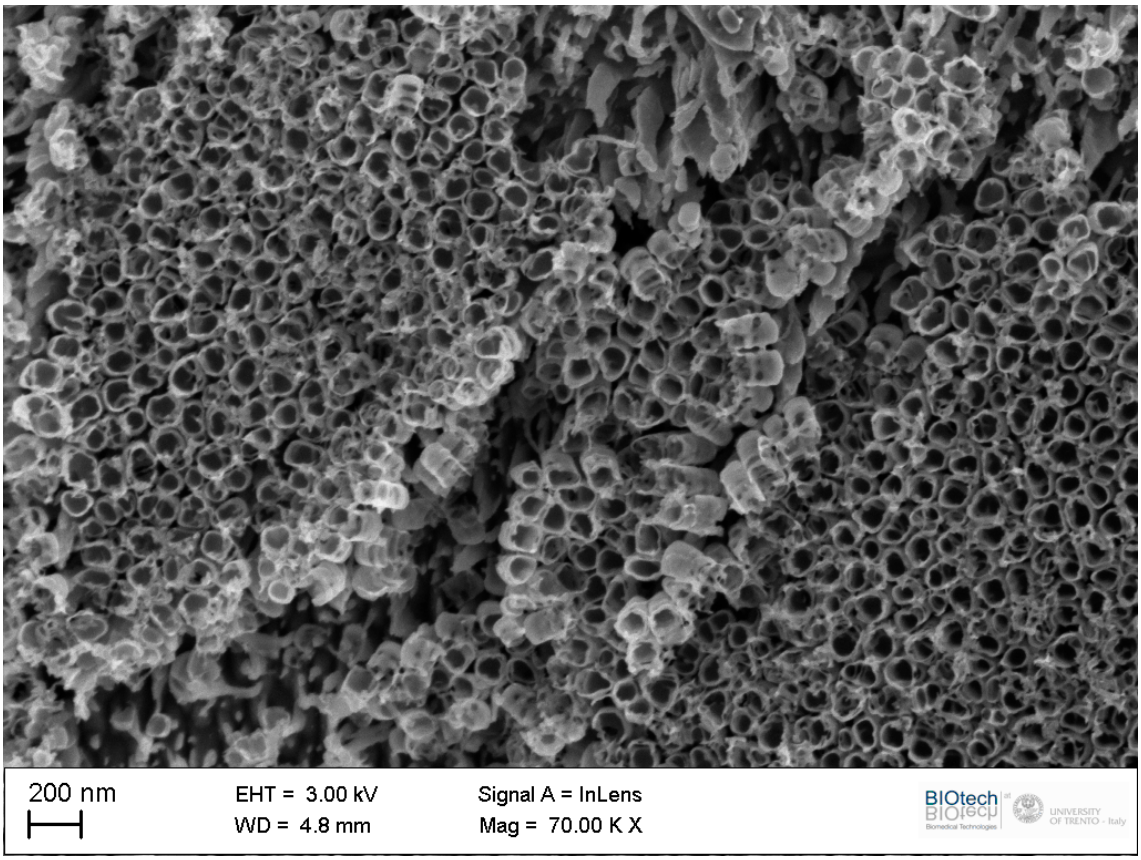

Figure 49. NNT6 nanotubes.

In figures 48 and 49 are presented images obtained from microscope. In them, it is possible to appreciate differences in nanotube characteristics such us internal diameter, length and thickness. However, the only difference between them is the use of the Ti o Pt as cathode; hence, we conclude that, in the same reaction conditions, for Ti cathode we achieved bigger diameters as well as smaller lengths and a certain honeycomb structure in

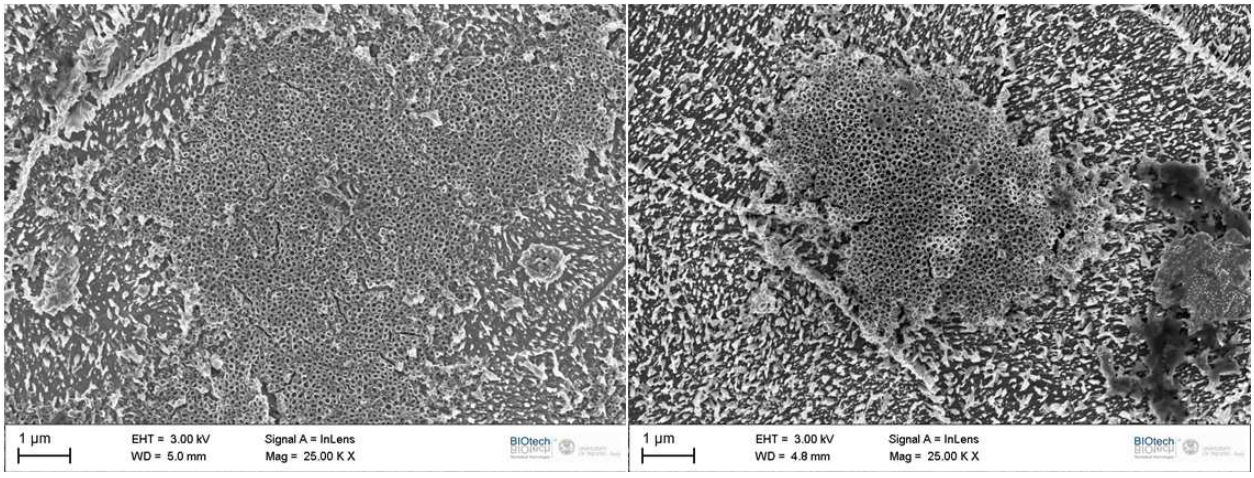

Figure 50. Island structures from NNT5 and NNT6

comparison with Pt.

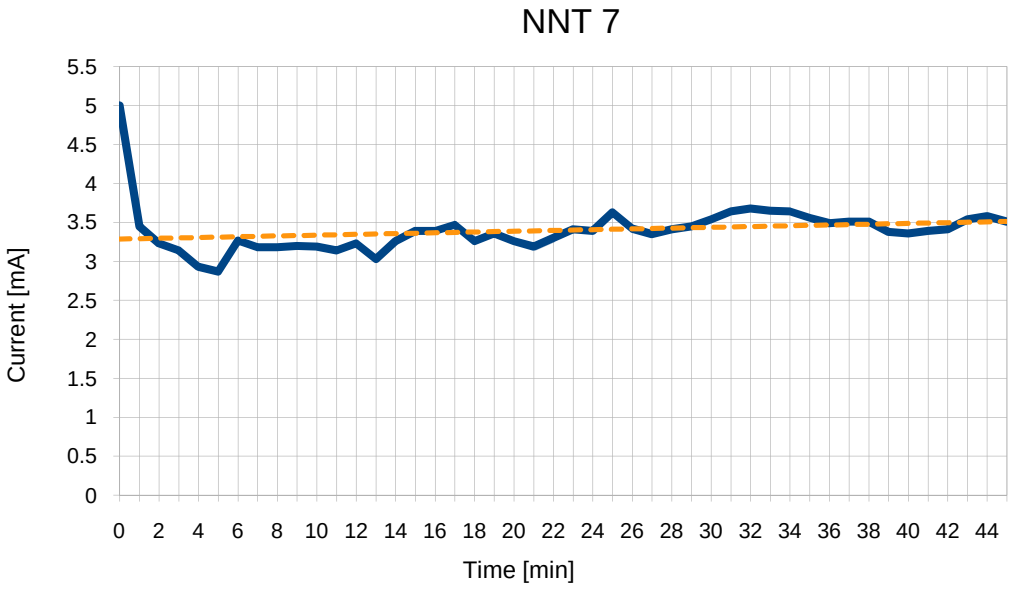

Stirring was used for the first time on NNT7 experiment. Since then, due to results reported on literature and obtained for us, a magnetic stirring was added in all the following reactions. For NNT5 rest of process parameters and the silicon container remains the same, in this case with a little stirring between anode and cathode, over a magnetic base.

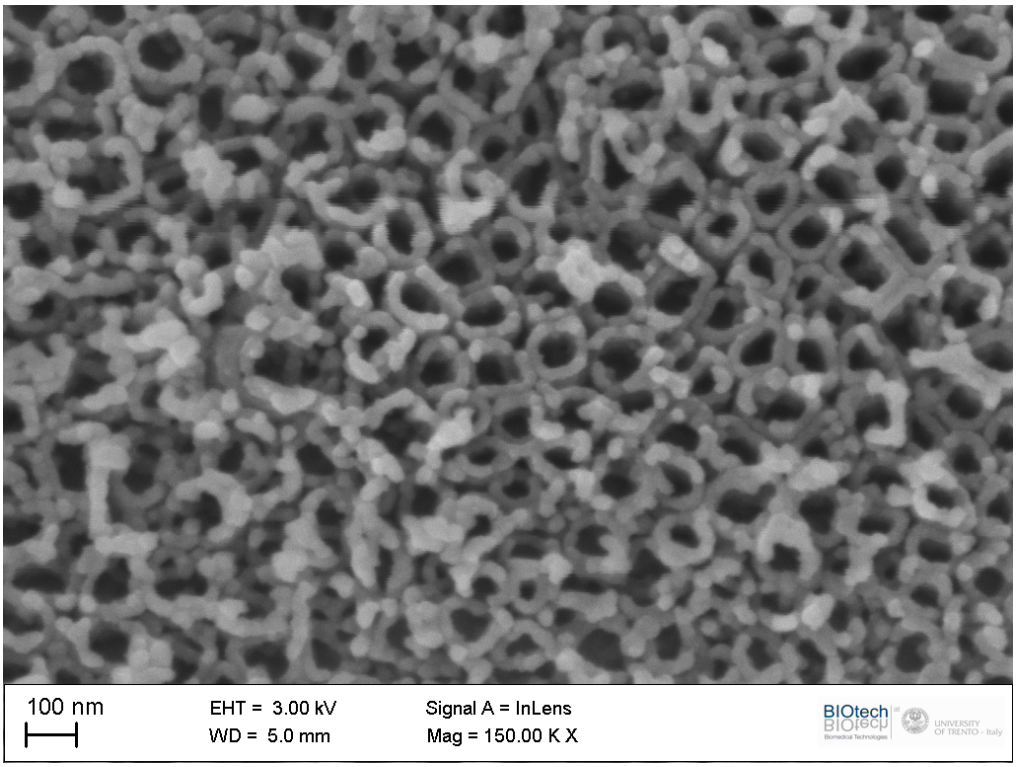

Figure 51. NNT7 nanotubes.

Surface images, as we can see, matched with the nanotube results; local islands where nanotube grows can be distinguished, length and diameter are similar, being thickness higher than for NNT5/6. The appearance of debris over the nanotube structures is another important aspect, justified by the presence of the stirrring.

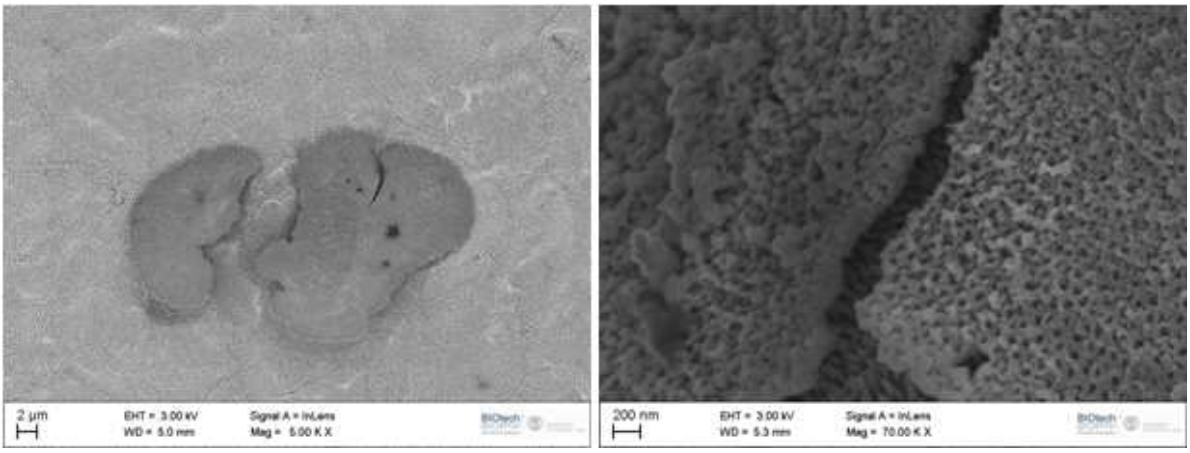

Figure 52. NNT7 ESEM images.

At this point, taking in consideration that nanotube conditions were achieved, our first objective was to extend the nanotube surface in all the sample instead of local areas as is shown above. In this manner, we tried to variate the temperature reaction with the purpose of finding a new way that give us an homogeneus nanotube area.

NNT8, NNT9 and NNT10 were carried out in Teflon receptacle with intial geometry described in figure 26. The entire assembly was inmersed in a temperature control device for the experiments. Electrolyte solution was the same that used before as well as platinum cathode and stirring. For the two first experiments time reaction were 45 min while third one were 60 min. Summarizing:

	Cathode	Time	Volt	Temperature	Stirring
NNT8	Pt	60 min	20	25°	SI
NNT9	Pt	45 min	20	35°	SI
NNT10	Pt	45 min	20	45°	SI

Table 3. NNT8, NNT9 and NNT10 process parameters.

This time,we have noted important results regarding the influence of the temperature. As is shown, the is an evident relationship between temperature and current flow during

reactions. Thus, when temperature is increased intensity increases too keeping constant the other conditions.

We did not find nanotubes in all these reactions. However, experiments served us to work with the new device, making a dynamic control of temperature and estimating its influence with current. In the same way, we realized that, with the equipment we had, a precise temperature control of more than 40° was difficult to obtain. More variability was observed using the ammeter.

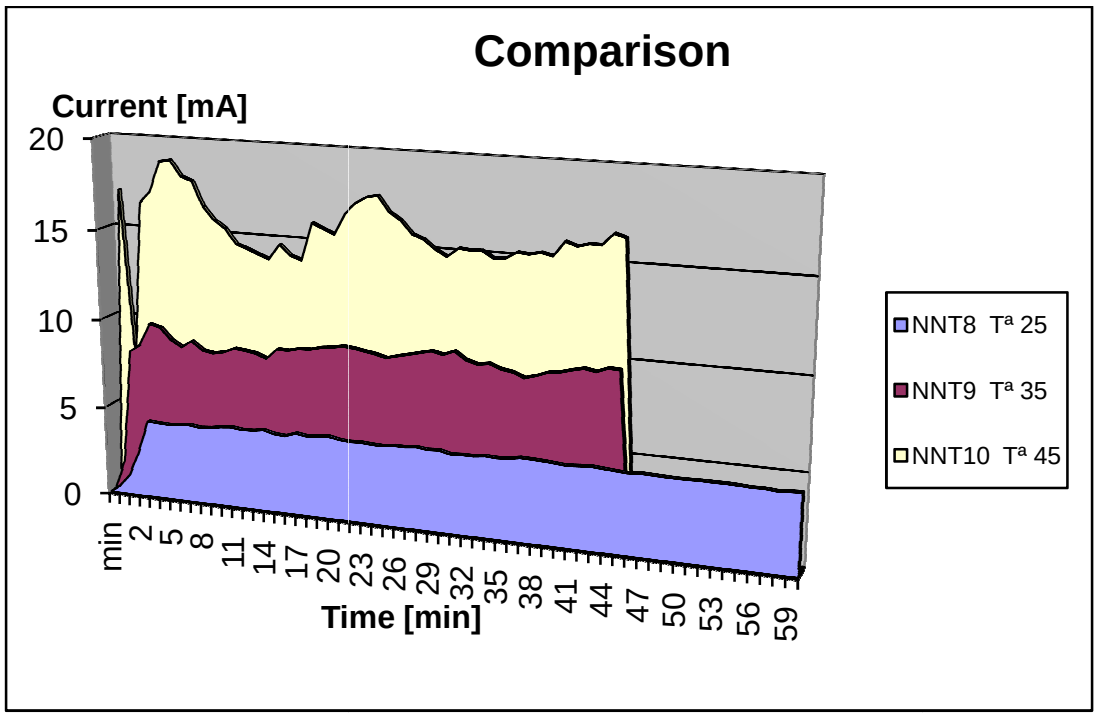

Next experiments were done changing time of anodizations. The idea was to prove that by adjusting temperature and reaction time we could achieve good results keeping constant the product of the previous variables. In this manner, we tried to join long times with low currents intensities (low temperatures), medium intensities with room temperatures, and high currents with short times. Temperature control device had a refrigerating system that allow us to work with lower temperatures than room conditions, taking advantage of this we decided to work around the room temperature with two experiments at 15° and 35°. To make sure of the first results a third reaction would be done.

Main parameters of NNT11, NNT12 and NNT13 anodizations are presented below. As we can observe, electrolyte, stirring and voltage are equal to the others; also, we used vertical geometry and immersed container in the temperature control. In order to maintain constant the parameters, the stirring was fixed at the speed of 350 rpm for the rest of the work.

	Cathode	Time	Volt	Temperature	Stirring
NNT11	Pt	90 min	20	15°	SI
NNT12	Pt	45 min	20	25°	SI
NNT13	Pt	22 min	20	35°	SI

Table 4. NNT11, NNT12, NNT13 process parameters.

Again, current versus time graphics give similar results as first nanotube anodizations; we can observe that the reaction begins with high currents for a period of 5 minutes, afterwards it is appreciated a slight rise ending practically constant on time. In the same way, this same relation between intensity and temperature are present for NNT11, where lower currents are achieved.

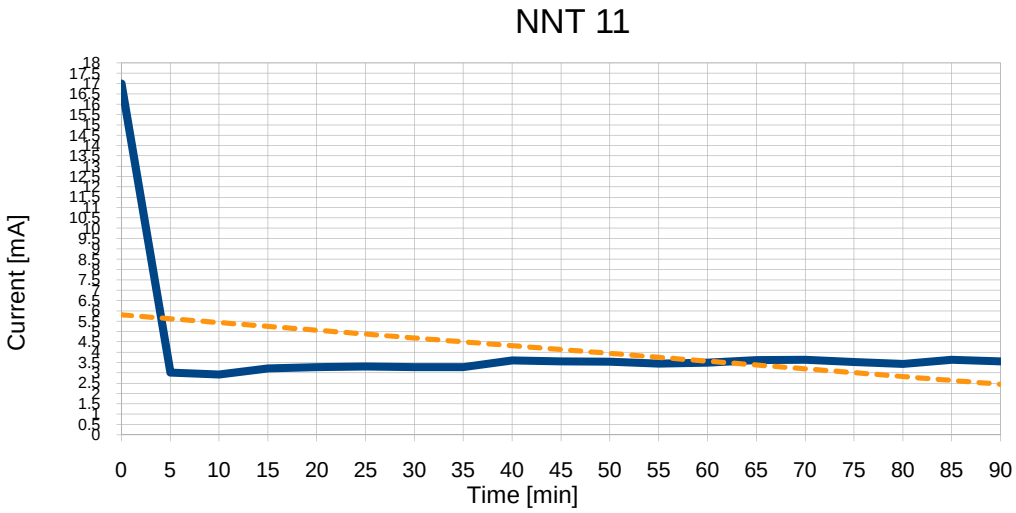

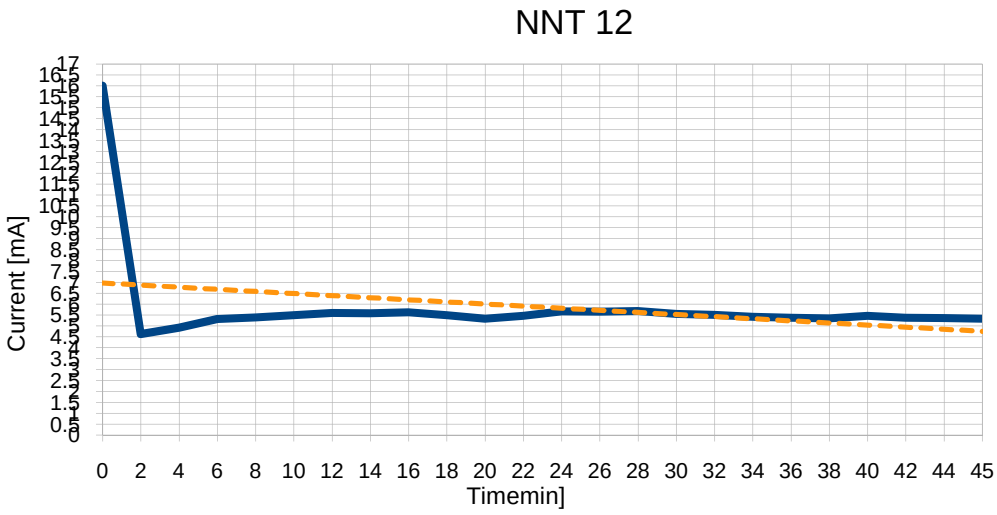

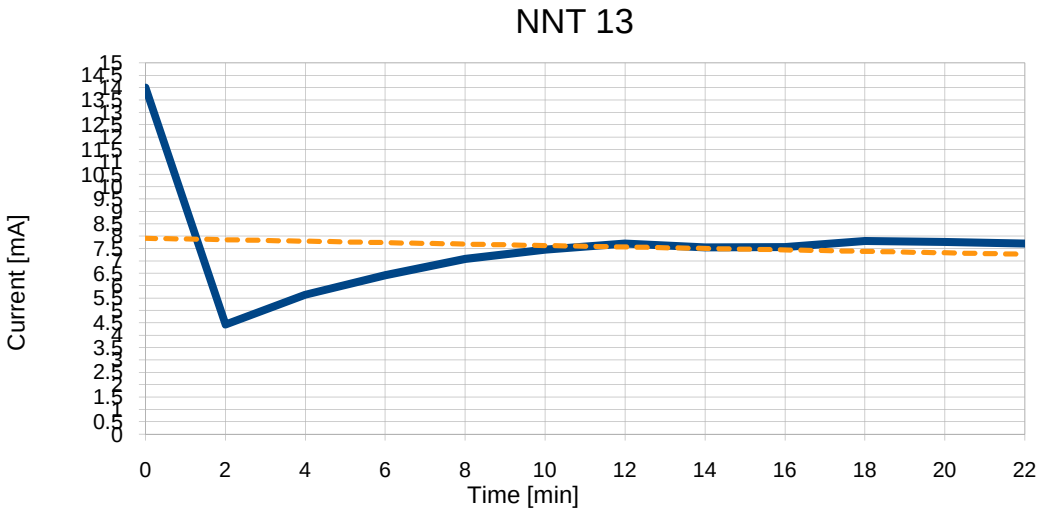

Concerning the ESEM analysis, nanotube areas were achieved again in more proportion than at the beginning. Nevertheless, we could not talk about an homogenous full space of nanotube as we expected, and only in zones close to the border were found.

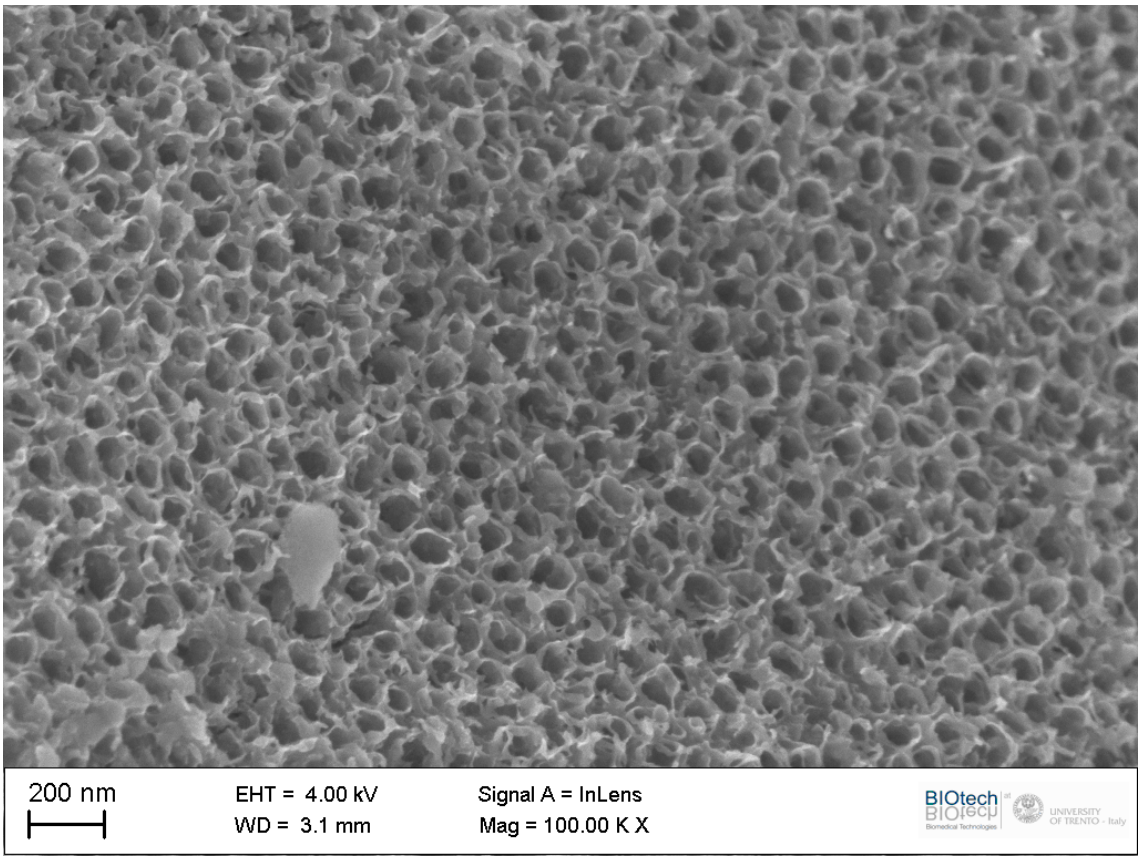

Figure 53. NNT12 surface.

Although in NNT11 were not found nanotubes, best results until now were obtained in NNT12 and NNT13. In both of these cases we achieved areas much bigger than in first experiments, disappearing island structures. Following reaction parameters, long anodization times were discarded in next experiments according to non-results obtained in NNT11.The product between current and time received a special worth.

By the same way, new nanotube properties were found such as a honeycomb structure with different thickness for the tubes. Is important to note that for these experiments we did not take special cares to analyze the structures obtained because our major purpose was to achieve an homogenous layer over the anodizated surface.

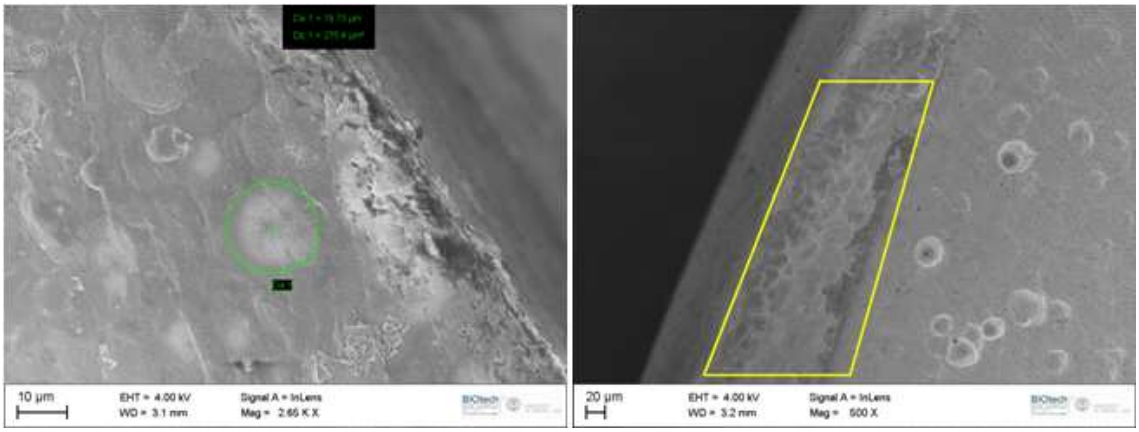

Figure 54. Delimitated area where nanotube structures were found.

Either way, it is noteworthy that for the first time we understood the influence of the electric filed concentration in areas close to the cathode, as is shown in figure 28. So, there were regions more affected by anodizations and it was impossible to get similar conditions in all the surfaces among the titanium plates.

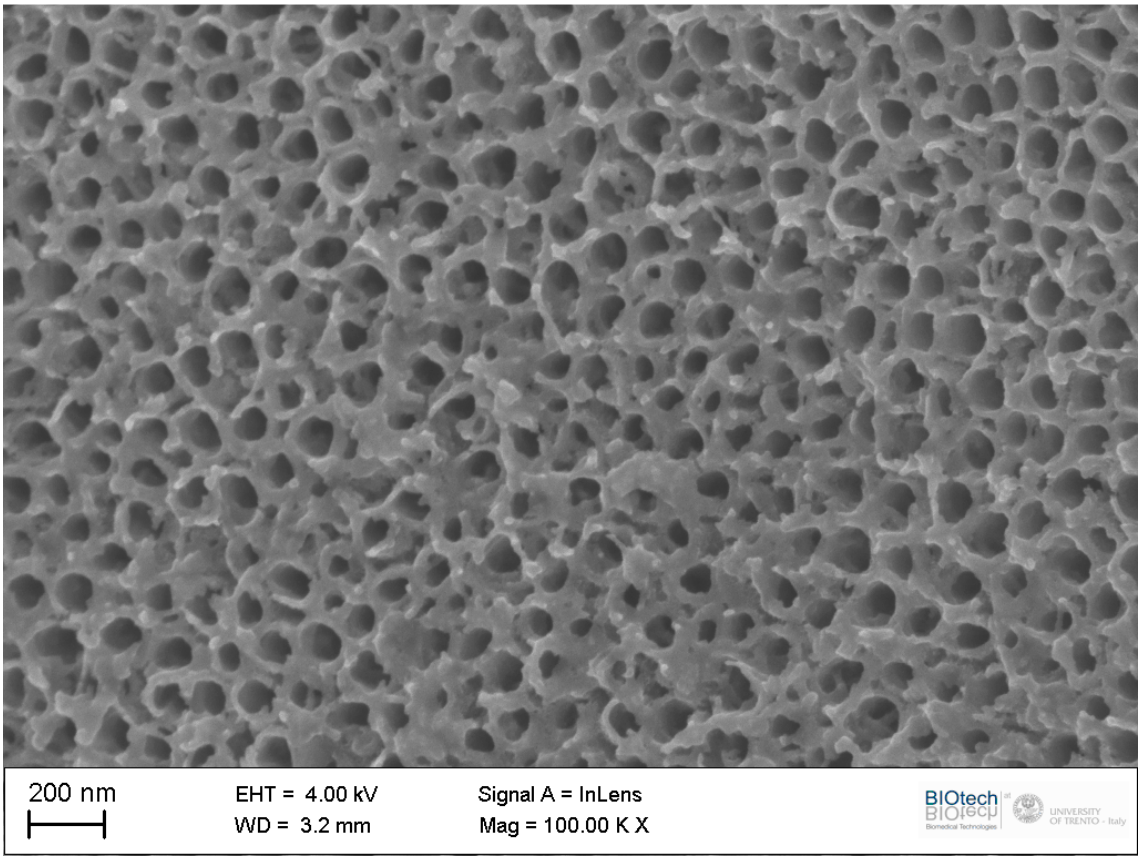

Figure 55. NNT13 nanotubes.

At this stage of work, oblique geometry was designed in order to resolve or minimize effects of the field concentration. In this mode, one test was carried out with NNT14, keeping NNT15 and NNT16 with the old geometry. Process parameters are as follow:

	Cathode	Time	Volt	Temperature	Stirring
NNT14	Pt	22 min	20	35°	SI
NNT15	Pt	22 min	20	35°	SI
NNT16	Pt	14 min	20	45°	SI

Table 5. NNT14, NNT15, NNT16 process parameters

As we can see, the only difference between NNT14 and NNT15, is the geometric arrangement. NNT16 is developed with a short anodization time due to good results obtained with NNT12/13 and for studying where it was the limit using brief times and high temperatures.

We did not achieved results confirming our hypothesis regarding no field concentration or short anodization time experiments because of a predictable mistake in electrolyte preparation. Thus, no nanotubes were found in ESEM analysis. However, it was understood that a small variation of process parameters could change our results.

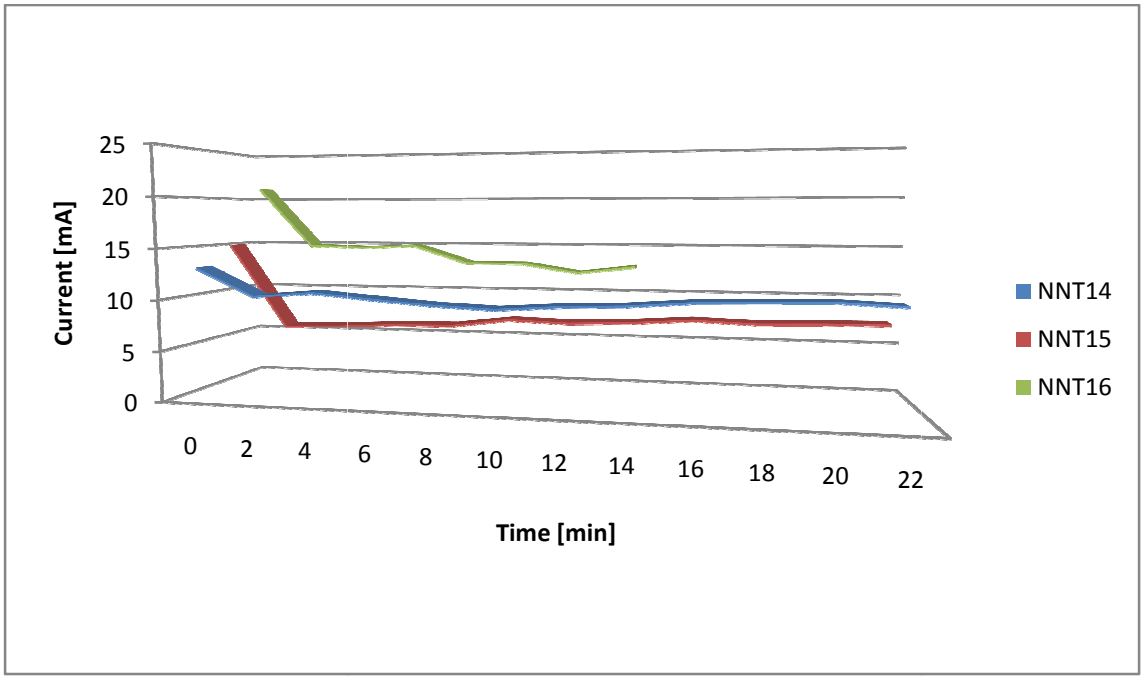

In the same way, and after taking one macro-photo of the surface sample, it was observed that the problem related with the concentration of current had been minimized but not

completely solved. In figure 56 are presented two pictures with the old and new geometry representing the visible no homogeneities.

Figure 56. Visible surface no-homogeneities for new and old geometry respectively.

Both NNT17 and NNT18 were carried out repeating conditions of NNT15 and NNT16 taking care in all the reaction stuff, this time the problem was the ESEM availability. Eventually, when we received an appointment, square plates of titanium arrived at our disposal. Since this moment, NNT17 and NNT18 analysis was discarded and we quickly started to work in new samples.

First step was to properly cut the original plate in others easier to use and suitable for experiments. Then, we built the plastic piece, shown in figure 30, to hold anode and cathode during anodization and samples were washed following steps described before.

Regarding process parameters used this time, we decided to repeat optimal conditions in nanotube growth achieved until now. So, NNT11/12/13 parameters were reproduced as follows.

	Cathode	Time	Volt	Temperature	Stirring
NNT19	Pt	45 min	20	25°	SI
NNT20	Pt	56 min	20	15°	SI
NNT21	Pt	38 min	20	35°	SI

Table 6 NNT19, NNT20 and NNT21 process parameters.

Specifically, anodization times were different from the previous experiments, in fact they were calculated in real time. We knew that good results had been found for 45 min, 20V at room temperature keeping constant the other parameters. Therefore, our idea was to note new current intensities for NNT20 NNT21 reactions (unknown for square plates) and estimate the experimental time keeping the same product "current per time" among all the reactions. As is mentioned, the experiments started and during anodizations we realize how long should be the reaction. For this method, NNT19 was used as reference in new titanium plates.

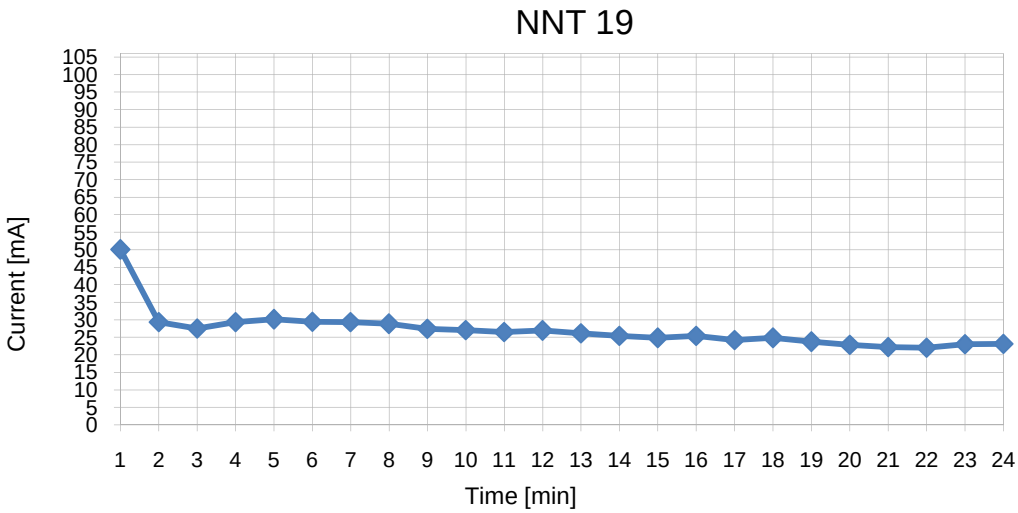

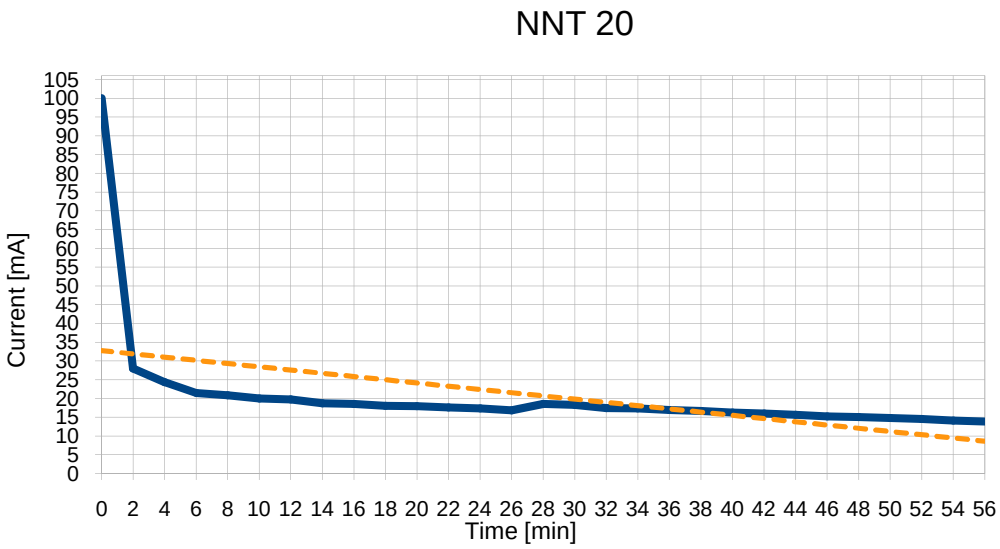

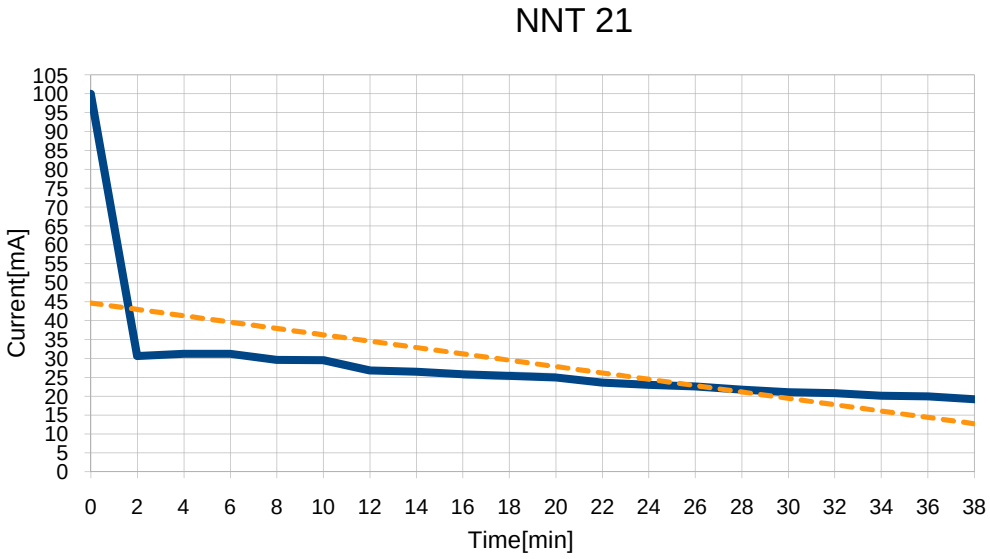

With these tests, our first surprise when we took the macro-images was to find a homogeneous surface after anodization never seen before in other reactions. Figure 57 shows, in the middle part of the sample, this characteristic.

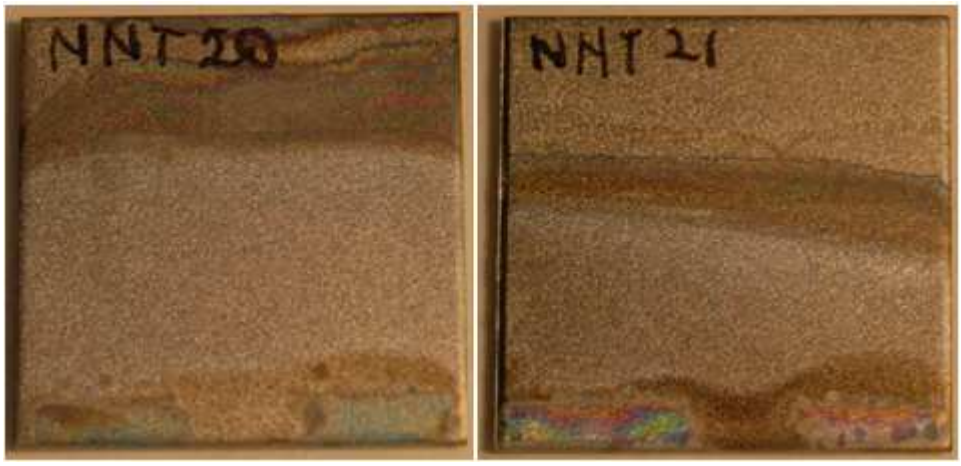

Figure 57. Entirely parallel surface.

By the same way, titanium plates were transported to Mattarello to ESEM analysis. The objective we were looking for appeared during the analysis: a full sea of nanotubes was found in NNT19. However, one of the most important result that in the others samples nanotube structures appeared homogeneously everywhere as well. Thus, our hypothesis in relation to control temperature and anodization time was correct.

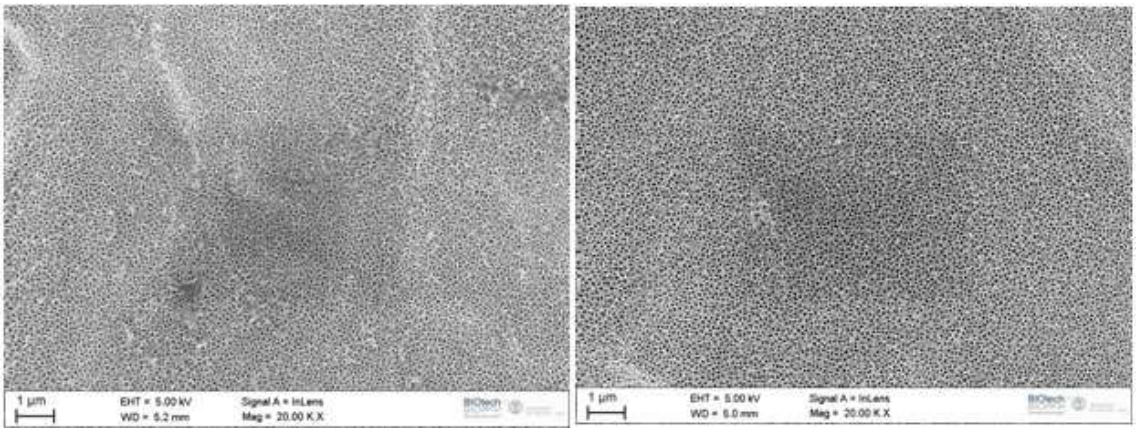

Figure 58. Sea of nanotubes

Next, pictures obtained from last experiments:

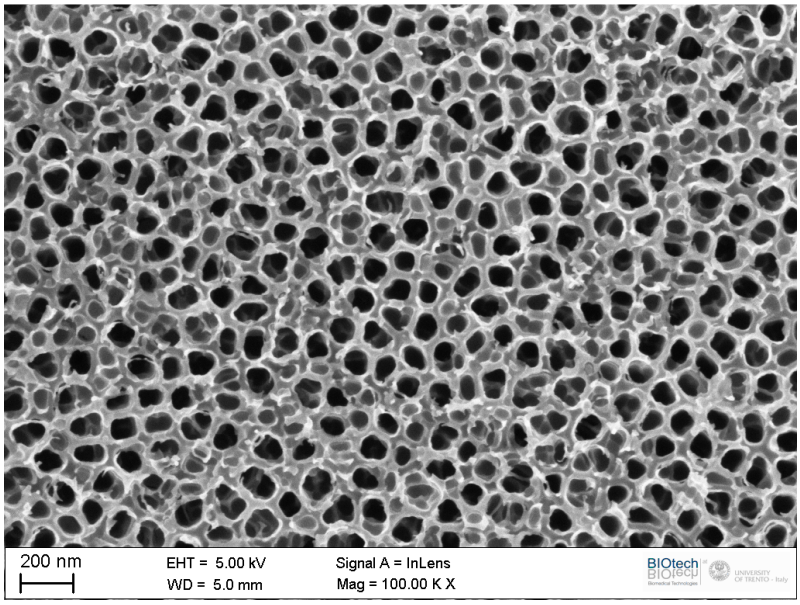

Figure 59. Detail of NNT19 surface

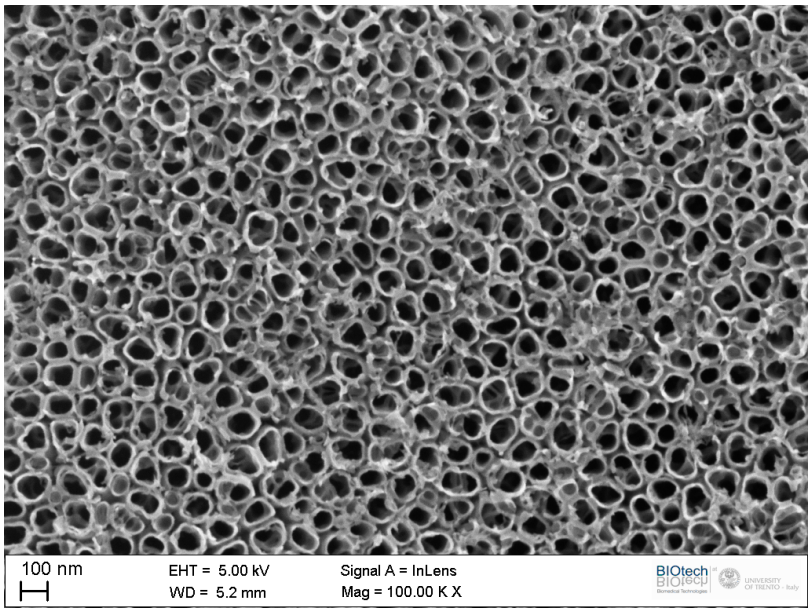

Figure 60. NNT20 image.

As we can see, different nanotube structures were obtained. First one, corresponding to NNT19 presents the most honeycomb likeness achieved, being the two next ones, NNT20/21 quite similar. Also is important to note the presence of debris; specially for NNT21. Parameters related with diameter and thickness is described in next section with the discussed methods.

At this stage of the work, our idea was make a spectrum following different reaction temperatures allowing us to understand main characteristic of nanotube growth and its evolution, geometric shape and ensure that conditions were reproducible.

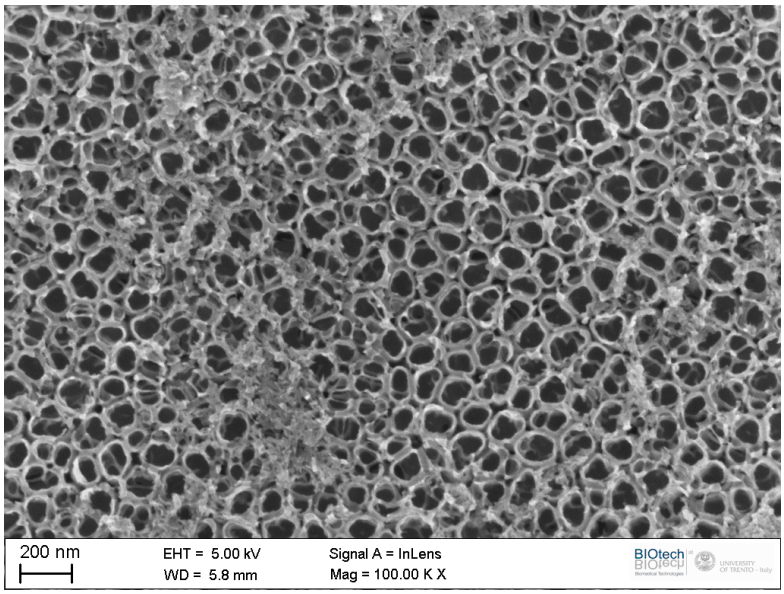

Figure 61. ESEM NNT21 picture

In this manner, next NNTs series were carried out keeping in mind that we had results for 15°, 25° and 35°. In this mode, we did tests for 18°, 22°, 28° and 32° where we were sure we are going to have good results.

Last experiments on titanium square plates were done like the others. Thus, water with 0.5 weight% of HF was used as electrolyte, Teflon container with temperature control and magnetic stirring was present during experiments and geometric arrangement was the same as well. The only difference this time was a new power supply that allows us, due to a connection with a PC that saves the current and voltage data of reactions, to focus on others arrangements during the anodization time.

One more time, data from NNT19 was taken as reference to decide, during anodizations, reaction times. At this point, samples were properly anodizated but a problem with the new power supply device appeared at the moment to check intensities measured after reactions. This was due to the measurement error of the machine (5 mA). Because of this non exact curves current vs time were achieved.

However, samples were analyzed and fulfilled our expectations. In fact, a homogeneous layers of nanotubes were present in each one of them. With this, the relative stage on nanotube growth in controlled conditions was finished; the only thing left was a special analysis of pictures obtained for characterizes geometric properties discussed in next paragraph.

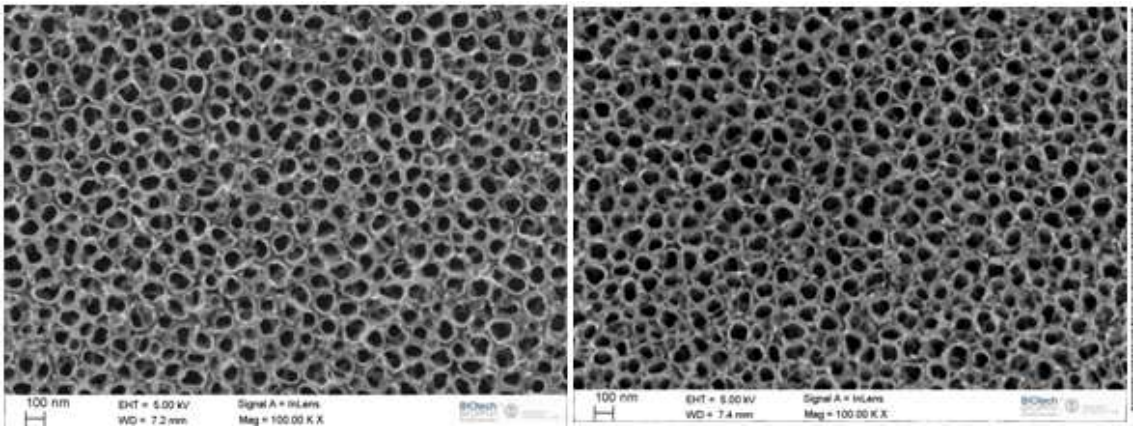

Figure 62. NNT22 and NNT23 nanotubes

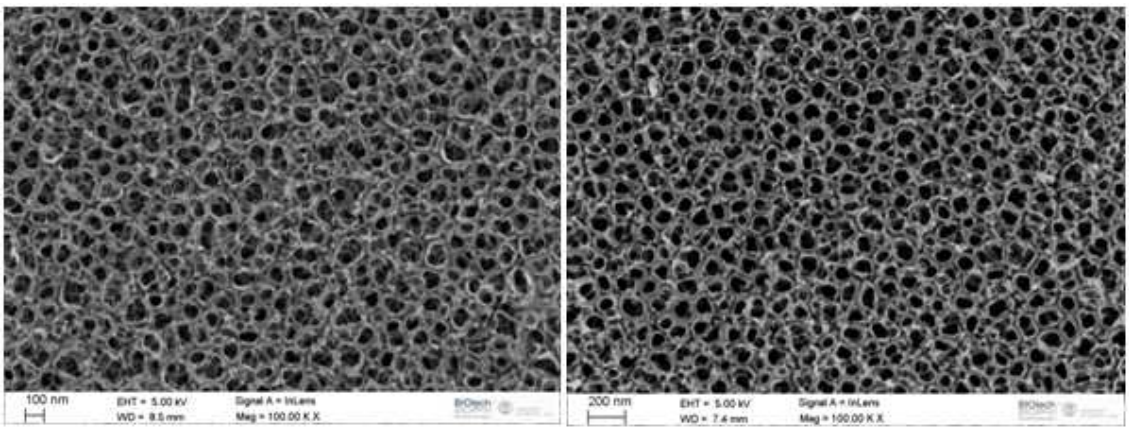

Figure 63. NNT24 and NNT25 images

3.1.1 Image analysis.

As is mentioned above, ImageJ software was used to analyze different pictures obtained from ESEM microscope to understand geometric properties within the spectrum developed depending on anodization temperatures.

In this mode, scale of images was defined following the legend before taking measurements. Then, a threshold was applied to differentiate pixels corresponding to dark areas inside of nanotubes and finally, measurement such as internal area and perimeter of nanotubes, diameter or circularity were checked. 30 measures were done per each image.

Another important parameter taken into account is the Feret's diameter defined as the longest distance between any two points along the selection boundary. Circularity of nanotubes correspond to 4π*area/perimeter^2; a value of 1.0 indicates a perfect circle. As

the value approaches 0.0, it indicates an increasingly elongated shape. Roundness is 4*area/(π*major_axis^2).

Following table shows average parameters from lowest temperature to highest.

	Area [nm^2]	Perim. [nm]	Circ.	FeretDiam. [nm]	Roundness	Temp
NNT20	44565	3314	0,510	1157	0,440	15°
NNT22	60712	3759	0,535	1336	0,448	18°
NNT23	45929	3472	0,473	1191	0,424	22°
NNT19	60349	4253	0,420	1434	0,392	25°
NNT24	30438	3518	0,312	1271	0,263	28°
NNT25	39314	3590	0,365	1265	0,322	32°
NNT21	52116	3450	0,548	1196	0,492	35°

Table 7. Process parameters.

In next graphs are collected data represented in function of temperature.

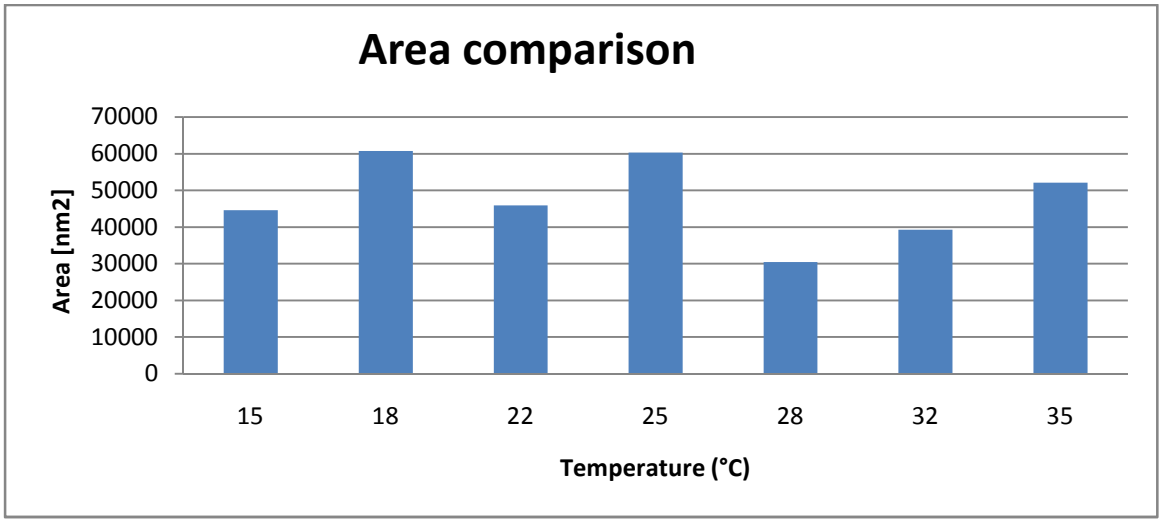

Internal area of nanotubes does not follow a lineal behavior for lower temperatures, however among 28°, 32° and 35° anodization temperatures an increase is appreciated.

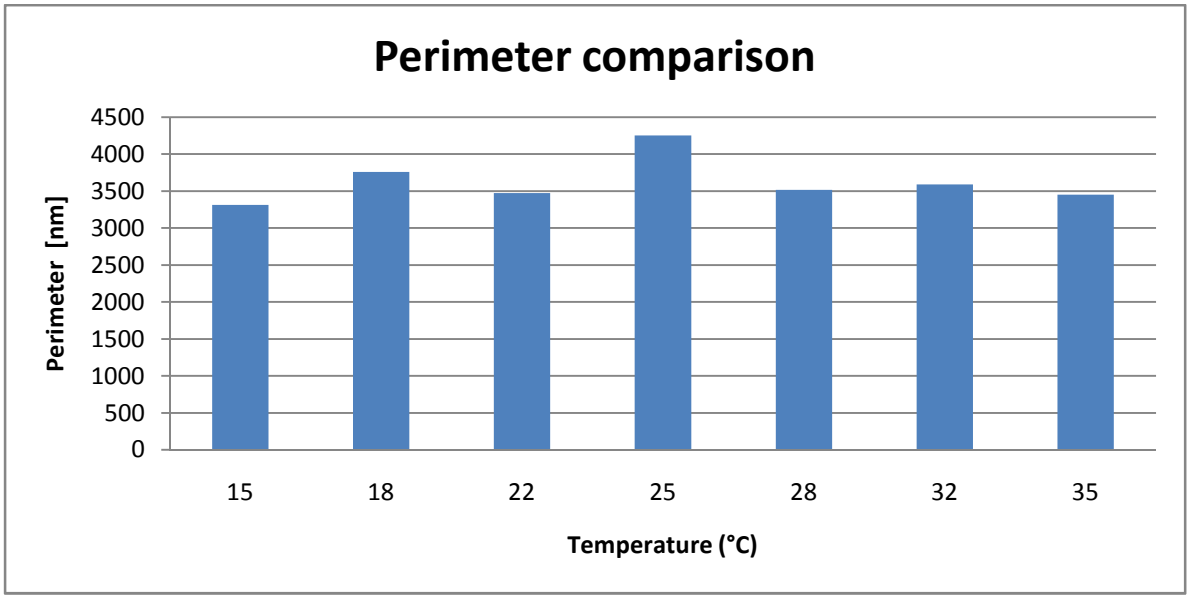

For internal nanotube perimeter no big differences on data distribution were distinguished, being NNT24 (28°) quite high if we compare it with its smallest area. Thus, we can think that if the area is low and the perimeter is high, circularity shape of NNT24 will be low. In the same way, is important to note that not only nanotube shape changes if taken images are depending on temperatures

With this I mean that the titanium oxide where are immersed the structures, has the borders completely differentiable for each nanotube at the beginning (low temperatures), figure 63a, instead of results observed for medium temperatures such us NNT24 (28°) or NNT19 (25°) where a honeycomb structure in titanium layer seems more "nanoholes" than nanotubes. Specifically, for NNT24 it is possible to talk about a chaotic nanohole distribution with no vertical dimension. However, for higher temperatures this behavior disappears again and borders are distinguished as in NNT21.

Nevertheless, factors such as solution experiments or exact location analysis during ESEM stage, can influence significantly in the results obtained. We remind that NNT19/20/21 were carried out different days than NNT22/23/24/25.

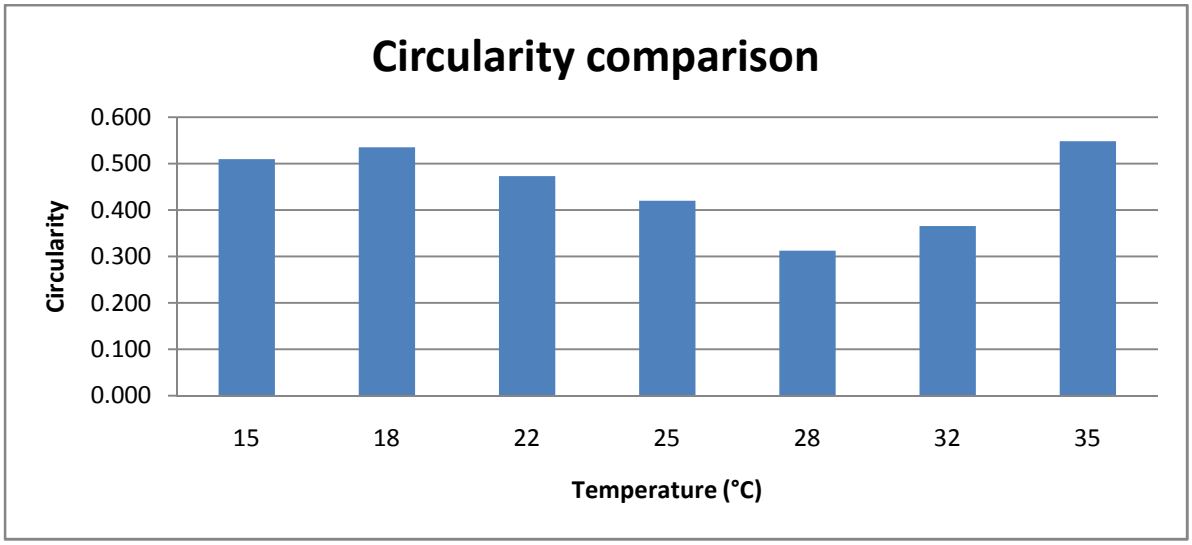

As expected, circularity follows a relation between area and perimeter; for lower areas and higher perimeters the nanotube loses its circular shape. As it was mentioned before, we can observe less well-defined nanotubes that have a lower circularity for middle temperatures.

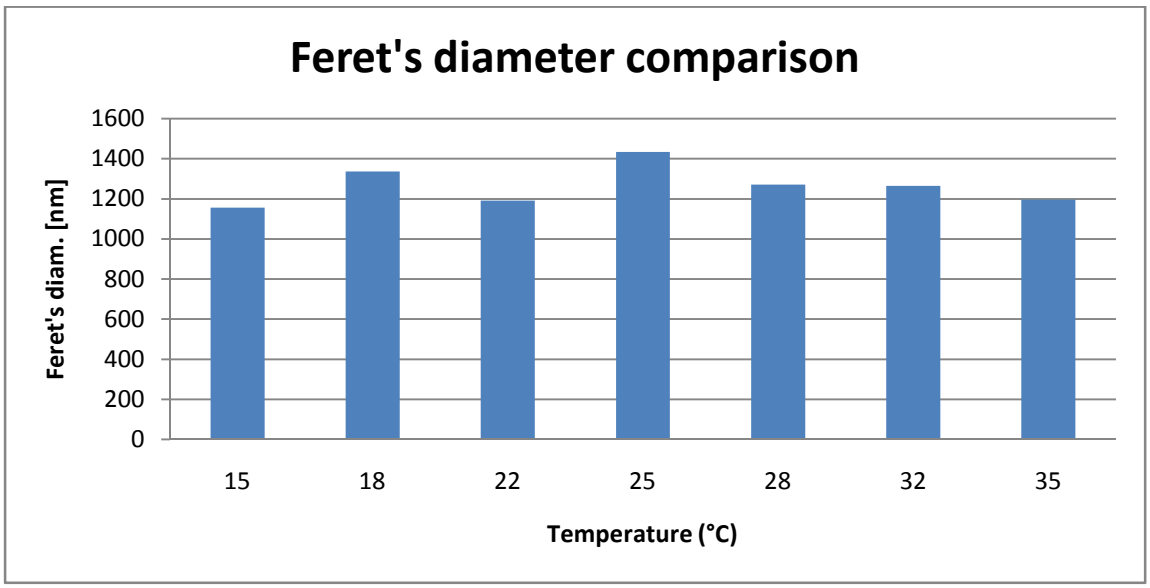

Both Feret's diameter and roundness comparison follow similar distribution than perimeter and roundness respectively and give us an idea that the major axis in each sample is close to diameter estimated.

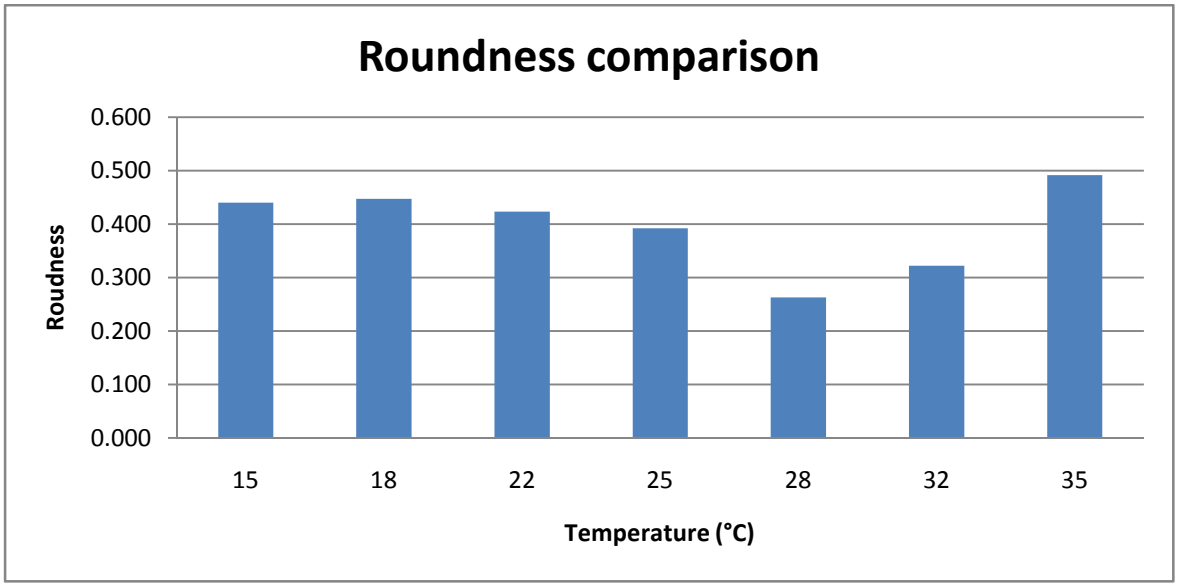

Regarding lengths of nanotubes, we tried to measure this parameter in different ways. First one was finding fissures during ESEM analysis and applying an angle in the base; in this manner, as shown in figures 49 and 52, there were estimated lengths of 175nm. However, once homogeneous surfaces were achieved it was much more difficult to find this advantage in microscope sessions.

Then, it was taken in consideration a possible surface breakage or X-ray analysis on the anodizated samples with good results but due to short time remaining for the work and availability of devices, we preferred to continue with the experimental procedure in Padova sputtering FTO glasses.

3.2 Anodization of sputtering samples.

Sputtering film reactions were carried out by the same way that was anodizated titanium plates. From the beginning we tried to reproduce conditions achieved for square plates such as solution, voltage and time but quickly we understood that the context were completely different.

In first samples, we realize that keeping attached the film during anodization was very difficult. Consulting literature [5] anodizations of single-layer titanium films was not successful because the material layer at the air-electrolyte interface etched rapidly away and

broke electrical contact with submerged portion of the film undergoing anodization before nanotube could be formed.

However, the solution disposed for this problem, consisted in a bilayer-film scheme for thin film deposition keeping the single layer region completely immersed in the electrolyte and the double-layer region at the air-electrolyte interface, unfortunately the bilayer-film was not at our disposal.

Therefore, we anodizated single deposition layers of titanium taking care during reactions of frequent pitting and fractures on the material. At this point of the work, we tried to obtain a valid conductive surface to assembly at least one solar cell from anodizating sputtering titanium films.

With more time and availability, the optimal solution would have been returning to Maggioni's lab in Padova to re-sputtering a second layer and then anodizate the samples.

Our first idea was to decrease the voltage trying to maintain the film on the FTO glass, because in the first sputtering anodizations the film was suddenly separated.

NNT30 was our first sample analyzed using ESEM. For this test it was chosen one of 500nm sputtering thickness from Padova; 1V was applied during 30 sec., then 2V during 30 sec. and finally 4 min at 5V keeping anodization conditions such as room temperature (25ºC), water with 0.5 vol% HF, stirring and Pt cathode. Superficial pitting on metal surface was noted as well as small bubbles. However, enough area remained to draw some conclusions with microscope pictures. Is important to mention that the samples after reaction were not full of titanium sputtering and some parts over the FTO glass were detached distinguishing two major regions; one of them grey and the other transparent corresponding glass.

As shown in the next figures, a nanoporous region is differentiated corresponding to grey zones and the other, with a dark color and granulose surface of the FTO glass, specially the conductive layer.

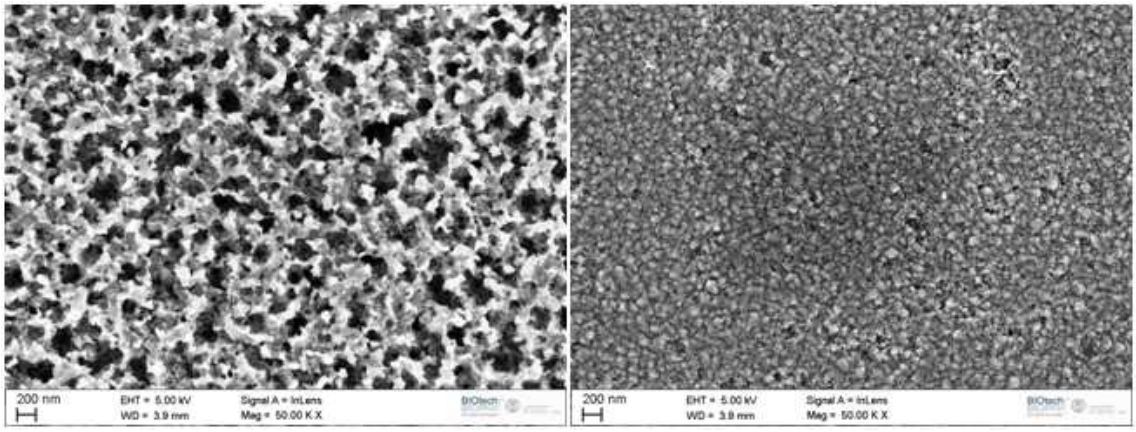

Figure 64. Right part corresponds to remaining titanium and left part conductive glass.

Nevertheless, another important result achieved checking images is the fracture mechanism of titanium film. At the beginning we thought that this process only was produced along the borders of titanium, but breaks in the middle of homogenous remaining film was also found. Figure 66 and 67 show this process.

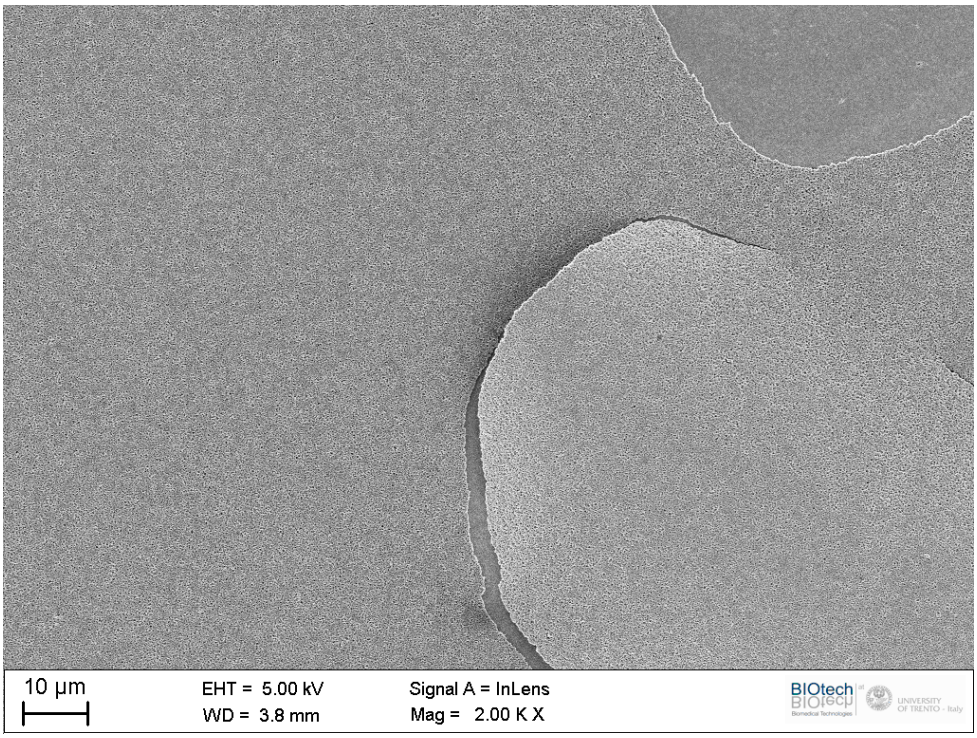

Figure 65. Internal surface fracture

Our first purpose in this stage was like with titanium plates: find the optimal conditions to achieve a homogeneous layer over the surface with the higher specific area as was possible, trying to produce nanotube growth situation.

One more time we took a 500nm sputtering sample for next anodization, process parameter of NNT30 were kept changing only the voltage to 10V. For this sample NNT31, anodization time was 5 seconds; this can give an idea of how much quick film were detached of the surfaces. In this case we had to stop manually power supply after checking that the metal film was being "volatilized".

However, again we had "material" to focus with ESEM microscope and similar images were obtained. An estimation of length was done with photo shows below around 150nm.

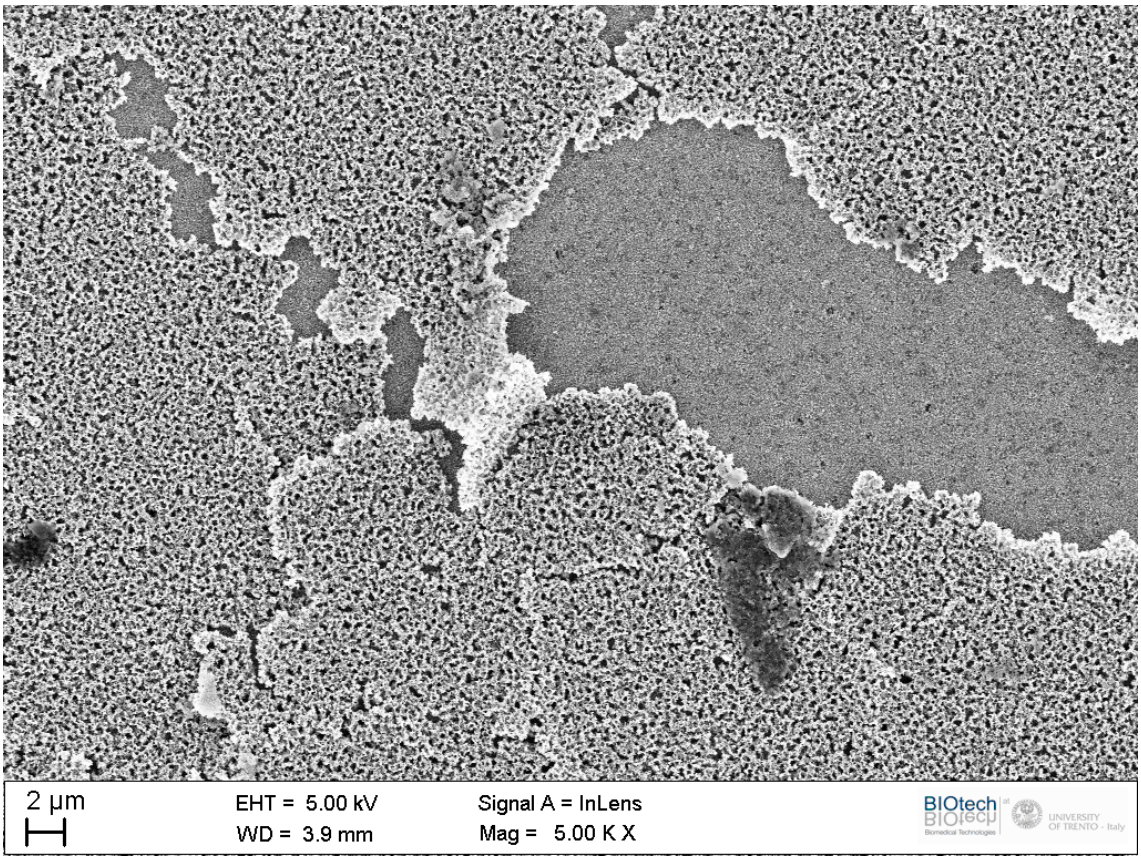

Figure 66. Limit surface fracture.

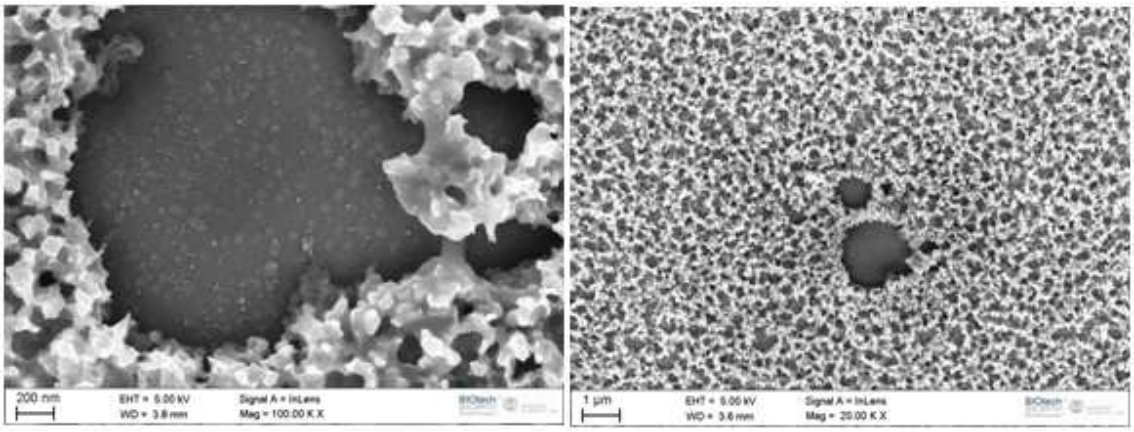

Figure 67. Anodization sputtering film.

At this point, we realized that it was necessary to introduce new changes among reaction conditions to move us towards somewhere. In this manner we decided to prove a decrease of one order of magnitude the voltage applied. Notation NNTX"b" is used to identify that each sample was anodizated twice as is commented before, as well as 500nm sputtering thickness was used in next anodizations. Process parameters of NNT32, NNT32b, NNT33 and NNT33b are described in next table.

	Cathode	Time	Volt	Temperature
NNT32	Pt	45sec	0,2V	25°
NNT32b	Pt	75sec	0,3V	25°
NNT33	Pt	30sec	1V	25°
NNT33b	Pt	30sec	0,5V	25°

Table 8. Process parameters.

By the same way, intensities during experiments were taken manually as well as different stage was noted. This is the case of NNT32; in first step 15 sec., the reaction started normally with no lost of material from the glass, but around 30 sec. a pitting appeared forcing us to stop the experiment after 45 sec. Also for NNT32, at 10 sec, were observed bubbles over the surface and for 30 sec. a black color appeared on the metal film, this time pitting arrived after 75 sec.

Carrying out NNT33s samples we realized that even before applying the voltage between cathode and anode the reaction started on titanium film. After 30 sec. the sputtering surface had become transparent.

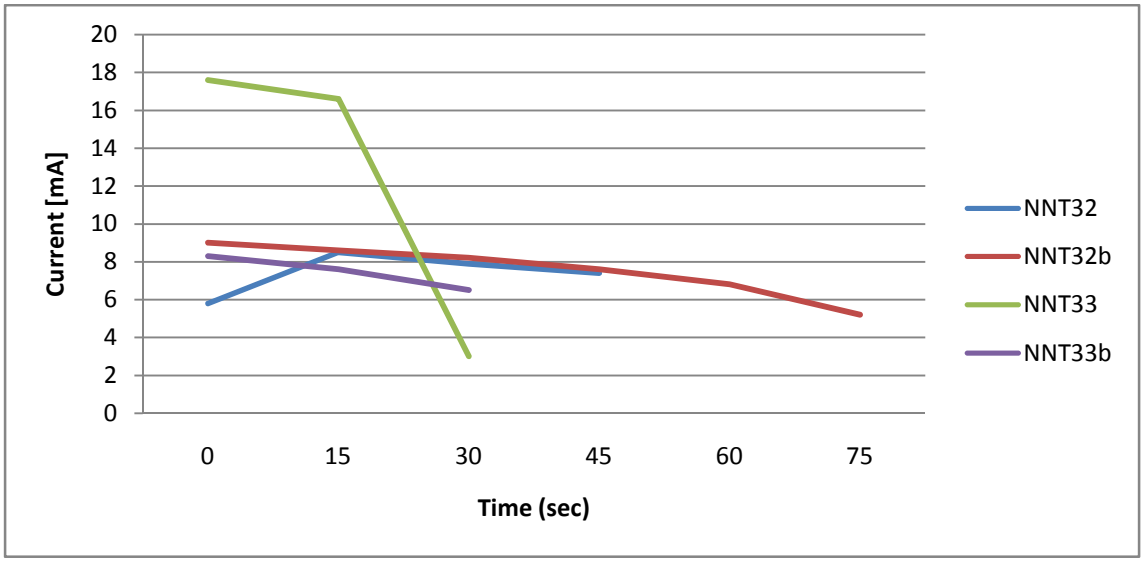

At least we could identify some homogenous surfaces over the black part of NNT32 and ensure that transparent results on samples were not transparent nanotube surfaces by analyzing ESEM images as we had wanted to dream.

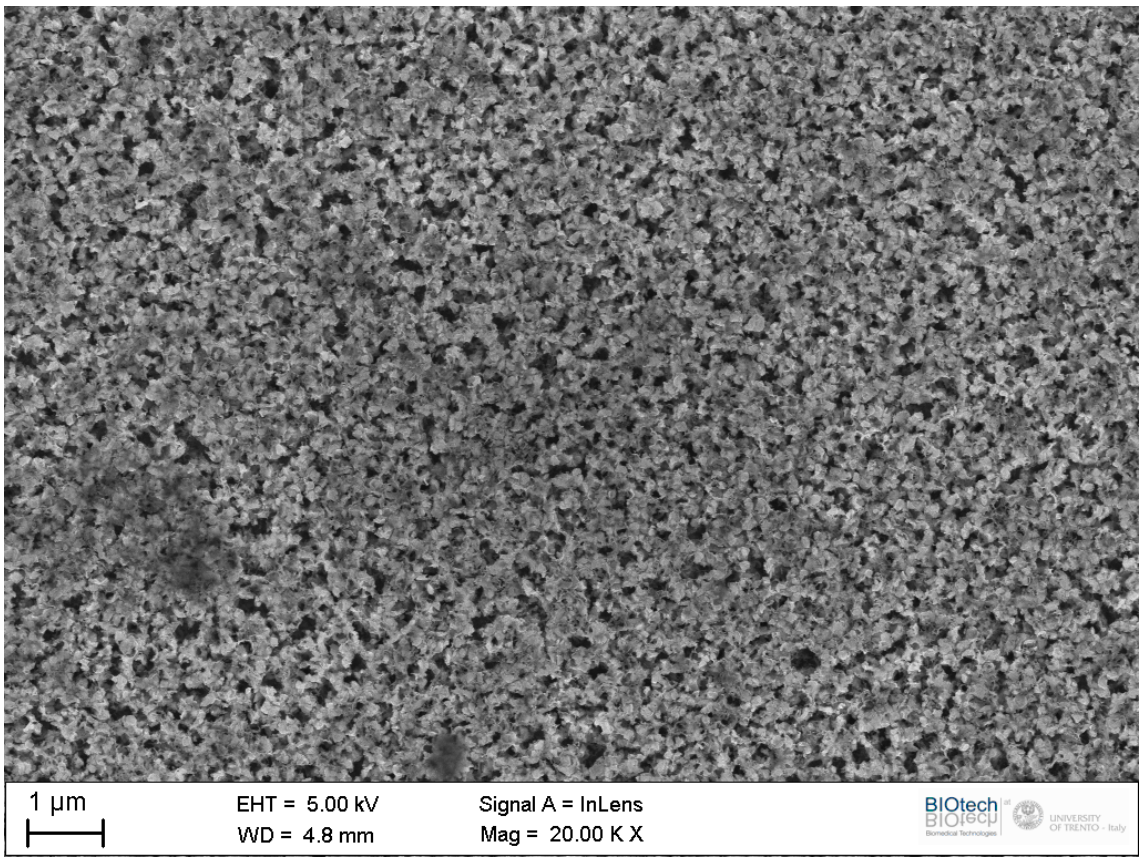

Figure 68. NNT32 surfacce.

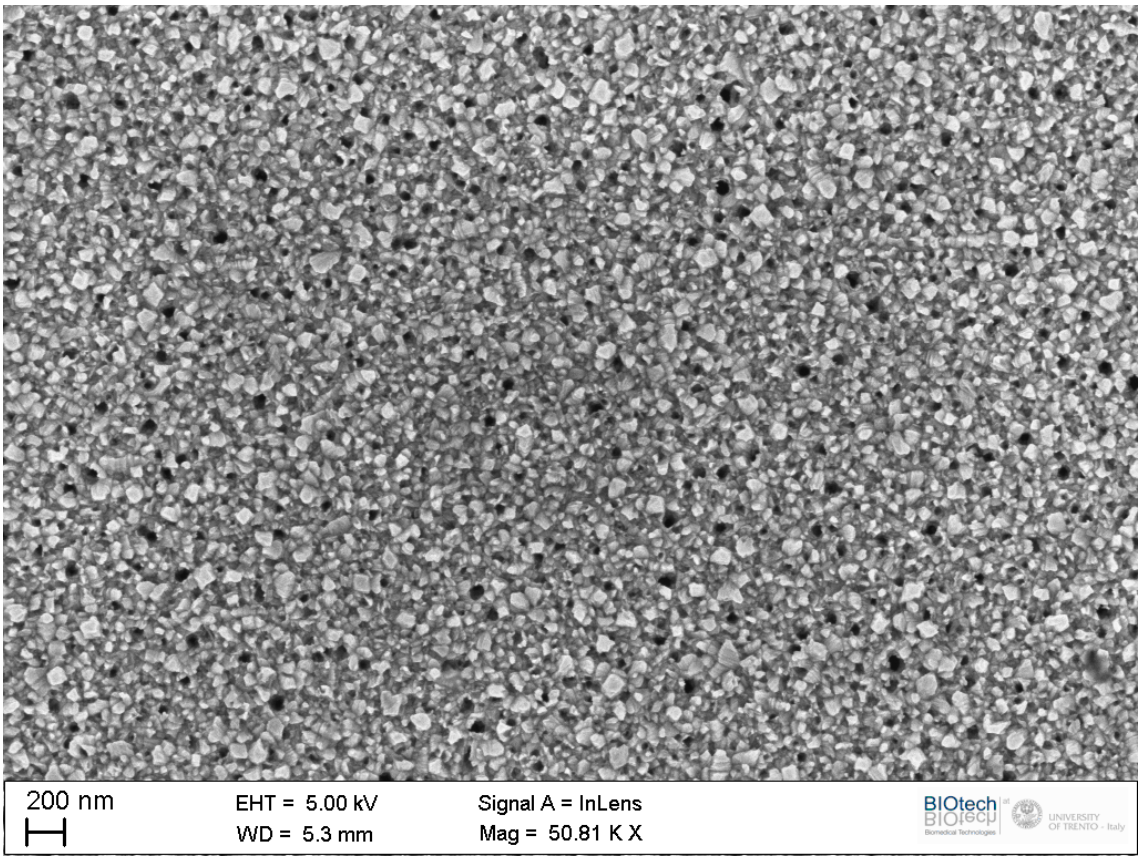

Figure 69. NNT33 ESEM image.

The figure 68 represents black parts in NNT32 that finally were identified as titanium partially oxidized and in figure 69 we can see the shape of the conductive layer with no presence of titanium on FTO glass for NNT33.

For NNT34s we decided to keep the voltage at 1V with short anodization times. Concretely, NNT34 was carried out for 10 sec. free of voltage and 5 sec. with 1V applied. NNT34b was in the electrolyte for 50 sec. and no voltage was used this time. All the another reaction conditions were the same than in NNT32/33s series.

In both NNT34 and NNT34b we achieved homogeneous surfaces after experiments, differencing another dark color in NNT34 and a semi-transparent film for NNT34b.

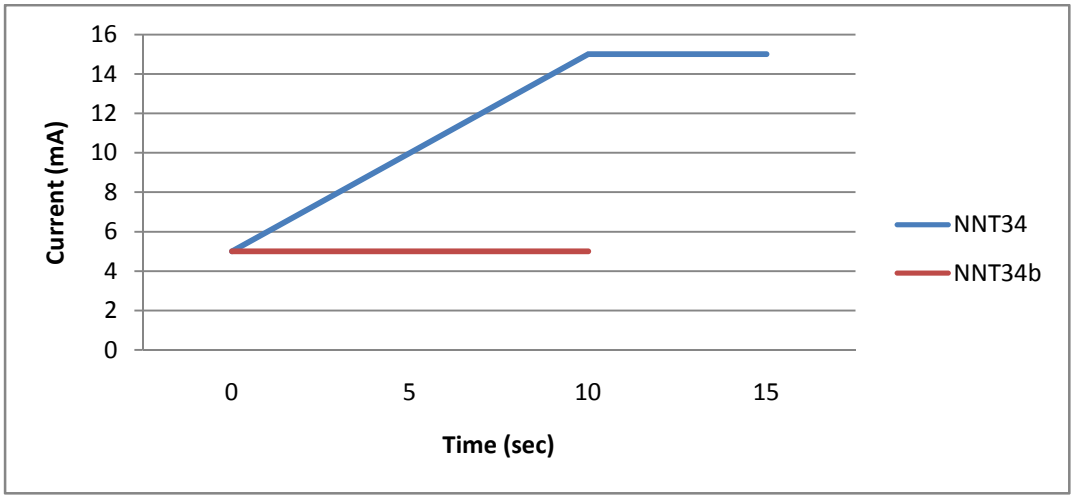

In ESEM analysis we observed a nanoporous surface over NNT34 as shown figure 70, instead of NNT34 where similar results as NNT32 were achieved.

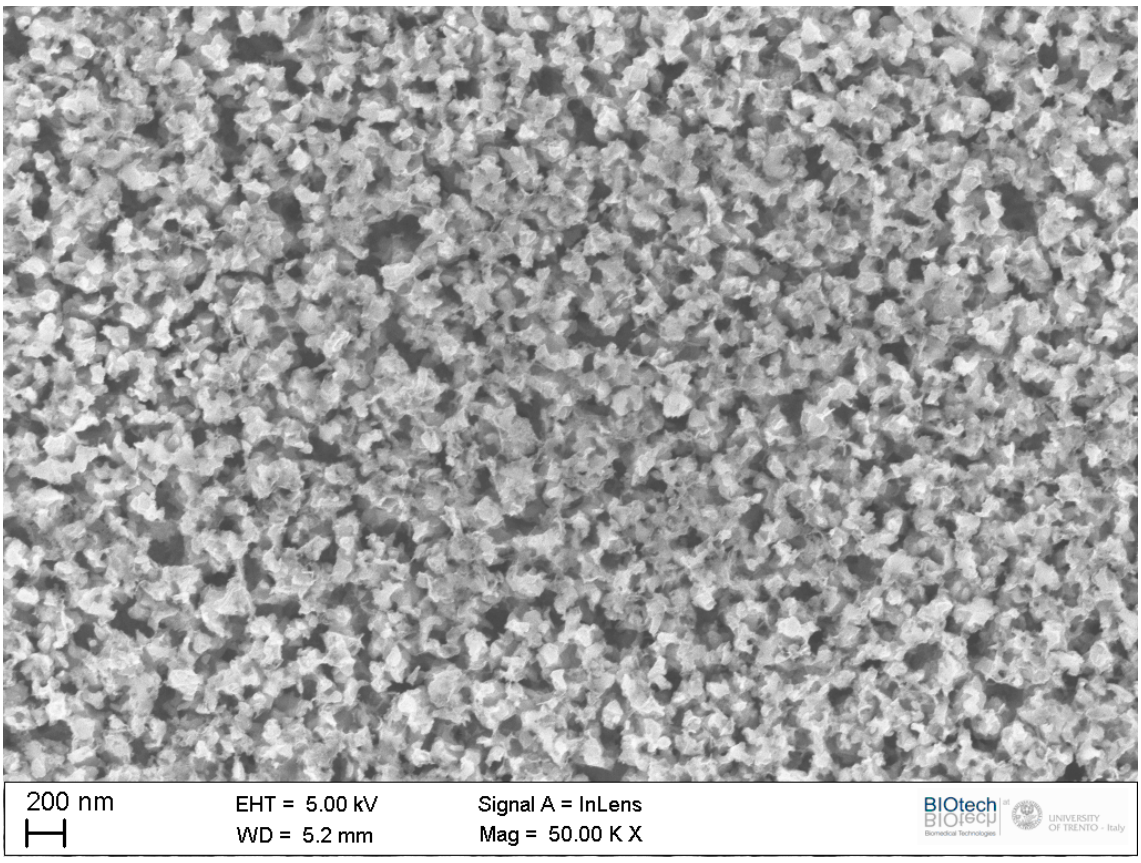

Figure 70. NNT34 nanoporous.

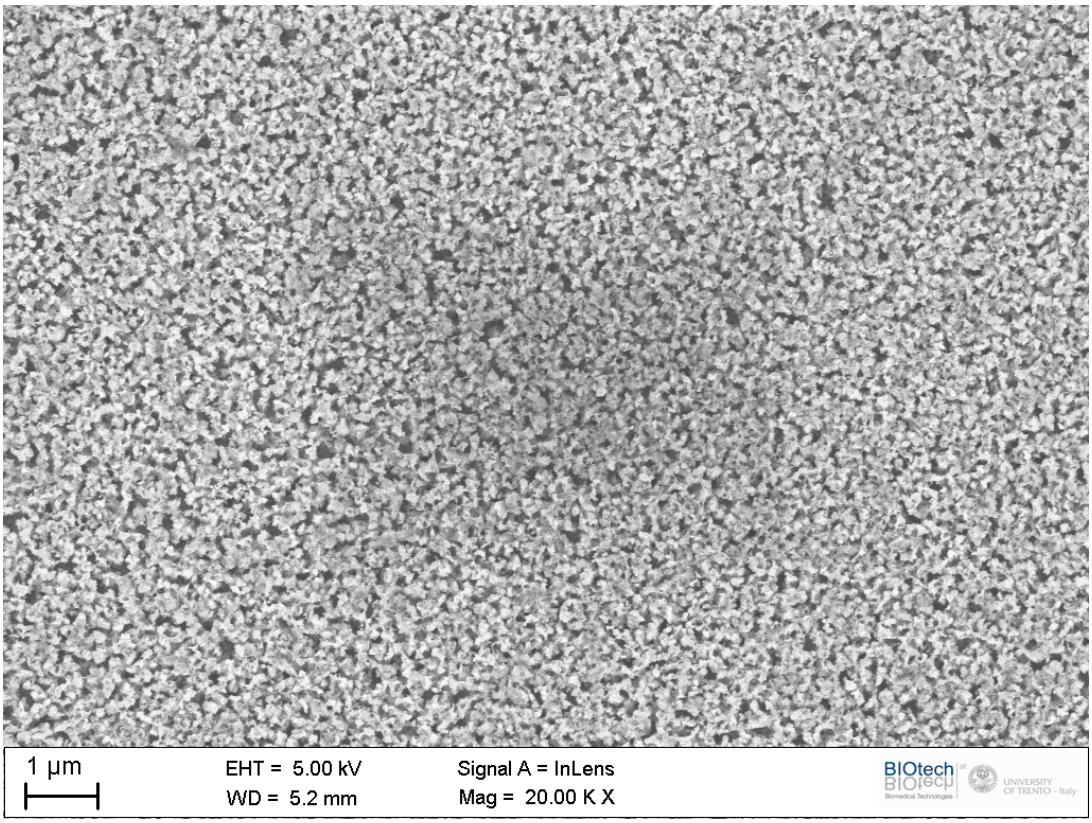

Figure 71. NNT34 image.

After this step, following last results in NNT34, various anodization were carried out on 500nm sputtering thickness individually. Our idea was to assembly some cells using nanoporous homogeneous surfaces with a good specific area of anodiziting samples.

By this way, similar experiments as NNT34s were repeated taking special care with the full sample.

3.3 Cell analysis.

Once anodizated, samples were sintered, the assembly was carried out following the steps commented before. Afterwards, we took advantage of sunny days we had in July to proceed with the cell measurements.

As expected, the performance of the cells was quite low. However, it was found a response to sunlight that justified their behavior as photovoltaic cell. Next graphics show voltage and power depending on current.

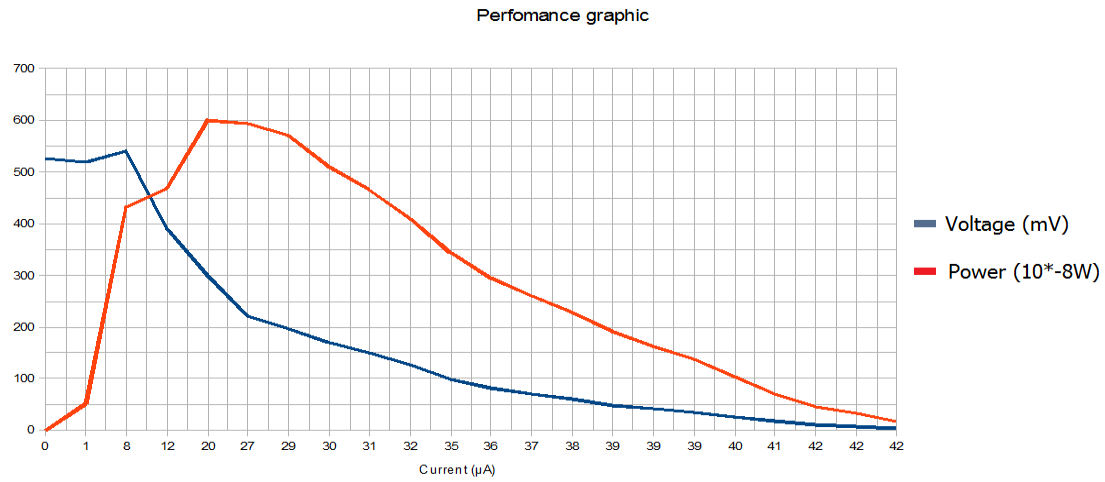

Figure 72 Current-Voltage curve and power for c1.

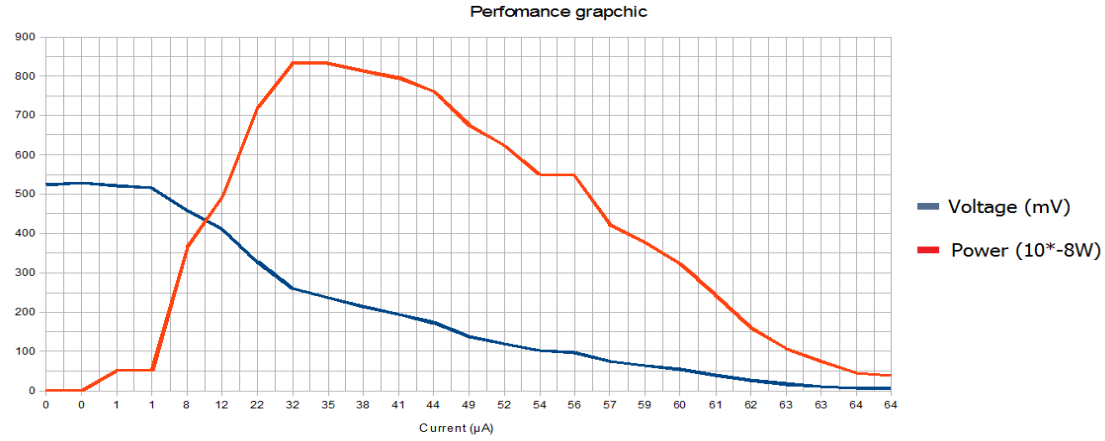

Figure 73 Current-Voltage curve and power for c2.

4. Conclusions.

The research work had as primarily objectives the fabrication and characterization of DSSC using titania nanotube as metal base. However, due to difficulties related with nanotube growth on sputtering samples, the project was refocused in the study of nanotubes on titanium plates with determinate conditions before continuing next parts.

After, we visit new labs to sputtering samples that we needed to go on with the work of anodizating metal film for building cells. Then, during next step we realize that new conditions with sputtering samples had appeared to achieve nanotubes. With methods and experience obtained on first step, anodizating on plates, we tried to reproduce nanotube conditions on sputtering samples unsuccessfully. Nevertheless a TiO2 nanoporous structure was found and used to fabricate two cells.

These cells had not the performance that we expected, but served us to understand that electric behavior existed and could be improved in next works.

However, I would like to note that anodization samples on plates were an important part in this work and that without it, it would have been impossible to achieve anything during sputtering samples. In the same way, ESEM image spectrum depending on temperatures could be interesting for next projects.

Is important to note that commented solution regarding of detaching film during anodization consisting on a sputtering double-layer would have been the better choice for continuing the experimental part anodizating the sputtering samples from Padova. In the same way, longer deposition times will be necessary to achieve competitive thickness as is reported in literature to get optimal cell conditions.

At this point, although the project was carried out with all available physical and material means, it would have been much better to have at our disposal, at least in the same city, fundamental elements and devices that would have allowed us the full cell fabrication.

5. Bibliography

1.The Official Journal of the European Union (OJ). *Opinion of the European Economic and Social Committee on the Current situation and prospects for traditional energy in a future energy mix* , C 28, 2006.

2 . U.S. Energy Information Administration. *International Energy Outlook,* 2010.
4. B. O'Reagan, M Grätzel, Low-cost, hig- efficiency solar cell based on dye-sensitized colloidal TiO2 films, Nature, 353, 1991.

3. U.S. Department of energy, *National laboratory renewable energy*, 2010.

5. Craig A. Grimes, Kopal K. Mor, *TiO2 Nanotube Arrays sysnthesis, properties and applications*, 2009.

6. F.O Lenzmann, J.M. Kroon, *Recent advances in Dye-sensitized Solar Cell,* Advaces in OptoElectronics, 2007.

7. Joseph George, C.S. Menon, *Electrical and optical properties of electron beam evaporated ITO thin films*,2000.

8. Massimo Sebastiani, *Costruzione e caratterizzazione di un dispositivo fotovoltaico a colorante organico*, Master thesis, 2007.

9. Ooman K. Varghese, M. Paulose, Craig A. Grimes, *Long vertically aligned titania nanotubes on transparent conducting oxide for highly efficient solar cells,* Nature nanotechnology, 2009.

10. Antii Tolvanen, *Characterization and manufacturating techniques of dye-sensitized solar cell,* Master thesis, 2003.

11. D. M. Mattox, *Handbook of physical vapor deposition (PVD) processing*, 1998.

12. Gallone, *La configurazione del campo elettrico nei sistema elettrochimici*.

13. Michael Gräetzel, *Photoelectrochemical cells,* Nature, 2001.